REPORT DOCUMENTATION PAGE

AFRL-SR-BL-TR-98-

0402

Public reporting burden for this collection of information is estimated to average 1 hour per response, and maintaining the data needed, and completing and reviewing the collection of information. Sen information, including suggestions for reducing this burden, to Washington Headquarters Services, Dir 1204, Arlington, VA 22202-4302, and to the Office of management and Budget, Paperwork Reduction F

188

ources, gathering this collection of s Highway, Suite

1. AGENCY USE ONLY (Leave Blank)	2. REPORT DATE	3. REPORT TYPE AND DATES COVERED
	December 1992	Final

4. TITLE AND SUBTITLE The Response of Prestressed Concrete Roof Elements of a Buried Shelter Subjected to a Surface Explosion	5. FUNDING NUMBERS
6. AUTHORS William Randal Burkett	
7. PERFORMING ORGANIZATION NAME(S) AND ADDRESS(ES) University of Texas at Austin	8. PERFORMING ORGANIZATION REPORT NUMBER
9. SPONSORING/MONITORING AGENCY NAME(S) AND ADDRESS(ES) AFOSR/NI 110 Duncan Avenue, Room B-115 Bolling Air Force Base, DC 20332-8080	10. SPONSORING/MONITORING AGENCY REPORT NUMBER
11. SUPPLEMENTARY NOTES	
12a. DISTRIBUTION AVAILABILITY STATEMENT Approved for Public Release	12b. DISTRIBUTION CODE

13. ABSTRACT *(Maximum 200 words)*

See attachment

DTIC QUALITY INSPECTED 4

19980504 167

14. SUBJECT TERMS	15. NUMBER OF PAGES
	16. PRICE CODE

17. SECURITY CLASSIFICATION OF REPORT	18. SECURITY CLASSIFICATION OF THIS PAGE	19. SECURITY CLASSIFICATION OF ABSTRACT	20. LIMITATION OF ABSTRACT
Unclassified	Unclassified	Unclassified	UL

THE RESPONSE OF PRESTRESSED CONCRETE ROOF ELEMENTS OF A BURIED SHELTER SUBJECTED TO A SURFACE EXPLOSION

APPROVED BY
DISSERTATION COMMITTEE:

Co-supervisor

Co-supervisor

CP Johnson

Dedicated To

My Wife and Children,

Our Parents and Families,

and

The Lord Jesus Christ

and

In Memory of

My Father

Eldreadge Lynn Burkett

THE RESPONSE OF PRESTRESSED CONCRETE ROOF ELEMENTS OF A BURIED SHELTER SUBJECTED TO A SURFACE EXPLOSION

by

WILLIAM RANDAL BURKETT, B.S., M.E.

DISSERTATION

Presented to the Faculty of the Graduate School of

The University of Texas at Austin

in Partial Fulfillment

of the Requirements

for the Degree of

DOCTOR OF PHILOSOPHY

THE UNIVERSITY OF TEXAS AT AUSTIN

December 1992

Acknowledgments

The author wishes to express his sincere appreciation and thanks to his Ph.D. Committee Co-supervisors, Dr. Ned Burns and Dr. Jose Roesset, for their professional guidance and personal encouragement during the development and completion of this dissertation. The author wishes to express a special thanks to committee member Dr. James Jirsa for his support and encouragement throughout the academic process of the last four years. Thanks is also expressed to the other committee members Dr. Philip Johnson, Dr. Michael Kreger, and Dr. Anthony Bedford for their guidance and support in the completion of this dissertation.

Thanks is extended to the faculty and staff of the Civil Engineering Department for their outstanding teaching and excellent support during the last four years.

Financial support for this study was supplied by the United States Air Force Office of Scientific Research via the Laboratory Graduate Fellowship Program and is gratefully acknowledged. Technical support for this study was provided by the Air Force Civil Engineering Support Agency, Tyndall AFB, FL, and is also gratefully

acknowledged. Thanks is expressed to the Office of Graduate Studies, The University of Texas at Austin, and the Southeastern Center for Electrical Engineering Education, St. Cloud, FL, for their timely and outstanding administration of the author's fellowship.

A special thanks is given to Randy James of the ANATECH Research Corporation for his time and support of this research study which used ANATECH's concrete constitutive model, UMAT91.

Sincere appreciation is expressed to Dr. Tom Kennedy and all the personnel at the Asphalt Research Program Office, The University of Texas at Austin, for their administrative support, encouragement, and friendship during the completion of this dissertation.

This paper is dedicated to my loving wife and children and our families without whose commitment, support, and encouragement this accomplishment would not have come to completion. This paper is dedicated in loving memory of my father who passed away during the course of this study and is deeply missed. Final and foremost, this paper is dedicated to The Lord Jesus Christ whose mercy and faithfulness has been and continues to be demonstrated in my life on a daily basis.

THE RESPONSE OF PRESTRESSED CONCRETE ROOF ELEMENTS OF A BURIED SHELTER SUBJECTED TO A SURFACE EXPLOSION

Publication No. _____

William Randal Burkett, Ph.D.
The University of Texas at Austin, 1992

Supervisors: Jose M. Roesset
Ned H. Burns

Dynamic nonlinear analyses were conducted on pretensioned and conventionally reinforced precast concrete members that were embedded in soil and loaded by a surface detonation of a high explosive. The single span members were analyzed as one foot wide solid sections in plane strain. The ends of the members were cantilevered past the supports to take advantage of additional restraint provided by the soil.

The soil was modeled as a uniform pressure applied to the top surface of the members with elastic, perfectly plastic springs distributed over the cantilevered portion of the members. The dynamic forcing function from the

explosion was modeled using commonly accepted formulas and was applied as a pressure to the top surface of each member. Soil-structure interaction effects were approximated in the analyses.

The dynamic analyses were conducted on a PC using a computer code, BLASTSDF, that was developed and validated within the study and was shown to have good correlation with results from more sophisticated analysis techniques and previously reported results. BLASTSDF implements a single-degree-of-freedom model that uses nonlinear shape and stiffness functions generated by a static nonlinear finite element analysis. BLASTSDF provides computer run time and cost savings when compared to dynamic nonlinear finite element analyses, especially for parametric studies when the member is kept constant.

It was observed that any additional restraint applied to the cantilevered portion of the members significantly improved the response of each member. However, the inertia force from the mass of the soil over the cantilevered portion of the members was shown to have very little influence on the dynamic response of the members and was ignored. Each prestressed member was shown to have an improved total response (combined static

and dynamic) when compared to the conventionally reinforced member. However, very little difference was observed in the dynamic responses of all the members when referenced from their static service load conditions. As expected, the prestressed members were shown to have reduced ductility when compared to the conventionally reinforced concrete member.

Table of Contents

		Page
List of Tables		xii
List of Figures		xiii
Chapter		
1	Introduction	1
	1.1 General	1
	1.2 Purpose and Scope	5
2	Background	7
	2.1 Introduction	7
	2.2 Protective Shelters	7
	2.3 Explosions	9
	2.4 Ground Shock	14
	2.5 Structure Design	27
	2.6 Prestressed Concrete	34
	2.7 Finite Element Method	42
3	Concrete Models	47
	3.1 Introduction	47
	3.2 General Modeling	48
	3.3 ABAQUS Concrete Constitutive Model	49

Chapter		Page
	3.4 ANATECH Concrete Constitutive Model .	55
	3.4.1 Preliminary Review and Static Analysis	56
	3.4.2 UMAT91 Concrete Model Validation.....	57
4	Dynamic Analysis	70
	4.1 Introduction	70
	4.2 Single-Degree-of-Freedom	71
	4.2.1 Theory	71
	4.2.2 Program Characteristics	79
	4.2.3 Validation	83
	4.3 Dynamic Nonlinear Finite Element	90
5	Soil Effects	95
	5.1 Introduction	95
	5.2 Soil Strength and Stiffness	95
	5.3 Inertia Forces	102
6	Static and Dynamic Response	104
	6.1 Introduction	104
	6.2 Member Details	106
	6.3 Static Nonlinear Analysis (FE).....	115
	6.4 Dynamic Nonlinear Analysis (SDOF)....	128

Chapter Page

7 Summary, Conclusions, and Recommendations 135

7.1 Summary 135

7.2 Conclusions 137

7.2.1 Response of Concrete Members . 137

7.2.2 Structure Configuration and Design 141

7.2.3 Finite Element Models and Method 142

7.2.4 Single-Degree-of-Freedom Model 143

7.3 Recommendations 145

Appendix

I ABAQUS Input File for Hamilton P/C Beam . 148

II FORTRAN Source Code for BLASTSDF 152

III BLASTSDF Static Input File Format 167

IV BLASTSDF Dynamic Input File Format 172

V ABAQUS Dynamic Input File for Member PC53-6 174

VI ABAQUS Static Input File for Member PC53-6 183

References 191

Vita 201

List of Tables

Table		Page
3.1	Material Properties for FE Analysis	60
3.2	Cross Sectional Stresses	65
5.1	Soil Effects Case Assumptions	99
6.1	Member Details	108
6.2	Material Properties	114
6.3	Static Load Steps	119
6.4	Significant Events	120
6.5	Maximum Response (W = 1014 lbs)	130
6.6	Maximum Response for Various Weights	134

List of Figures

Figure		Page
1.1	Generic P/C Protective Shelter	5
2.1	Typical Buried R/C Protective Shelter	10
2.2	General Shock Wave Form	11
2.3	Indirect Ground Shock	15
2.4	Direct Ground Shock	16
2.5	Peak Pressure vs Distance	19
2.6	Pressure vs Time	20
2.7	Plane Stress Wave	23
2.8	Radial and Transverse Stresses	26
2.9	Single-Degree-of-Freedom System	29
2.10	Typical P/C Cross Sections	39
2.11	Harped Tendon Profile	41
3.1	Weidlinger and Hinman One-way R/C Slab ...	50
3.2	ANATECH Example	53
3.3	Concrete Models: ABAQUS vs ANATECH	54
3.4	Hamilton Prestressed Concrete Beam	58
3.5	Finite Element Mesh	59
3.6	Finite Element	60
3.7	ANATECH Concrete Stress-Strain Curve	61
3.8	Stress-Strain Response for #3 Bar	62

Figure		Page
3.9	Stress-Strain Response for Strand	62
3.10	Hamilton P/C Beam: Load-Deflection	66
3.11	Extreme Fiber Concrete Strain	67
3.12	Various Concrete Cracking Strains	68
4.1	Idealized Beams	72
4.2	Static Shape and Load Vector	74
4.3	Approximate Shape Function	76
4.4	Weidlinger One-way R/C Slab	84
4.5	ABAQUS and BLASTSDF Slab Models	85
4.6	Linear Dynamic Analysis	86
4.7	Dynamic Nonlinear Analysis	88
4.8	Load Distribution Effects	89
4.9	Dynamic Nonlinear Analysis: WS53-2.7	91
4.10	Dynamic Nonlinear Analysis: PC53-6	92
4.11	Deflected Shape: PC53-6	93
5.1	Soil Effects Case Geometries	97
5.2	Load-Deflection for Soil Effects	98
5.3	Soil Mass Effect on Response	103
6.1	Member Details	107
6.2	Static Load Capacities	111
6.3	Static Load-Deflection Curves	116

Figure		Page
6.4	Member Ductility	126
6.5	Total Response (W = 1014 lbs)	130
6.6	Dynamic Response (W = 1014 lbs)	131
6.7	Dynamic Response for Various Weights	133

Chapter 1

Introduction

1.1 General

Today reinforced concrete, prestressed concrete, or a combination of the two are common construction materials and techniques used throughout the world for a wide range of civilian and military applications including nuclear reactor containment vessels, single story and high-rise buildings, parking garages, bridges, highways, airport runways, storage tanks, dams, drainage pipes, earth retaining walls, hardened aircraft shelters, and underground bomb shelters. As a composite material, the use of steel reinforced concrete dates back to the mid 1800's, while the initial use of prestressed concrete began in the mid 1880's. However, the first attempts at using prestressed concrete were not successful because the maximum initial tensile stress which could be applied to the low strength steel of that day was soon lost by shrinkage and creep of the concrete. With the development of high strength steels, the modern development and application of prestressed concrete began in the late 1920's.[1,2]

Structures which are required to resist the effects of explosions are commonly constructed of reinforced concrete. They are normally massive, heavily reinforced, cast-in-place concrete structures used to provide safety and protection for personnel, equipment, materials, and other buildings from the harmful effects of explosions.

These structures can be classified as one of two types; containment or protective.[3] Containment structures are designed to confine an explosion within the structure and minimize the damage to nearby surroundings. An example would be a munitions manufacturing plant where people outside the structure and adjacent buildings and materials need to be protected from effects of an accidental explosion. Protective structures, on the other hand, are designed to resist the effects of an external explosion and provide protection to people, material, or equipment inside the structure. An example would be a civil defense or military "bomb" shelter used to provide protection from an enemy attack. Discussions and issues in this study will be limited to protective structures.

The design of a protective structure is affected by many factors including the degree of protection required, the source of the explosion, and the type of structure

being designed. When considering the degree of protection required, the contents of the structure and their sensitivities to various harmful effects of the explosion must be considered. The possible contents within any given shelter and their corresponding sensitivities are far beyond the scope of this paper. Therefore, only the response of the structure itself will be considered in this effort.

The source of the explosion greatly impacts the characteristics and types of harmful effects produced. Sources of explosion include nuclear, high explosives such as trinitrotoluene (TNT) and composition C-4, and common commercial materials such as fuels and chemicals. Types of harmful effects produced by these sources include electromagnetic pulse, blast overpressure, fragments, ground shock, fire, heat, and dust. The characteristics and magnitudes of these effects are not only a function of the explosive material but also of the charge weight, shape, encasement, and location with respect to the structure.[3,4]

The type of structure, buried or aboveground, will also impact the characteristics and type of harmful effects that must be resisted. An aboveground concrete structure might have to resist blast overpressure,

fragments, and ground shock while an underground structure will normally only have to resist ground shock. The scope of this study is limited to underground concrete structures subjected to high explosives; a very common type of military protective structure.

Underground protective shelters are commonly heavily reinforced cast-in-place concrete structures. They use large amounts of material and are labor intensive and time consuming to construct. The Air Force Civil Engineering Support Agency in Florida is interested in using prefabricated modular units to construct underground protective shelters. The use of prefabricated modular units has the potential to provide substantial economic savings through efficient material usage, repetitive usage of standardized modular units, and reduced erection labor. Additional advantages could be achieved by stockpiling the modular units at a site until they are needed. Stockpiling of the modular units would allow additional shelters to be constructed relatively fast as the need arises and would allow the repair of structures by the replacement of damaged units. One aspect of interest is the use of precast prestressed concrete sections as roof elements for the buried protective shelters. A generic buried protective shelter

configuration using modular concrete units is shown in Figure 1.1.

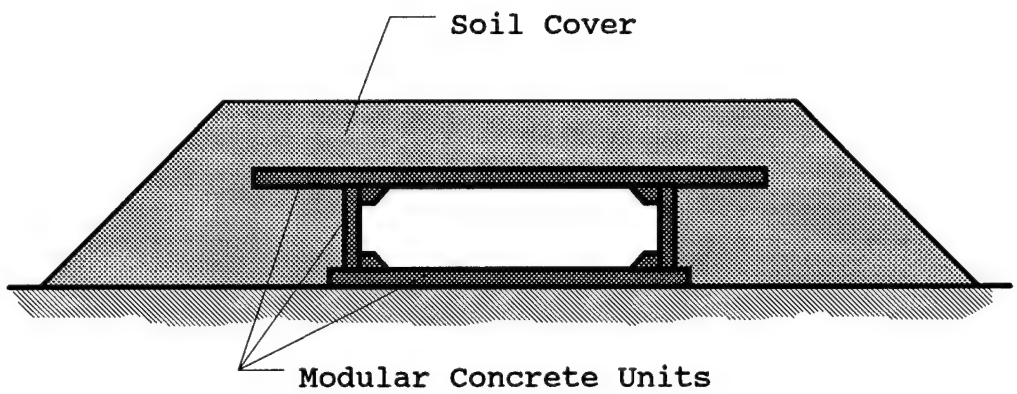

Figure 1.1 Generic P/C Protective Shelter

1.2 Purpose and Scope

The primary objective of this research is to look at the response of precast prestressed concrete elements as a roof for a buried protective shelter subjected to non-nuclear munitions (high explosives) loading condition, commonly referred to as conventional weapons effects. This objective will be accomplished by dynamic nonlinear analyses using a FORTRAN computer code, BLASTSDF, which models a single-degree-of-freedom system. BLASTSDF is developed in Chapter 4 of this study. The mid span

response, as a function of time, of single span concrete members similar to the one shown in Figure 1.1 will be investigated. The response of concrete members with variations in structural geometry, tendon profile, partial prestressing, and conventional reinforcement will be considered.

Two secondary objectives are addressed in the study. The first is to develop and validate a single-degree-of-freedom system computer code for dynamic nonlinear analyses of conventional weapons effects on buried concrete structures. The second is to validate the applicability of using ABAQUS,[5,6] a commercially available general purpose finite element program, to conduct dynamic nonlinear analyses for conventional weapons effects on buried concrete structures. Validation will be accomplished by comparing results obtained in this study for a reinforced concrete protective shelter against previously reported results.

Chapter 2

Background

2.1 Introduction

The issues addressed and concepts used in this study cover a broad spectrum. A comprehensive literature review of these issues and concepts was completed with the results being provided in the six sections of this chapter. The six topics are Protective Shelters, Explosions, Ground Shock, Structure Design, Prestressed Concrete, and Finite Element Method.

2.2 Protective Shelters

Technology to design shelters to provide protection from detonations of high explosives had its beginnings in research conducted in the 1940's with much of the research appearing to have been sponsored by the National Defense Research Committee and the National Research Council. Since that time, research has continued providing reports and papers too numerous to list. However, a large amount of recent research is documented in the proceedings from four symposia held in 1983,[7] 1985,[8] 1987,[9] and 1989[10] on the interaction of non-nuclear munitions with structures. The technology

developed through the years to design protective shelters against high explosives has also been combined in several key documents; *Structures to Resist the Effects of Accidental Explosions (Volumes I - VI)*,[3,11,12,13,14,15] *Fundamentals of Protective Design for Conventional Weapons*,[4] and *Protective Construction Design Manual*.[16]

Protective shelters are commonly buried below ground using the soil to reduce or remove some of the harmful conventional weapons effects that the structure must resist, namely blast overpressure and fragments. This leaves ground shock, which will be discussed in Section 2.4, as the major threat to buried structures for explosions on or within the ground.[17] Buried protective shelters are often heavily reinforced concrete box structures as shown in Figure 2.1. Flexural reinforcement in this type of structure can be in the order of 1% in each direction and at each face. The same percentage of steel that is in the loading tension face is commonly placed in the loading compression face to supply tensile capacity during stress reversals due to rebound. The steel mats of each face are connected by steel ties to provide confinement to the concrete and resist the tensile stress created when the compressive

stress wave in the concrete reflects off the free inside surface.

A concrete burster slab, shown in Figure 2.1, or a layer of rock rubble is often placed at the ground surface over the structure to minimize the distance the explosive charge can penetrate into the soil. By minimizing this distance, the magnitude of the compressive stress wave traveling through the soil (ground shock) that the structure must resist is reduced. However, the explosive charge in this study is assumed as a point source at the ground surface, and the burster layer is omitted.

2.3 Explosions

An explosion is defined by Henrych[18] as a, "Sudden physical or chemical change of the state of a mass accompanied by a release of energy and by motion," and is defined by Ayvazyan,[11] et al, as a, "Very rapid and stable chemical reaction." In our area of interest, solid high explosives, the material is changed almost instantaneously from a solid to a hot, dense gas. This transformation takes place as a chemical reaction progresses throughout the material at a rate called the detonation velocity. The detonation velocity varies with

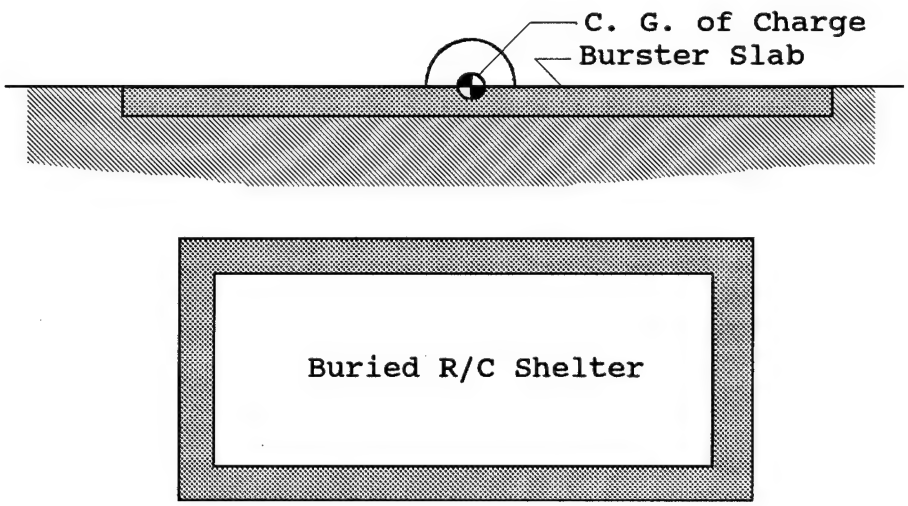

Figure 2.1 Typical Buried R/C Protective Shelter

high explosive materials but is in the order of magnitude of 25,000 feet/second.[11] For a spherical charge with a radius of 1.5 feet, the time required for detonation would be in the order of 6×10^{-5} seconds.

Associated with the chemical reaction which transforms the high explosive from a solid to a gas is a large increase in temperature and volume. The temperature in the explosion process can be as high as 7000 degrees Fahrenheit.[18] The large increase in volume causes the gas to rapidly expand radially outward creating a high pressure region which compresses the surrounding material. Pressures in this region can be in the order 4,600,000 psi.[11,18] It is this rapid outward

expansion of hot gases that creates the blast wave or shock wave.

The general form of a shock wave from an explosion is shown in Figure 2.2. The pressure rises from the ambient condition to a maximum or peak pressure almost instantaneously. It then decreases monotonically below the ambient pressure to a minimum and then increases back to the ambient pressure. The pressure regions above and below the ambient pressure are called the positive and negative pressure phases, respectively. The positive phase is the significant aspect of the shock wave, and the common practice of addressing only the positive phase will be used in this study.

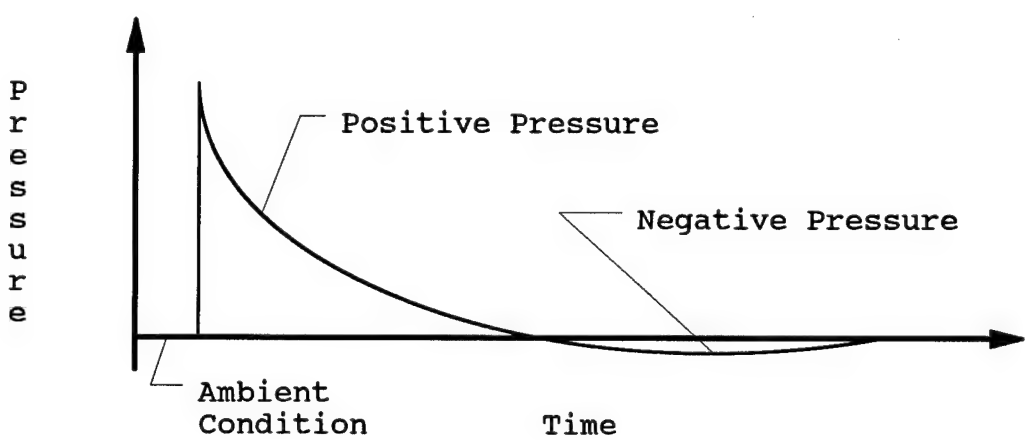

Figure 2.2 General Shock Wave Form

The characteristics and effects of an explosion are a function of many parameters including the explosive weight, material, shape, and casing as well as the distance from the explosion (standoff distance). The weight of the explosive material and the standoff distance are the key parameters. Through the years, much of the data and experimental work pertains to trinitrotoluene (TNT) which is used as the standard and will be used as the standard in this study.

The shape of the charge, spherical versus cylindrical, has an impact on the distribution of the shock wave produced. However, this effect is significant only at points close to the explosion and diminishes with increasing standoff distance. The charge dimensions in relation to the standoff distances of interest in this study are such that the shape of the charge will have little effect on the ground shock produced and will be ignored.

The characteristics of the explosion and the load on the structure will be altered if the explosive charge is "cased" as opposed to "bare." When the charge is encased, the detonation process produces internal stresses in the case material until the failure strength is exceeded. The case then ruptures hurling thousands of

particles or fragments of various sizes in all directions at very high initial velocities. For typical charges, it would not be uncommon for fragments weighing several ounces to be initially traveling at velocities around 8,000 feet per second. For aboveground structures located near the charge, these fragments impacting the structure would have to be considered in conjunction with the blast pressure of the explosion. However, the fragments quickly lose their velocity as they penetrate into common soils and will have little impact on the buried structures investigated in this study. The casing also affects the magnitude of the shock wave produced but this effect is thought to be small for ground shock[19] and will be ignored in this study.

The characteristics of an explosion, as indicated above, are greatly affected by two main parameters, standoff distance and charge weight. To correlate characteristics of explosions having various combinations of these two parameters, Hopkinson or cube-root scaling is used. The scaled distance, which is given the symbol λ, is defined as

$$\lambda = R / W^{1/3} \tag{2.1}$$

where R = Distance from explosion

W = Weight of the explosive

For example, the blast pressure for an explosion of weight W_1 at distance R_1 would be equal to the blast pressure of an explosion of weight W_2 at distance R_2 if the following was true:

$$R_1 / W_1^{1/3} = R_2 / W_2^{1/3} \tag{2.2}$$

Cube-root scaling has been proven experimentally true for an extremely wide range of charge weights when ambient conditions, charge shape, and charge-to-surface ratio are identical. However, reasonable results are still obtained when only similar conditions exist.[4]

2.4 Ground Shock

Ground shock is produced by the detonation of explosive charges in the air, at the ground surface, or within the ground. These types of detonations are commonly referred to as air burst, surface burst, and ground burst, respectively. Indirect ground shock is

produced as the shock wave from a surface burst travels along the surface of the ground as shown in Figure 2.3. Direct ground shock is produced by direct coupling of the explosion with the ground in a surface or ground burst as shown in Figure 2.4. Direct ground shock is the dominant threat to the buried structures of interest, and it alone will be addressed in this study. The general configuration for this study is shown in Figure 2.4, with the charge located at mid span to provide the critical loading condition.

Explosions can occur in direct contact with or near a buried structure because of charge penetration into the soil. Depth of penetration is a function of soil properties and presence of burster layers above the

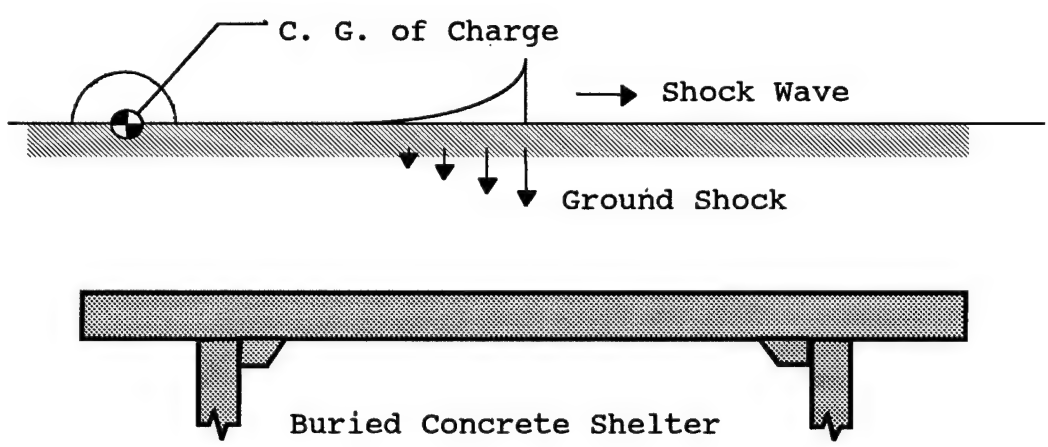

Figure 2.3 Indirect Ground Shock

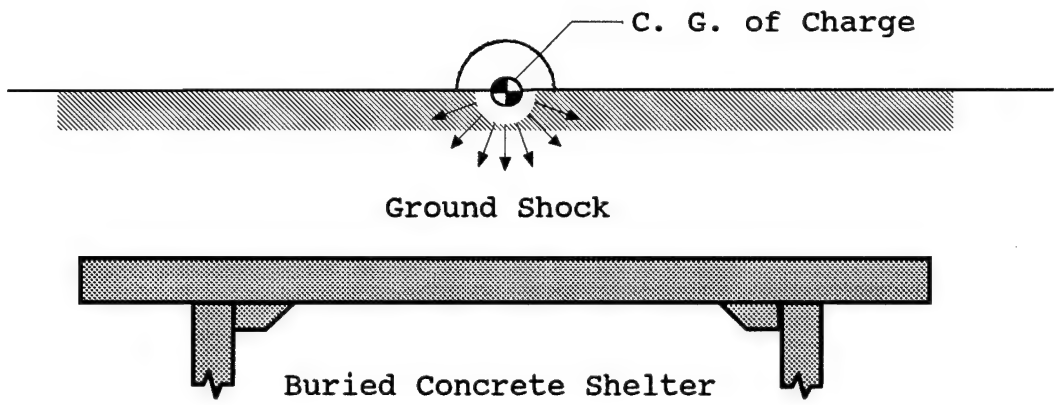

Figure 2.4 Direct Ground Shock

structure as well as weapon physical characteristics, velocity, and fusing. Near structure detonations are defined as scaled distances less than 1.0 and are likely to cause localized breaching of the structure.[4] This study will be limited to surface burst with scaled distances greater than 1.0 which will allow the overall global response of the members to control in lieu of a localized material failure.

The magnitude of the ground shock that reaches a buried structure varies greatly as the physical properties and moisture content of the soil through which it propagates varies. At a scaled range of 2 $ft/lb^{1/3}$, the peak stress ranges from 200 psi to 10,000 psi as the soil varies from a loose dry sand to a saturated clay, respectively.[17] The soil type and physical condition

greatly affect the ground shock transmission and should be considered in protective shelter design. This study will be limited to a granular soil which is a common backfill material and provides better resistance to weapon penetration.[15] Specific soil material properties used by Weidlinger and Hinman[20] will be used throughout this study and are identified in Section 4.2.3.

Ground shock is characterized by free-field parameters such as stress, impulse, and soil particle displacement, velocity, and acceleration. Predictions for peak values of these parameters are made by commonly accepted empirical equations developed by Drake and Little.[17] The key parameter used in this study is the peak free-field pressure that is predicted by

$$\sigma_o = f * \rho c * 160 * (R/W^{1/3})^{-n} \qquad (2.3)$$

where σ_o = Peak pressure (psi)

f = Coupling factor

ρc = Acoustic impedance (psi/fps)

R = Distance from charge (ft)

W = Charge weight (lb)

n = Attenuation coefficient

The peak free-field pressure (σ_o) which decreases greatly with increased distance from the explosion, as shown in Figure 2.5, can then be used to define the free-field pressure at any given point as a function of distance and time, $\sigma(x,t)$. The pressure pulse, $\sigma(x,t)$, is characterized by an almost instantaneous rise time (t_r) from the ambient condition to the peak value σ_o at the associated time t_o followed by an exponential decay back to the ambient condition. The time of arrival (t_a) and the rise time (t_r) of the pressure pulse can be approximated, respectively, by

$$t_a = R/c \tag{2.4}$$

$$t_r = 0.1 * t_a \tag{2.5}$$

where R = Distance from explosion

c = Compressive wave speed of soil

The pressure pulse in this study was broken into three phases: prior to arrival, rise time, and exponential decay. The three phases are defined as follows:

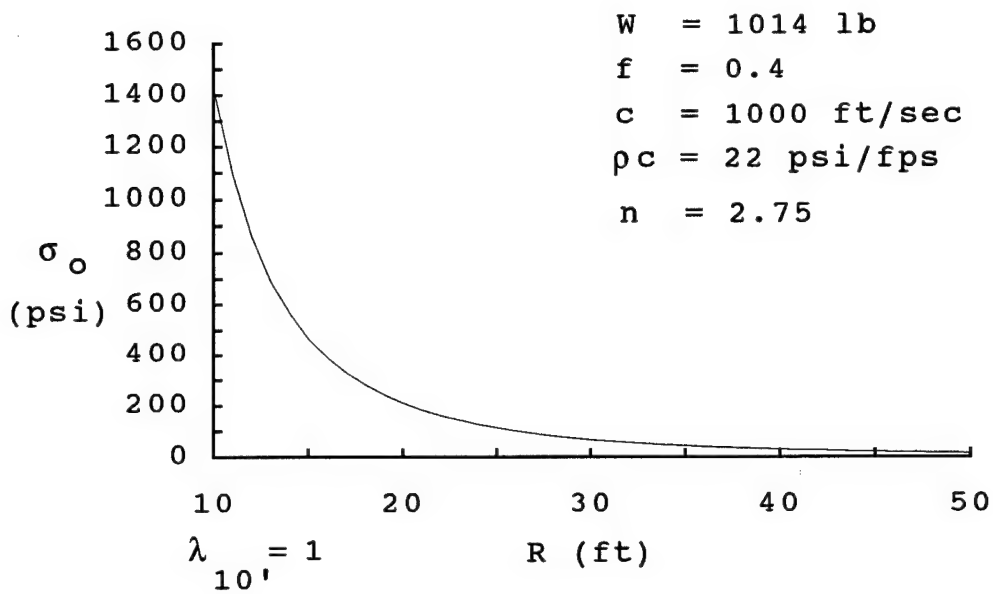

Figure 2.5 Peak Pressure vs Distance

For $t < t_a$

$$\sigma(x,t) = 0.0 \tag{2.6}$$

For $t_a \le t \le t_o$

$$\sigma(x,t) = \sigma_o * (t-t_a)/t_r \tag{2.7}$$

For $t > t_o$

$$\sigma(x,t) = \sigma_o * e^{-[(t-t_a)/t_a]} \tag{2.8}$$

The pressure, $\sigma(x,t)$, is shown in Figure 2.6 for distances of 21 ft and 30 ft using the soil parameters in this study. Distances from the explosion of 21 ft and 30 ft correlate to points on the top surface of the buried structure at mid span and the support, respectively, for the configuration shown in Figure 4.4. It should be noted that the coupling factor of 0.4 used by Weidlinger[20] and this study conservatively assumes the charge as a point source at the ground surface.

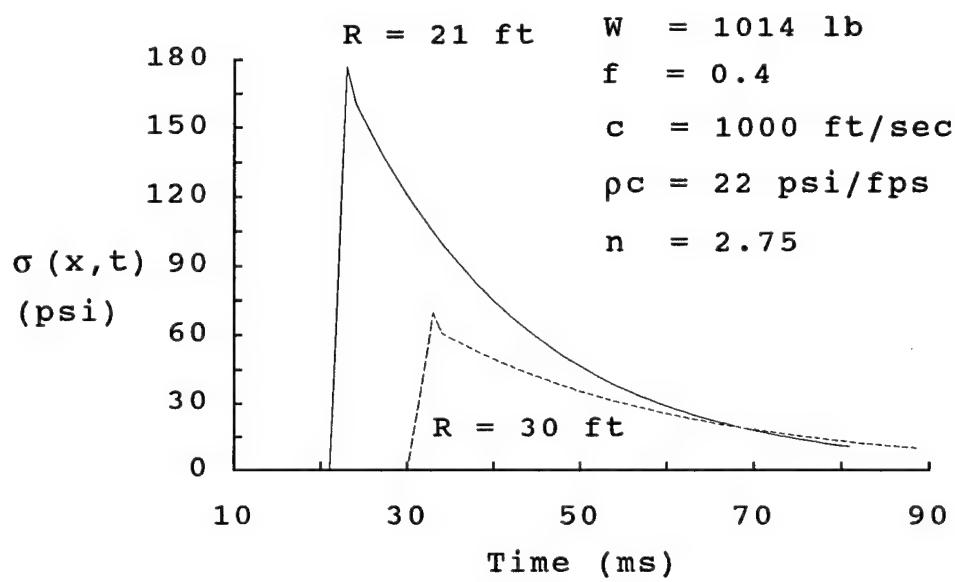

Figure 2.6 Pressure vs Time

Up until now, the discussion on ground shock has considered only the free-field parameters, that is, the compressive shock wave traveling through the soil in the absence of a structure. However, in this study, there is a structure embedded in the soil which is greatly affected by the ground shock and in turn greatly affects the ground shock. As the initial compressive shock wave travels through the soil, it interacts with the structure. The shock wave is reflected off the structure back into the soil and also transmitted across the soil-structure boundary to the structure.

The stress pulse that is reflected (σ_R) from the boundary of two materials is a function of the physical properties of the two materials and the incident stress pulse (σ_I). It can be calculated for a plane wave front using one-dimensional wave propagation theory[21] as

$$\sigma_R = \sigma_I * [(\rho_2 c_2 - \rho_1 c_1)/(\rho_1 c_1 + \rho_2 c_2)] \qquad (2.9)$$

while the relationship of the interface stress (σ_{int}) to the incident, reflected, and transmitted (σ_T) stresses is given by

$$\sigma_{int} = \sigma_I + \sigma_R = \sigma_T \tag{2.10}$$

where

σ_{int} = Interface stress

σ_I = Incident stress

σ_R = Reflected stress

σ_T = Transmitted stress

ρ_i = Mass density of material "i"

c_i = Compressive wave speed of material "i"

The relationship defined in Equation 2.10 can be observed by discussing the triangular stress pulse and two materials shown in Figure 2.7. Before the incident stress wave reaches the boundary as in Figure 2.7.a, the interface, reflected, and transmitted stresses are zero. During the time that the incident stress is in contact with the boundary as shown in Figure 2.7.b, the interface stress is equal to the sum of the incident and reflected stress and must also equal the transmitted stress to maintain equilibrium. Once the incident stress pulse ends as in Figure 2.7.c, the interface stress returns to zero, and the reflected and transmitted pulses propagate away from the boundary.

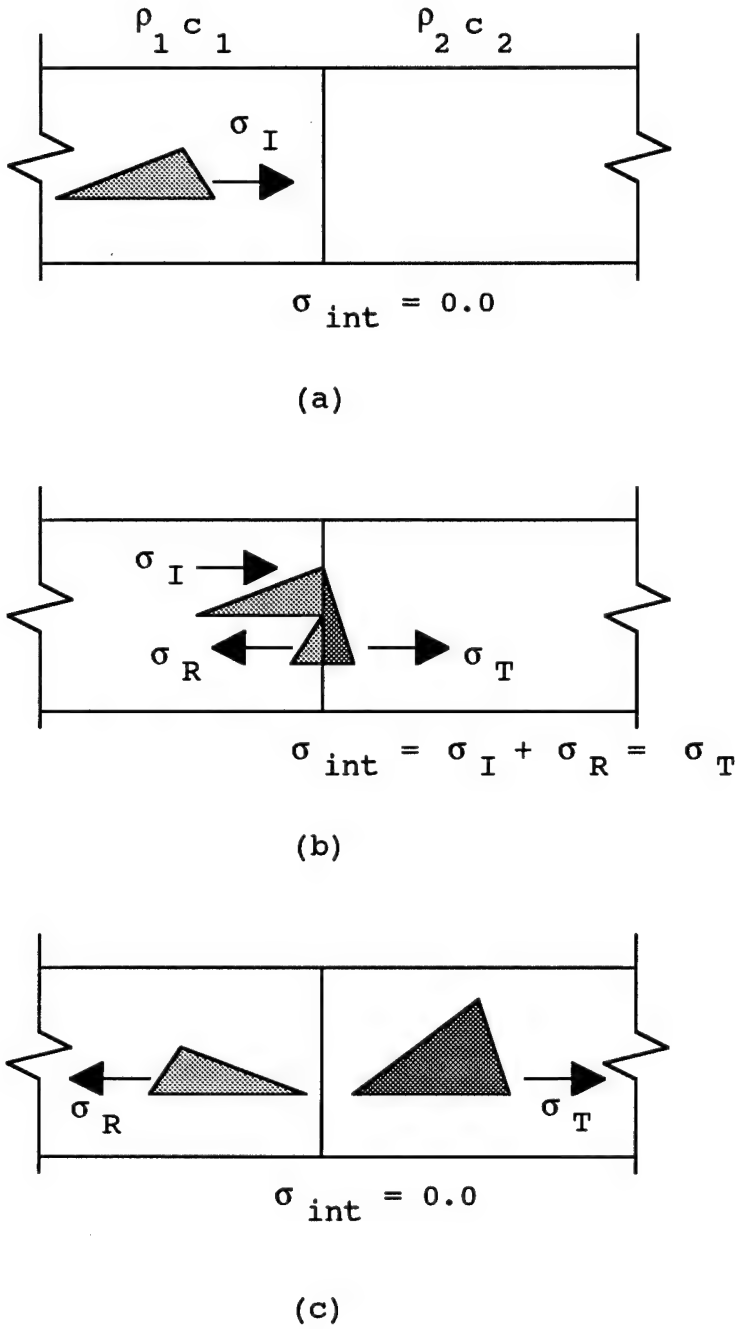

Figure 2.7 Plane Stress Wave

Significant insight can be achieved by looking at the two extreme cases: the second material as a rigid boundary and as a free boundary. First, the second material assumed as a rigid boundary, $\rho_2 c_2$ much greater than $\rho_1 c_1$, allows Equation 2.9 to approach

$$\sigma_R = \sigma_I * (\rho_2 c_2 / \rho_2 c_2) = \sigma_I \tag{2.11}$$

Substituting into Equation 2.10 gives

$$\sigma_{int} = \sigma_I + \sigma_I = 2\sigma_I \tag{2.12}$$

which indicates that at a rigid boundary the reflected stress equals the incident stress and that the interface stress is twice the incident stress. This is a conservative estimate for the ground shock loading on a buried shelter and will be discussed in more detail in Section 2.5. Second, the second material assumed as a free boundary, $\rho_1 c_1$ much greater than $\rho_2 c_2$, allows Equations 2.9 to approach

$$\sigma_R = \sigma_I * (-\rho_1 c_1 / \rho_1 c_1) = -\sigma_I \tag{2.13}$$

which indicates that at a free boundary a compressive incident stress will reflect as a tensile stress. This is the phenomenon that occurs at the concrete/air

interface on the inside of a protective shelter and is why steel ties are used as was indicated earlier.

The free-field pressure or stress wave in the soil propagates radially from the center of the explosion creating a spherical shock front which is only normal to the embedded structure at one location, directly below the explosion. This creates a three-dimensional time and space dependent stress function which must be broken into components acting on the structure. However, slabs can be conservatively designed for one-way action which reduces and simplifies the analysis to a two-dimensional problem and is the approach that will be used in this study.

Ross,[22] et al, reported that transverse stresses in the soil in the range of 30 to 40 percent of the radial stress have been noted in sandy soils with moisture contents around 5 to 7 percent. In the two-dimensional problem, the transverse stress (σ_t) combined with the radial stress (σ_r) at a point forms a biaxial state as shown in Figure 2.8 which can be used to determine the magnitude of the stress acting normal to the structure (σ_n). The magnitude of the normal stress can be

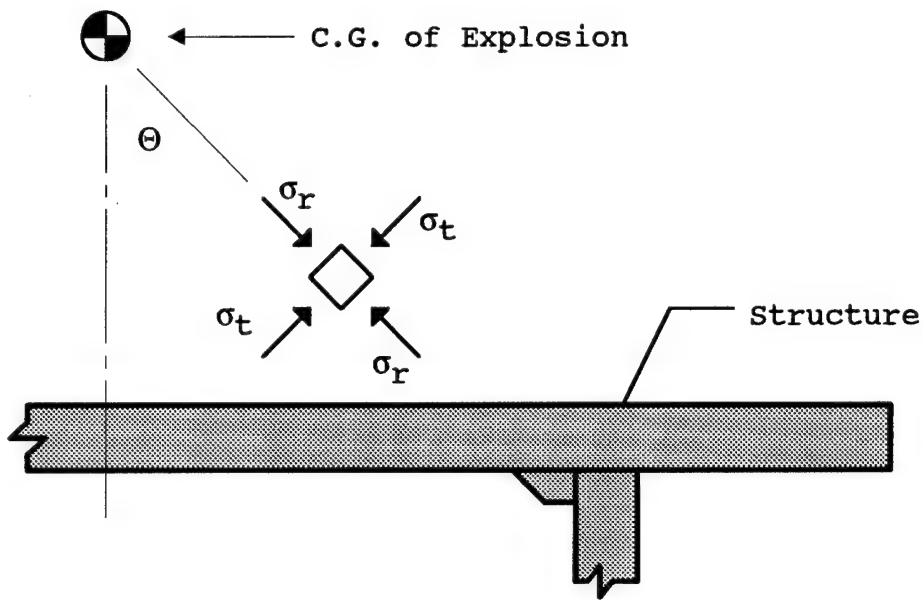

Figure 2.8 Radial and Transverse Stresses

expressed as

$$\sigma_n = (\sigma_r+\sigma_t)/2 + [(\sigma_r-\sigma_t)*\cos 2\Theta]/2 \qquad (2.14)$$

with the angle theta as shown in Figure 2.8. Equation 2.14 can be developed directly from the Mohr circle of stresses[23] and has been verified experimentally.[22] Ross,[22] et al, showed that for values of σ_t equal to σ_r, $0.5\sigma_r$, and zero that the normalized values of peak normal stress were 1.0, 0.97, and 0.94, respectively. From this, the mid range value of σ_t equal to $0.5\sigma_r$ was

selected for use in this study and reduces Equation 2.14 to

$$\sigma_n = \sigma_r * (0.75 + 0.25\cos 2\Theta) \qquad (2.15)$$

Knowing σ_r equals $\sigma(x,t)$ as expressed in Equations 2.6, 2.7, and 2.8 and substituting into Equation 2.15 gives

$$\sigma_n(x,t) = \sigma(x,t) * (0.75 + 0.25\cos 2\Theta) \qquad (2.16)$$

Equation 2.16 is used in this study to predict the component of the free-field pressure pulse in the soil that is normal to the structure.

2.5 Structure Design

Shelters used to protect personnel, material, and equipment from blast effects are often designed to resist only a single load application. The load imposed on a buried structure by ground shock from a surface explosion is a high intensity load of short duration with very localized effects. The investigation of survivability normally addresses individual elements as opposed to the overall response of a multi-element structure; therefore, the term structure and element will be used

interchangeably with the mid span deflection being used as the measure of response. Inelastic response is allowed since the structure must resist only one load application. The amount of inelastic response allowed is controlled by the ductility of the member which is defined as

$$\text{ductility} = \delta_{max} / \delta_{elastic} \tag{2.17}$$

which is the ratio of maximum response to the elastic response with a value between 5 and 10 used for protective shelters.[15]

The ground shock reflecting off the buried structure creates a dynamic system which is affected by the structural stiffness, damping and inertial forces, and soil-structure interaction (SSI). Older and current methods which produce conservative designs use a single-degree-of-freedom (SDOF) system as shown in Figure 2.9 where m*, k*, c*, and p(t)* represent the equivalent mass, stiffness, damping, and loading of the structure, respectively, and the displacement 'u' represents the mid span deflection of the structure. Structural damping has little influence on the maximum response which occurs

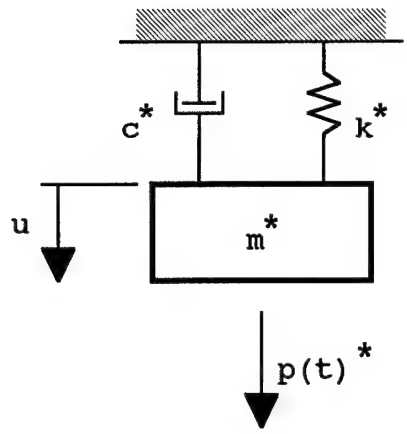

Figure 2.9 Single-Degree-of-Freedom System

during the initial cycle of vibration and is commonly neglected.

The loading function, p(t)*, for the SDOF model is assumed as a uniform load distribution. In early designs, the magnitude of the loading function was assumed as 2 times the peak free-field stress in the soil distributed uniformly across the entire span.[24] The reflection factor of 2 comes from Equation 2.12 where the structure is assumed rigid. The actual reflection factor for normal weight concrete and sandy soils ranges from 1.94 to 1.79 for loose and dense sandy soils, respectively. The assumed distribution of the free-field stress is not uniform across the span but decreases significantly with increasing distance from the explosion

as shown in Figure 2.5. These load assumptions led to extremely conservative designs.

The current design methods compensate for the extreme conservatism discussed above by using a reduced reflection factor and by using an equivalent uniform load in lieu of the peak uniform load. The equivalent uniform load is defined as the uniform load that will produce the same static mid span deflection as that produced by a non uniform distribution (commonly a cubic distribution) which better approximates the peak load variation across the span. The time of duration of the ground shock also varies across the span and is accounted for by using an average time of duration for the span.

Current design methods are still extremely conservative with responses predicted by the current SDOF design method often being much greater than those observed in actual tests. Drake,[25] et al, stated that it is "widely acknowledged that buried protective structures are often grossly over designed," and reported that in the mid 1980's structures tested to loads well above their expected structural capacity exhibited little or no damage.

The conservatism of the current design method partially comes from neglecting the interaction of the

soil and the structure. The load that the shock wave in the soil imparts to the structure is directly coupled to and affected by the response of the structure. As the shock wave loads the structure, the structure accelerates moving away from the soil which reduces the load the structure must resist. This would suggest that a flexible ductile structure may provide better designs than the stiff rigid structures used to-date.

Significant research on soil-structure interaction (SSI) has been conducted since the late 1970's[19,20,25,26,27,28,29,30,31,32,33] showing that SSI has a definite impact on the magnitude and distribution of the loading and should be included in the design and analysis of buried protective shelters. Drake,[25] et al, in some cases showed a reflection factor applied to the free-field stress slightly larger than one at mid span as compared to commonly used reflection factors ranging from 1.5 to 2.

Since the early 1980's, dynamic finite element methods have been commonly used in research to analyze buried protective shelters and have produced results that are in good agreement with experimental results.[20,27,28,29,31,34,35] One dynamic finite element approach used by Nelson,[36] called the soil island approach, models the

surrounding soil, the structure, and the interface between them. Even though this approach is able to reproduce the effects of SSI, it is a time consuming and costly process for iterative design applications.

The cost of computer run time to complete the dynamic finite element approach described above can be minimized by decoupling the structure from the soil allowing only the structure to be modeled. Drake,[25] et al, reported that an approximation for the blast induced normal interface stress at a point between the soil and a structure was suggested by Crawford,[37] et al, as

$$\sigma_{int}(t) = \sigma_{ff}(t) + \rho c*[V_{ff}(t)-\dot{u}(t)] \qquad (2.18)$$

where $\sigma_{int}(t)$ = Normal interface stress

$\sigma_{ff}(t)$ = Normal free-field soil stress

ρc = Soil acoustical impedance

$V_{ff}(t)$ = Normal free-field soil velocity

$\dot{u}(t)$ = Structure velocity

Wong[26] linked the normal interface stress approximation of Equation 2.18 to the structural deformation by applying the general plane wave relationship

$$\sigma = \rho c V \tag{2.19}$$

to the soil and substituting into Equation 2.18 which gives

$$\sigma_{int}(t) = 2*\sigma_{ff}(t) - \rho c*\dot{u}(t) \tag{2.20}$$

Knowing the expression for the normal free-field stress in the soil (Equation 2.16), we can rewrite Equation 2.20 for any point along the structure as

$$\sigma_{int}(x,t) = 2*\sigma_n(x,t) - \rho c*\dot{u}(x,t) \tag{2.21}$$

By using $\sigma_{int}(x,t)$ as the loading function and rearranging with $\rho c*\dot{u}$ becoming a damping term, the general dynamic equation of motion for a multiple-degree-of-freedom system can be written as

$$\mathbf{M}\ddot{\mathbf{U}} + \rho c\dot{\mathbf{U}} + \mathbf{KU} = 2\boldsymbol{\sigma}_n(x,t) \tag{2.22}$$

The decoupled SSI approximation described above has been shown to provide results in good agreement with test results and with results from more detailed analyses[20,25,28,31,38] and will be used in this study.

2.6 Prestressed Concrete

The use and understanding of prestressed concrete has continued to increase since the beginning of its modern development in the late 1920's. Today, it is a common construction method used in a wide range of structural applications including years of successful use in dynamic applications. Various research efforts and authors[1,15,39,40,41,42,43,44,45] indicate that prestressed concrete is a good material for use in impact and shock loaded structures characterized by pulses of high magnitude and short duration. However, no experimental or analytical investigations on dynamically loaded prestressed concrete elements identified by the author to-date used load functions, distributions, or magnitudes which simulate the load applied to a buried structural element caused by a surface detonation of a high explosive. Also, no research on dynamically loaded prestressed elements has been identified that includes the important effects of soil-structure interaction.

Some design guidance for precast prestressed concrete members subjected to blast loads is provided in *Structures to Resist the Effects of Accidental Explosions - Volume VI*,[15] but no specific research is referenced as a basis for this guidance. General background and design

information concerning prestressed concrete used in this study has been drawn from five main sources: *Design of Prestressed Concrete Structures*,[1] *Reinforced Concrete Design*,[2] *Structures to Resist the Effects of Accidental Explosions - Volume VI*,[15] *PCI Design Handbook*,[46] and *Building Code Requirements for Reinforced Concrete (ACI 318-89)*.[47]

The concept of prestressing as applied to concrete uses the high tensile strength and elasticity of the steel to offset the weak tensile strength of the concrete. Correct precompression can eliminate cracking of the concrete section at service load. This allows the member to respond elastically, helps control deflection, and provides protection for the steel. For buried protective shelters which are designed to survive a single worst case detonation while undergoing inelastic deformations, it is important to maintain the integrity of the steel and structure during daily service loads to insure that adequate strength is available during inelastic response. If cracking occurs due to soil overburden or other superimposed loads prior to blast loading, corrosion of the steel could occur resulting in loss of strength and possible structural collapse during blast loading.

Prestressing of concrete is accomplished by two methods: pretensioning and post-tensioning. The post-tensioning method is accomplished by releasing elongated steel tendons which are inserted through ducts cast in the concrete. As the steel tries to contract to its original length, the concrete is compressed as the tensile force in the steel is transferred to the concrete via anchors at the ends of the member. A larger prestressing force can be applied to the concrete by the post-tensioning method because of the higher concrete strength at the time of transfer. The post-tensioning method has an additional advantage over the pretensioning method if the steel tendons are left unbonded after transfer. Unbonded strand allows any additional elongation in the steel, caused by loads applied to the member, to be distributed along the length of the strand reducing high strain concentrations and the possibility of strand failure. However, the post-tensioning method increases the amount of time, the skill of labor, and the complexity of equipment required for erection when compared to the pretensioning method. Because of these erection disadvantages, the post-tensioning method will not be addressed in this study.

The pretensioning method is accomplished by releasing pre-elongated steel which is embedded in hardened concrete. As the steel tries to contract to its original length, the concrete is compressed as the tensile force in the steel is transferred to the concrete via the bond. Pretensioned members are produced in a controlled shop setting, hauled to the site, and placed into position minimizing the disadvantages during erection listed above. Because limiting construction time, skill, and equipment at erection is of prime importance, this study will be limited to pretensioned members and any use of the term prestressed will imply pretensioned.

Prestressed concrete combines high strength materials (steel and concrete) which work effectively as a composite to resist transverse loads. The steel tendons are normally 7-wire strand conforming to ASTM A416, with Grade 270 low-relaxation strand now becoming more common.[46] The minimum yield strength for Grade 270 steel is 243 ksi which allows sufficient prestressing force to remain in the steel after the concrete shortens due to its elasticity, shrinkage, and creep. Initial attempts to prestress concrete using lower strength

steels were unsuccessful because the prestressing force was lost over time.

The concrete commonly used in prestressed applications has a 28 day design strength in the range of 5000 to 6000 psi and has a high early strength to allow for stress transfer and form removal on a daily basis. A practical value for concrete strength of 3000 psi is required at transfer.[46] Even though these high strength materials normally have a higher unit cost than materials used in conventional reinforced concrete, economy can be achieved by reduced sections and repetitive casting of standardized sections.

Common prestressed concrete sections with typical dimensions and spans for conventional load applications taken from PCI[46] and Lin and Burns[1] are shown in Figure 2.10. These are generic sections which may vary depending on the local manufacturer. The dimensions and spans are listed to provide a general range for each section. However, each member must be evaluated considering the span, transverse loading, material properties, concrete cross section, prestress force, and tendon profile that are unique to each application. Even though there are numerous sections available, this study

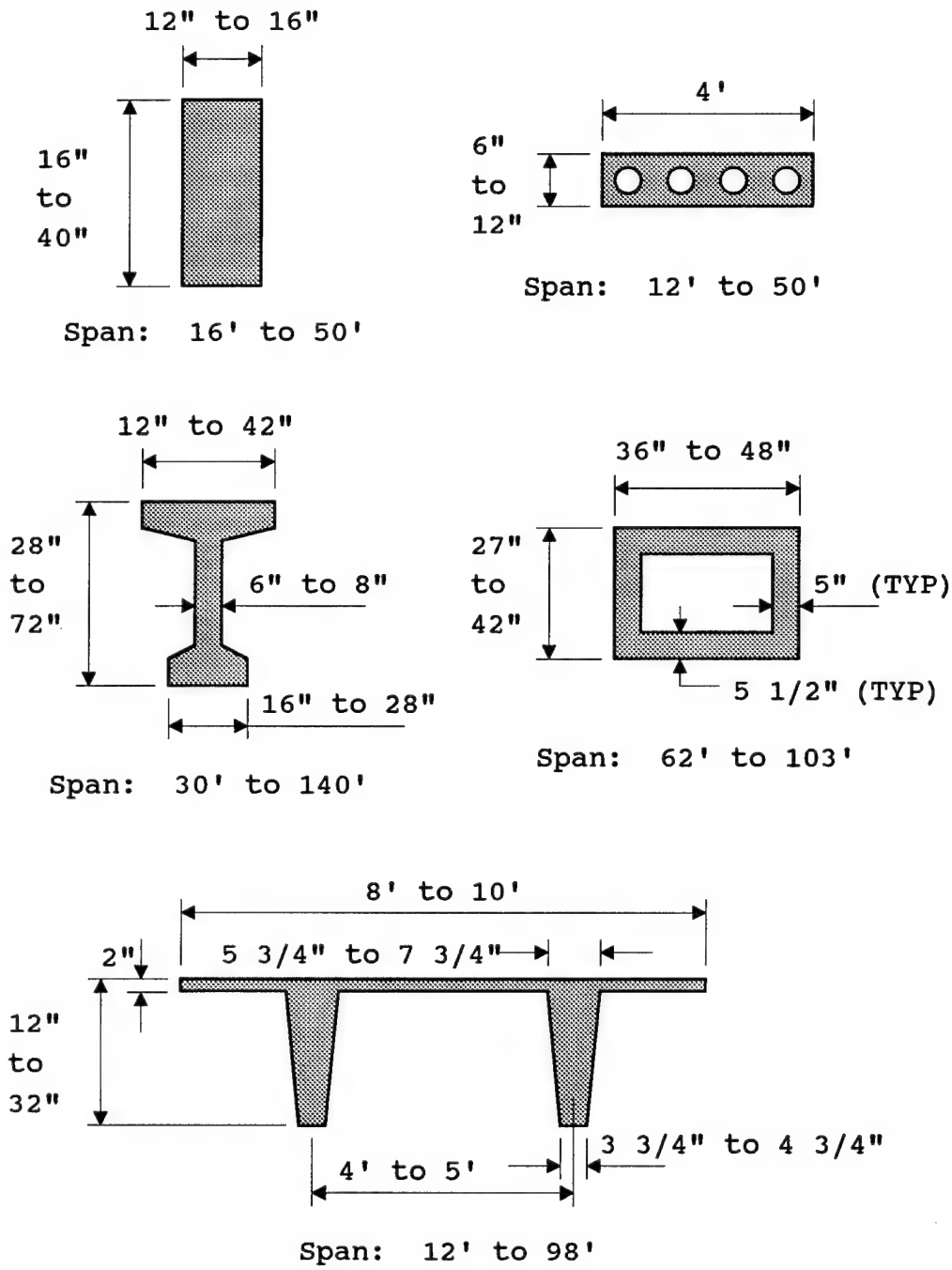

Figure 2.10 Typical P/C Cross Sections

will be limited to the response of solid rectangular sections. Additional research will be required for hollow or flanged sections to determine if localized failure of the top flange occurs and what influence it would have on the global response of the member.

Three loading stages must be considered in the design or analysis of prestressed concrete: transfer, service, and ultimate. The prestressed concrete members in this study will be designed to control crushing and cracking of the concrete at transfer and at service load, with service load defined as the dead weight of the concrete and the soil overburden. The members investigated in this study will also be designed to have ultimate static load capacities comparable to the reinforced concrete slab reported on by Weidlinger,[20] et al, which is discussed in detail in Section 4.2.3.

The location and profile of the prestressing tendons within the member has a significant effect on the stresses in the concrete. A straight tendon located at the neutral axis of the member creates only an axial prestress. By moving the tendon away from the neutral axis, bending stresses can be developed which oppose those created by transverse loads improving the efficiency of the prestress. This is especially

advantageous at locations where bending moments due to transverse loads are maximum. However, care must be taken where the transverse load bending moments go to zero to control prestress induced tensile stresses and cracking in the concrete. Tensile stresses in the concrete at locations of reduced applied bending moments can be controlled by varying the eccentricity of the prestressing tendon with respect to the neutral axis of the member as shown in Figure 2.11. The harped tendon profile shown in Figure 2.11 develops bending moments that oppose and closely follow the anticipated applied load bending moments and was selected for use in this study.

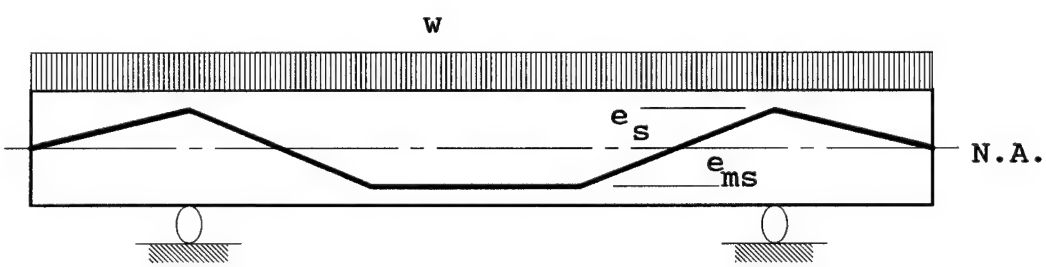

Figure 2.11 Harped Tendon Profile

Two other advantages can be obtained by using the harped tendon profile shown in Figure 2.11. First, an initial camber can be developed in the member which helps

offset vertical deflection caused by transverse loads. Second, a vertical component in the prestressing force is developed which can help resist the vertical shear forces.

The economy of a member may be improved under certain loading conditions by combining prestressed and non-prestressed reinforcing in a member. For conditions with low service loads and high ultimate strength requirements, such as some blast loaded structures, economical designs may be achieved using non-prestressed reinforcing to provide 50 percent or more of the ultimate strength of the member.[1] Non-prestressed reinforcing has very little effect in the elastic range, prior to cracking. However, in the inelastic range, the non-prestressed reinforcing helps to distribute cracks and minimize their size and adds to the ultimate strength of the member. This combination of reinforcing will also be considered in this study.

2.7 Finite Element Method

The finite element method is a commonly used and accepted technique in structural analysis of reinforced and prestressed concrete as is evidenced by the quantity of programs, information, and validation tests available

in the literature. It was recognized as a "powerful tool" for research in the early 1980's,[48,49] and in recent years, it has progressed to the point of being a method for the nonlinear analysis of concrete structures which can be used with a relatively high degree of certainty.[50,51,52,53,54] Even so, it is not a practical approach for common engineering design applications because of the high cost and time requirements associated with input development and output evaluation. Its use is often restricted to design and analyze structures with complex geometries or with complex load histories as encountered with blast loads.

The finite element method has a more significant role in research. Once the method has been proven effective for a specific application, it provides a point of reference to which the results of new or simplified models or new analysis techniques can be compared helping to reduce the need for expensive experimental work.[31,48,55]

The finite element method was initially developed in the early 1950's and grew out of work by the Structural Dynamics Unit of the Boeing Airplane Company.[56] Its first significant application to concrete was in the late 1950's and early 1960's at The University of California-

Berkeley where it was used to analyze a large concrete dam.[57] However, one had to wait until the mid 1960's before any work was published using the finite element method to analyze reinforced concrete beams and until the 1970's for prestressed concrete.[49] Since that time, the published literature on these topics is too numerous to list, but in 1982, a state-of-the-art report, *Finite Element Analysis of Reinforced Concrete*,[49] was published with a comprehensive literature survey up until that time. The report gives 67 references on the application of the finite element method to reinforced and prestressed concrete alone for the period from 1967 to 1978. It has a similar quantity of references for the other related topics it addresses: material constitutive relations, failure theories, cracking, shear transfer, dynamic analysis, and modeling of reinforcement and bond.

The development of the finite element method and its application to reinforced and prestressed concrete has continued to grow since publication of the above report. Again, the vast number of publications prohibits listing all of them here, but a selected number are given to provide a general feeling about the method and its applicability to this study.

Static nonlinear finite element analysis has been successfully applied to a wide range of reinforced and prestressed concrete structures including beams, slabs, and single and double box girder bridges.[50,52,53,58,59,60,61,62,63,64,65,66,67] It has provided results that are in good agreement with experimental work for the full range of loading stages from elastic to ultimate. Results include but are not limited to mid span load-deflection curves, steel and concrete stresses, deflected shapes, and crack propagation. In these cases, the loads are applied incrementally so that the structural response can be traced through the entire load range.

Dynamic nonlinear finite element analysis has also received a great deal of attention through the last ten years.[30,34,35,51,54,68,69,70,71,72,73,74,75] It has provided results that are in good to reasonably good agreement with experimental work for various concrete structures subjected to dynamic loads, blast and impact. However, van Wees and Weerheijm[74] did report premature failure of a concrete beam during their simulation and attributed it to the concrete model which did not account for the increased strength of concrete at high strain rates. This does flag a very important point; regardless of the overall reliability of the technique, care must be

taken in the modeling process to insure that material behavior is properly simulated to achieve good results.

A detailed evaluation of the large number of finite element programs, material models, and modeling techniques now available is beyond the scope of this study. However, *Finite Element Analysis of Concrete*[49] provides an in-depth discussion of the method and modeling techniques and identifies 25 finite element codes for possible use with concrete structures. *Investigation of Existing Computer Codes with Linear and Nonlinear Dynamic Capabilities*[76] provides information about 12 computer codes and references several other investigations of available computer codes. In addition, the references previously listed in this section address many computer codes, material models, and modeling techniques.

In summary, the finite element method has produced results from nonlinear analyses of reinforced and prestressed concrete members which are in good to reasonably good correlation with experimental results. Therefore, the finite element method will be used within this study.

Chapter 3

Concrete Models

3.1 Introduction

It was initially intended to use the nonlinear constitutive model for concrete resident in the program ABAQUS[5,6] for this study. However, preliminary static analyses conducted to evaluate this model, described in Section 3.3, showed premature failure of doubly reinforced concrete members. As a result, a different nonlinear model was sought. The concrete constitutive model UMAT91, developed by ANATECH Research Corporation[77,78] to interface with ABAQUS via the user defined material option, was selected, and the preliminary static analyses were repeated with this model. The ANATECH concrete model when linked with ABAQUS was shown to yield good overall results with close correlation between nonlinear finite element analyses and ultimate design theory. The studies conducted to validate the ANATECH concrete model are described in detail in Section 3.4.

3.2 General Modeling

The members analyzed in this phase of the study were modeled with two-dimensional 8-noded rectangular elements with reduced integration. Slabs were modeled in plane strain while beams were modeled with plane stress elements. Each finite element mesh was uniform within a given member but varied between members due to changes in geometry. However, aspect ratios were restricted to reasonable values and ranged between 3.6 to 1.0 and 1.7 to 1.0. The number of elements through the depth of the member was selected to provide a sufficient number of integration points to account for the variation in the nonlinear properties of the concrete.

All reinforcing steel, conventional and prestressed, was modeled using the "REBAR" option in ABAQUS[5] which superimposes the steel onto the corresponding concrete element and combines their effects into a composite element. All conventional reinforcing steel (longitudinal bars and stirrups) was modeled as elastic, perfectly plastic in this phase of the study. Prestressing steel was modeled using multiple linear steps small enough to simulate typical stress-strain behavior. Details are provided in Section 3.4.2.

Loads were applied to the members incrementally to trace the nonlinear behavior of the concrete through the entire load range of each member. Loads were applied incrementally from zero to a value 20 to 25 percent greater than the ultimate capacity predicted by ultimate design theory. Uniformly distributed loads were input as pressure along element surfaces as required by ABAQUS.[5]

3.3 ABAQUS Concrete Constitutive Model

The concrete model resident in ABAQUS was initially selected on the basis of example problems 2.2.6 and 4.2.7 in the *ABAQUS Example Problems Manual*.[79] These two example problems show that results using the ABAQUS concrete model compare well with experimental results. However, example problems 2.2.6 and 4.2.7 are limited in scope. The structures addressed in the examples are one-way and two-way reinforced concrete slabs, respectively, which are reinforced only on the bottom face.

Problems occurred when ABAQUS and its resident concrete model were used to perform static analyses on a protective shelter reported on by Weidlinger and Hinman,[20] shown in Figure 3.1, which contains reinforcing at both faces of the roof slab. The structure was

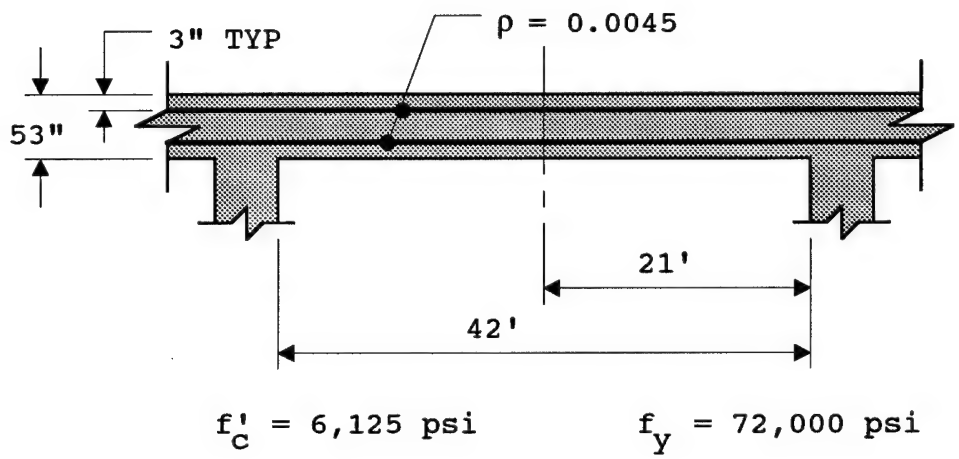

Figure 3.1 Weidlinger and Hinman One-way R/C Slab

analyzed as a one-way slab with a 28 x 10 mesh and an element aspect ratio of 1.7 to 1.0. The structure was loaded with a uniform pressure along the entire top surface of the slab applied in 1 psi increments. The material strength of the concrete and reinforcing steel was modeled by Weidlinger and Hinman[20] and in this study as shown in Figure 3.1 in lieu of their static values of f'_c of 4,900 psi and f_y of 60,000 psi to account for strength increases at the high strain rates expected in the dynamic analysis.[4,13]

The structure was initially analyzed assuming both ends were fixed against rotation. During this analysis, numerical problems were encountered which terminated the execution of the finite element analysis at a pressure of

24 psi which is less than 50 percent of the predicted ultimate value. The maximum applied uniform pressure for this configuration was predicted by ultimate design theory as 49.8 psi using

$$\sigma_{ult} = 16 \times M_p / L^2 \tag{3.1}$$

where

σ_{ult} = Ultimate applied pressure

M_p = Ultimate moment capacity per unit width

L = Length of the span

The structure was then modeled with simple supports in an effort to determine if end restraint conditions affected the numerical stability of the ABAQUS algorithm and its concrete model. Again, numerical problems were encountered when the finite element analysis terminated prematurely at an applied pressure of 15 psi, 60 percent of the predicted ultimate capacity. The ultimate capacity of the protective shelter with simple supports was predicted by ultimate design theory as 25 psi using

$$\sigma_{ult} = 8 \times M_p / L^2 \tag{3.2}$$

A finite element analysis using ABAQUS and its concrete model was later run on the example problem from ANATECH's User's Manual[78] for comparative purposes. The singly reinforced concrete beam, shown in Figure 3.2, was loaded with a uniformly distributed load applied in 1.0 psi increments. The beam was modeled using a 6 x 4 mesh with an element aspect ratio of 3.6 to 1.0. The finite element analysis was able to progress through the entire load range of the beam without numerical problems. The load-deflection curves shown in Figure 3.3 show that the ABAQUS and ANATECH concrete models produce similar results for this member but that the ABAQUS concrete model is stiffer after cracking. However, the results from each model converge to the same ultimate load between 21 and 22 psi with the ultimate design theory predicting 20.1 psi.

A finite element analysis using the ABAQUS concrete model was also completed on a doubly reinforced prestressed concrete beam tested by Hamilton.[42] Details of the Hamilton beam are provided in Section 3.4.2. Once again, the finite element analysis was terminated due to numerical problems with a maximum load of 16 kips, 73

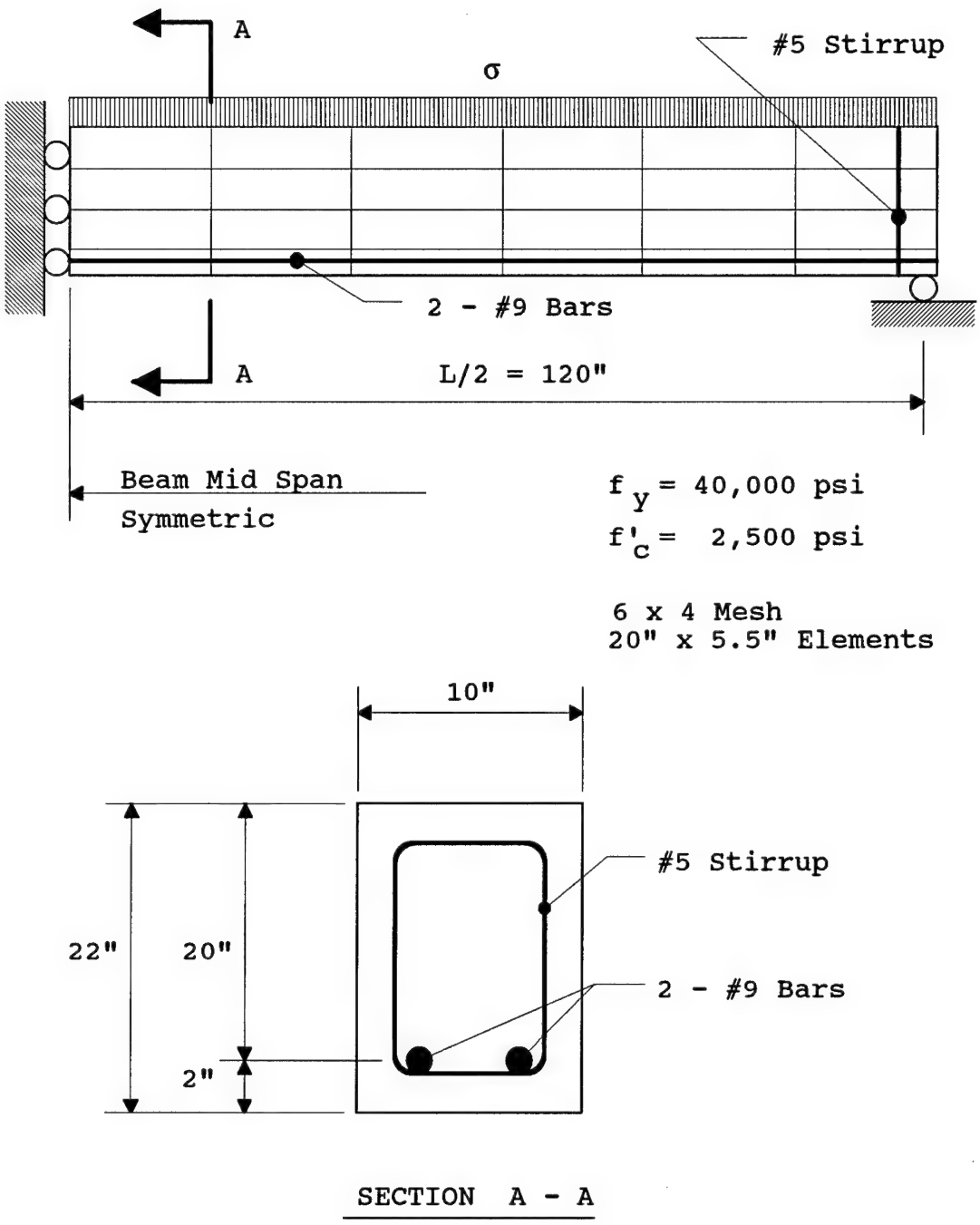

Figure 3.2 ANATECH Example

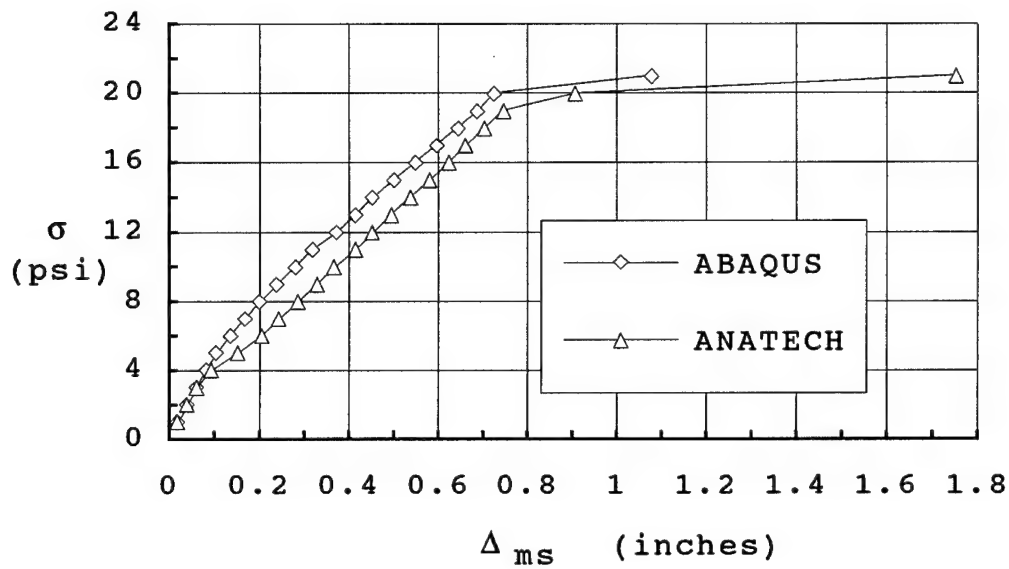

Figure 3.3 Concrete Models: ABAQUS vs ANATECH

percent of the predicted ultimate capacity and 69 percent of the experimental ultimate capacity.

Difficulties were encountered in each analysis performed on doubly reinforced members. The largest loads that were reached during these analyses were in the range of 50 to 73 percent of the ultimate capacities as predicted by ultimate design theory. Each analysis performed on a doubly reinforced member was terminated either internally by ABAQUS because of "negative eigenvalues" in the "system matrix" or by the CRAY computer because of a "floating point error." Smaller

load steps were tried to minimize the nonlinearity in any given step, but the maximum load attained in each analysis just converged to the values mentioned above. Since the members of interest in this study are required to be doubly reinforced due to rebound, it was necessary to find an alternative to the ABAQUS concrete constitutive model.

3.4 ANATECH Concrete Constitutive Model

The ANATECH concrete model, UMAT91, is an advanced concrete constitutive model that is a result of over 10 years of research conducted by the ANATECH Research Corporation.[77,78] It was developed for two and three dimensional analysis of plain, reinforced, and prestressed concrete structures. UMAT91 contains four separate concrete models which allow structural analysis of different applications with various levels of refinement. Model 3, the default model, is the general purpose, full plasticity model that was used in this study.

UMAT91 was used in an object file form and was linked directly to ABAQUS during execution. Material input values are passed between ABAQUS and UMAT91 via the

"*USER MATERIAL" option in ABAQUS.[5] Model 3 requires five input values: (1) concrete model selection, (2) static crushing strength, (3) static tensile cracking strain, (4) static elastic modulus, and (5) Poisson's ratio. UMAT91 provides default values for all of the input values except for the static crushing strength of the concrete.

3.4.1 Preliminary Review and Static Analysis

An initial review of ANATECH's example problem (Figure 3.2) from their User's Manual[78] shows good agreement between a finite element analysis completed using ABAQUS with UMAT91 and values predicted by elastic beam theory and ultimate design theory. The finite element analysis was able to determine the applied load at which first cracking of the concrete occurred. It also predicted the ultimate capacity of the member between 21 and 22 psi with ultimate design theory predicting 20.1 psi. However, the beam was only singly reinforced so further preliminary investigation was conducted using UMAT91.

The beam reported on by Weidlinger and Hinman[20] was used for further preliminary analyses. Both end

restraint cases previously analyzed (fixed against rotation and simply supported) yielded good agreement between finite element analysis using ABAQUS linked with UMAT91 and ultimate design theory. When the ends were fixed against rotation, the finite element analysis determined an ultimate capacity of 52 psi which is within 4 percent of the value of 50 psi predicted by ultimate design theory. Failure was defined as the strain in the extreme fiber of the concrete exceeding 0.003. For the simply supported case, the finite element analysis determined an ultimate capacity of 26 psi which is within 4 percent of the value of 25 psi as predicted by ultimate design theory. Failure was determined by UMAT91 internally and was indicated by a warning message from UMAT91.

3.4.2 UMAT91 Concrete Model Validation

The doubly reinforced prestressed concrete beam tested by Hamilton[42] was used for final validation. In an effort to validate the concrete model UMAT91, output from a finite element analysis using ABAQUS and UMAT91 was compared with: (1) experimental results from Hamilton, (2) values predicted by elastic beam theory,

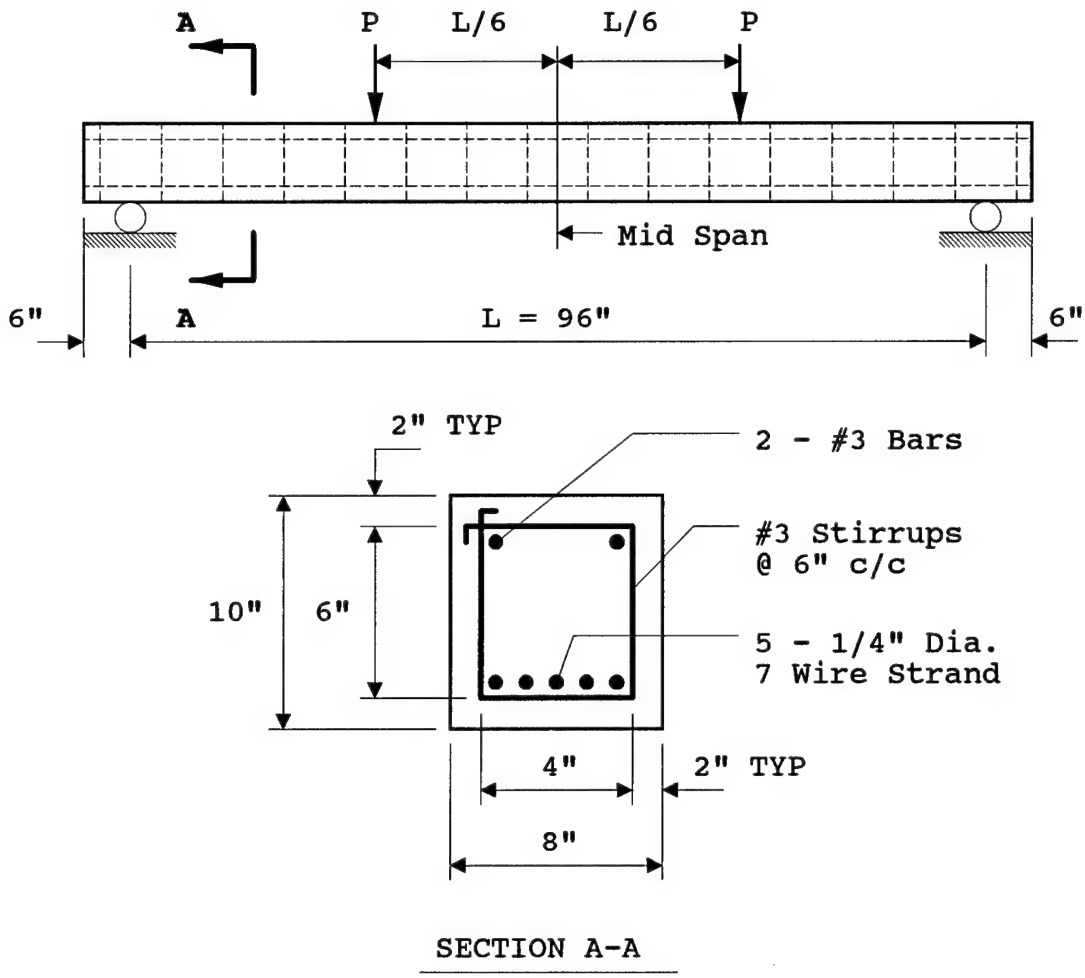

Figure 3.4 Hamilton Prestressed Concrete Beam

and (3) known material behavior. The details of the prestressed concrete beam tested by Hamilton[42] are shown in Figure 3.4. The beam was loaded statically at its third points in concentrated load 'P' increments of 1,000 lbs until failure. The Hamilton[42] beam shown in Figure 3.4 was modeled for the finite element analysis using

plane stress elements. Symmetry was applied with only half of the beam being modeled as shown in Figure 3.5. Half the length of the beam was modeled using nine elements (each 6 inches long) while the depth of the beam was modeled using four elements (each 2.5 inches deep) as shown in Figure 3.5 and Figure 3.6. This gives an element aspect ratio of 2.4 to 1.0 which should yield good results. Four elements through the depth of the beam also provide eight integration points through the depth which should be adequate to account for the variation in nonlinear concrete properties.

Material properties used in the finite element analysis are given in Table 3.1 while a complete ABAQUS input file for the above example is provided in

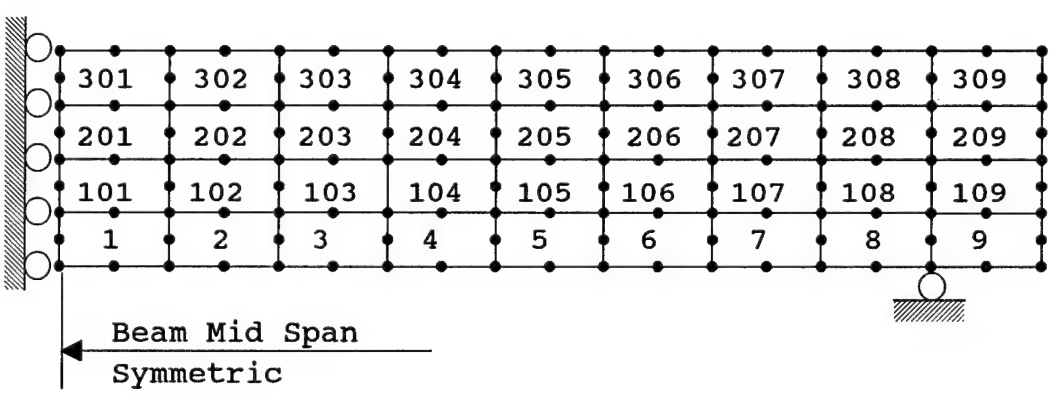

Figure 3.5 Finite Element Mesh

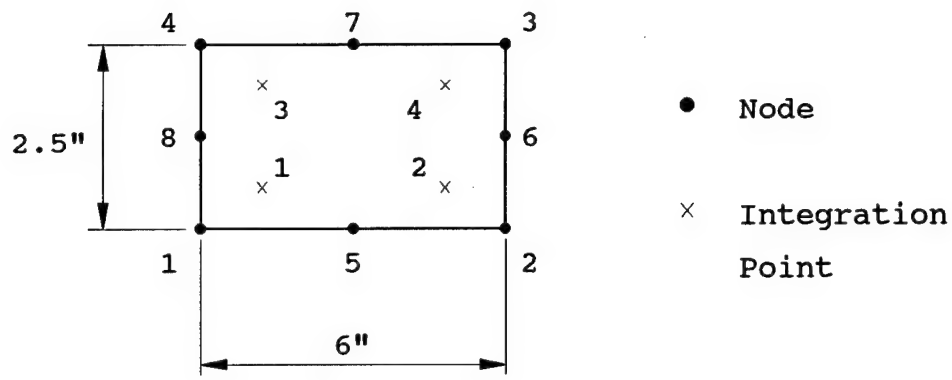

Figure 3.6 Finite Element

Appendix I. The stress-strain relationship for the concrete is generated internally within UMAT91. Figure 3.7 is a plot of the stresses and corresponding strains generated at integration point 3 of element 301 of this example during the finite element analysis. It can be seen from Figure 3.7 that UMAT91 generates a typical form for the stress-strain curve of concrete.

Table 3.1 Material Properties for FE Analysis

Concrete	Strand	Rebar
E_c = 4,370 ksi	E_{ps} = 28,000 ksi	E_s = 29,000 ksi
ν = 0.15	ν = 0.3	ν = 0.3
f'_c = 5.88 ksi	f_u = 270 ksi	f_y = 40 ksi
$\varepsilon_{cr} = 1.0 \times 10^{-4}$	f_{se} = 118.5 ksi	

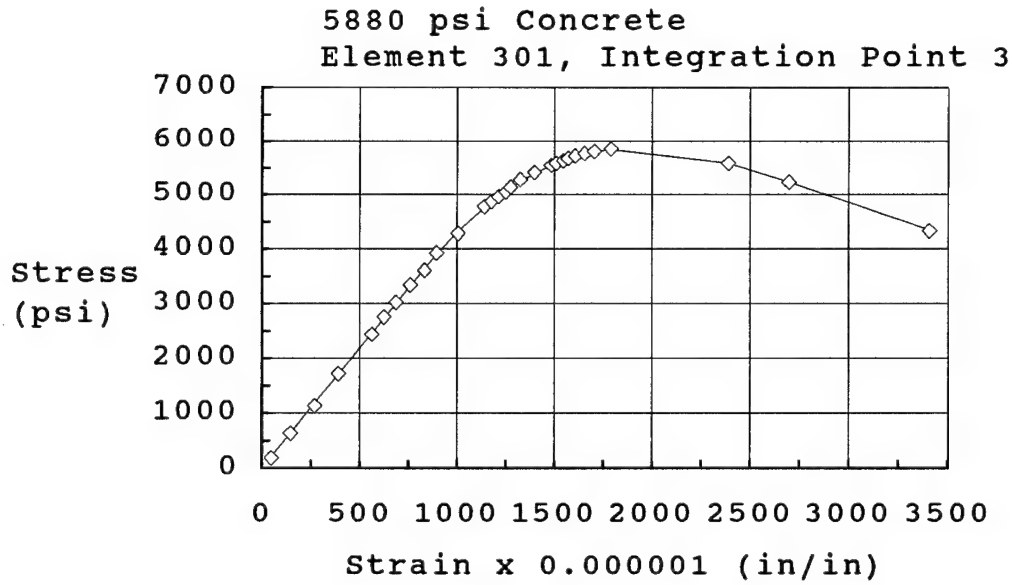

Figure 3.7 ANATECH Concrete Stress-Strain Curve

The constitutive material model for the Grade 40 steel was idealized as elastic, perfectly plastic as shown in Figure 3.8. The constitutive material model for the prestressing steel was idealized as piecewise linear as shown in Figure 3.9 which duplicates the typical stress-strain curve given by PCI.[46] Loading during the finite element analysis was broken into three phases: (1) prestress and dead weight of the member, (2) concentrated load 'P' from zero to 10,000 lbs in 1,000 lb increments, and (3) concentrated load 'P' from 10,000 lbs to 12,000 lbs in 100 lb increments.

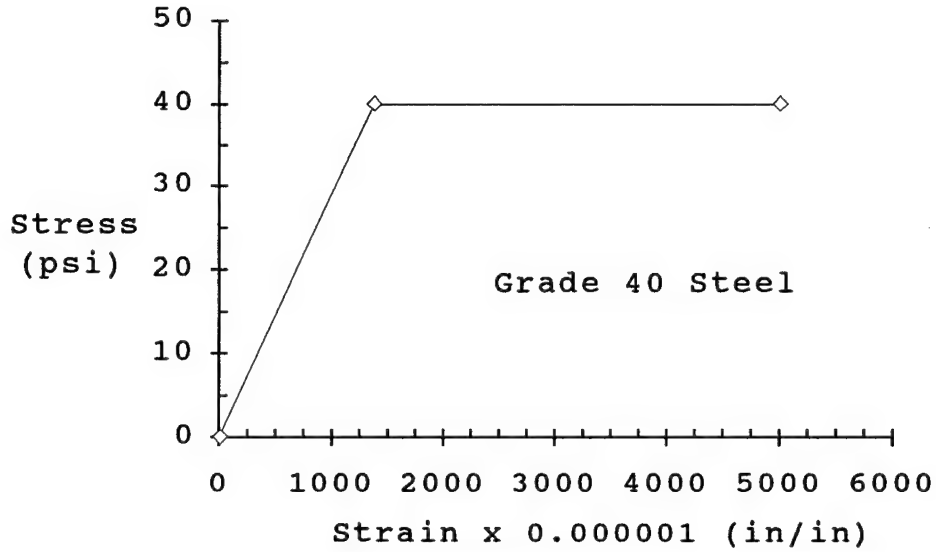

Figure 3.8 Stress-Strain Response for #3 Bar

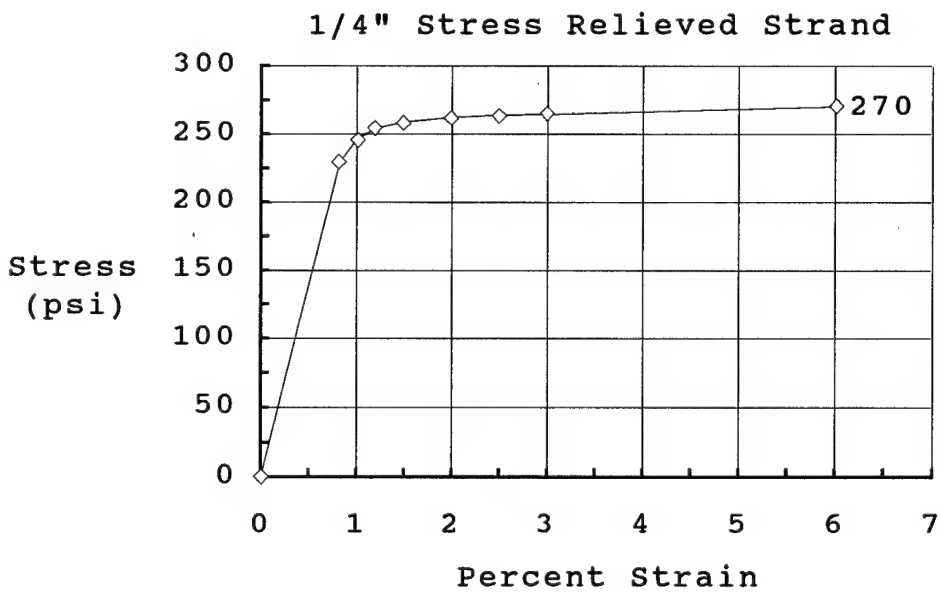

Figure 3.9 Stress-Strain Response for Strand

In the first load phase, an effective prestress of 118,500 psi in the prestressed steel was applied to the member via the five 7-wire strands using the "*INITIAL CONDITIONS" and "*PRESTRESS HOLD" options in ABAQUS.[5] The effective prestress was used along with the 28 day strength and modulus of elasticity of the concrete to account for losses from the initial prestress in the strands of 141,600 psi as reported by Hamilton.[42] The dead weight of the concrete was also applied during the first phase as a global body force. During the second and third phases of loading, the concentrated loads were applied to the member in addition to the loads in phase one. The smaller load increment of 100 lbs was used during the highly nonlinear third phase.

A comparison of the mid span camber and the distribution of stresses through the depth of the section (as determined by the finite element analysis and elastic beam theory) was performed at the end of the first loading phase. Mid span cambers compare very favorably with values of 0.0223 inches and 0.0226 inches of upward deflection from the finite element analysis and elastic beam theory, respectively. Stresses using elastic beam theory were calculated at the level of the integration

points through the depth of the section at mid span and at the support. These stresses are compared to finite element output at the corresponding integration points in Table 3.2. Overall results are good except at element 308, integration point 2, where the percent error is 73.6. The high percentage of error is due in part to the small magnitude of the stress near the neutral axis. Also, some numerical problems could be caused by the two #3 reinforcing bars near that level.

The mid span deflections from the finite element analysis and the experimental data reported by Hamilton[42] are shown in Figure 3.10. The finite element analysis results are stiffer than the experimental data in the elastic range. After predicted concrete cracking at 11 kips, the finite element analysis follows very closely the experimental data points through ultimate. Ultimate loads shown in Figure 3.10 are 23.2 kips and 22.4 kips as determined by the Hamilton[42] test and finite element analysis, respectively.

A comparison was also made of extreme fiber strain in the concrete as determined by finite element analysis and experimental work reported by Hamilton.[42] Results

Table 3.2 Cross Sectional Stresses

Element	I.P.	Mid Span		
		Stress (psi)		
		FEM	Theory	% Error
301	3	108.6	107.2	1.3
	1	-11.4	-12.7	10.5
201	3	-99.3	-100.3	1.0
	1	-219.4	-220.2	0.4
101	3	-307.4	-307.8	0.1
	1	-427.6	-427.7	0.0
1	3	-515.4	-515.3	0.0
	1	-635.4	-635.2	0.0
		Support		
		Stress (psi)		
		FEM	Theory	% Error
308	4	151.8	160.8	5.6
	2	6.3	23.7	73.6
208	4	-79.9	-76.7	4.2
	2	-183.9	-213.8	14.0
108	4	-298.9	-314.2	4.9
	2	-456.7	-451.3	1.2
8	4	-546.9	-551.7	0.9
	2	-701.9	-688.8	1.9

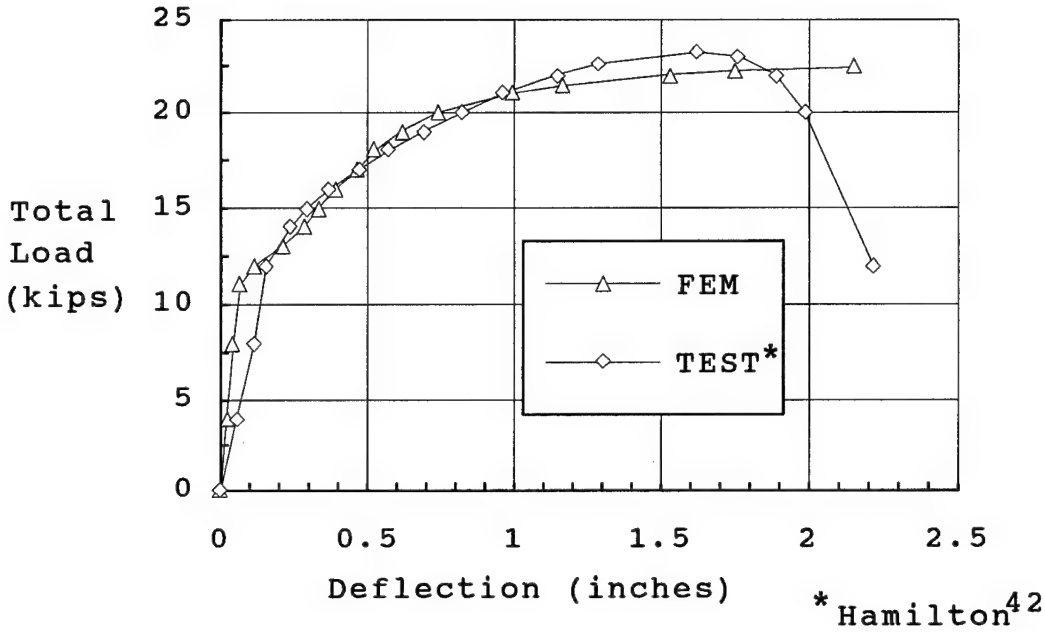

Figure 3.10 Hamilton P/C Beam: Load-Deflection

are shown in Figure 3.11 with good correlation throughout the entire load range.

The effect of the tensile cracking strain of the concrete, ε_{cr}, as an input parameter of UMAT91 was investigated. Three values of ε_{cr} were used, and the associated load-deflection curves are shown in Figure 3.12. The values of ε_{cr} were selected as: (1) 0.00013 from the ACI[47] formula

$$\varepsilon_{cr} = [7.5 \times (f'_c)^{1/2}] / E_c \qquad (3.4)$$

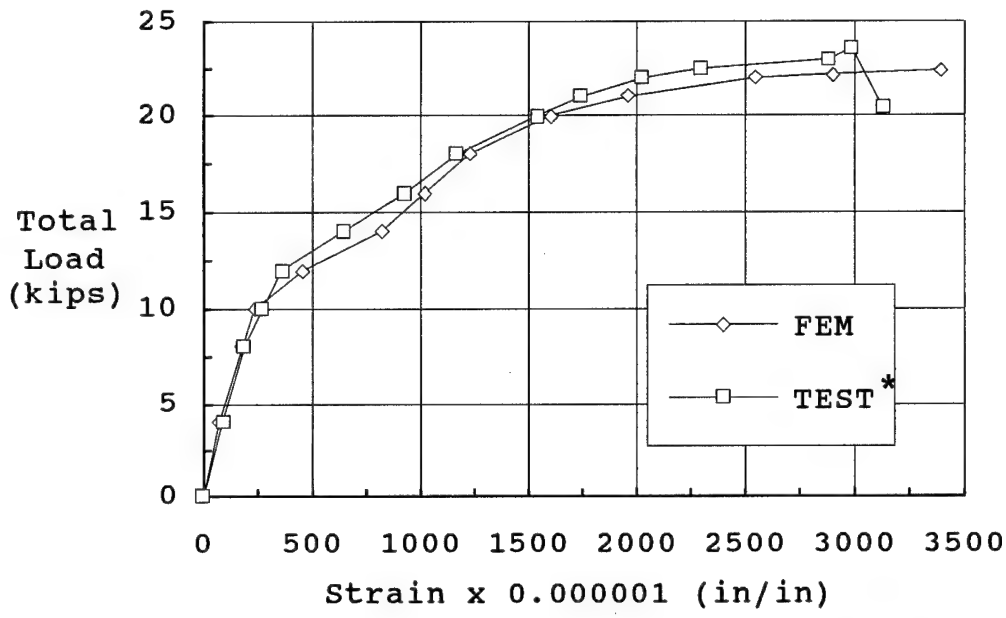

*Hamilton[42]

Figure 3.11 Extreme Fiber Concrete Strain

(2) 0.0001, the UMAT91 default value, and (3) 0.000075 from discussions with ANATECH personnel who indicated that input values for ε_{cr} as low as 0.00005 had yielded closer correlation to reported results in some instances. As illustrated in Figure 3.12, the input cracking strain of the concrete does have some impact on the load-deflection response generated by the ANATECH concrete model. The default value of 0.0001 for the cracking

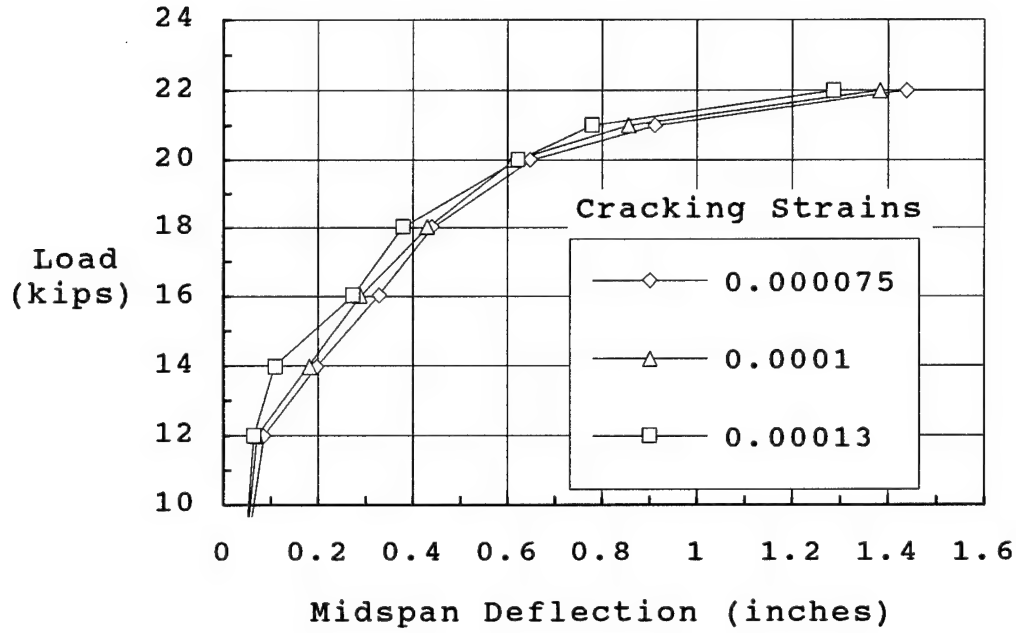

Figure 3.12 Various Concrete Cracking Strains

strain gives the best correlation with the experimental load-deflection curve reported by Hamilton[42] and should yield the best overall results since it was selected as the default value by ANATECH. Therefore, the default value of 0.0001 was selected for use in this study.

It has been shown in this section that finite element analysis using ABAQUS with UMAT91 provides good response predictions for concrete members subjected to static loads through the full range of loads. It has also been shown that the concrete material properties

generated within UMAT91 closely follow the expected values. Therefore, ABAQUS and UMAT91 will be used to perform the finite element analysis of reinforced and prestressed concrete members in this study.

Chapter 4

Dynamic Analysis

4.1 Introduction

It was initially intended to conduct all nonlinear dynamic analyses in this study using the finite element program ABAQUS.[5,6] However, the concrete model, UMAT91, selected for use in this study required a special option to conduct dynamic analyses which was not standard in the version of ABAQUS (version 4.9) currently available on the Cray computer at The University of Texas at Austin.

It was then decided to write a single-degree-of-freedom (SDOF) program to perform the dynamic analyses. Nonlinear effects from the concrete would be accounted for by using results from static nonlinear finite element analyses as member stiffness input into the SDOF dynamic analyses. The high strain rate effects[4,13] during the SDOF dynamic analyses would also be accounted for by increasing the ultimate strength of the concrete and the yield strength of the conventional reinforcing steel during the static finite element analyses. The SDOF program was written and provided near identical results when compared to those of a linear dynamic finite element

analysis completed using ABAQUS. It also provided good results when compared to a nonlinear dynamic finite element analysis reported by Weidlinger and Hinman.[20] The formulation and validation of the SDOF model are presented in Section 4.2.

Once this work was completed, a special version of ABAQUS was obtained which allowed the nonlinear dynamic analysis of concrete members using ABAQUS linked with UMAT91. Analyses using ABAQUS with UMAT91 and analyses using the SDOF program were compared showing close correlation. The two nonlinear dynamic analysis procedures are compared and discussed in Section 4.3.

4.2 Single-Degree-of-Freedom

4.2.1 Theory

The beam shown in Figure 4.1.a with mass m(x), structural damping c(x), structural stiffness k(x), and dynamic load w(x,t) can be modeled as discrete segments shown in Figure 4.1.b. The structural damping c(x) will have little effect on the maximum response of the beams with the loading function of interest in this study and will be ignored. However, the damping term c will be retained and lumped at the center of mass of each segment to approximate soil-structure interaction (SSI) effects

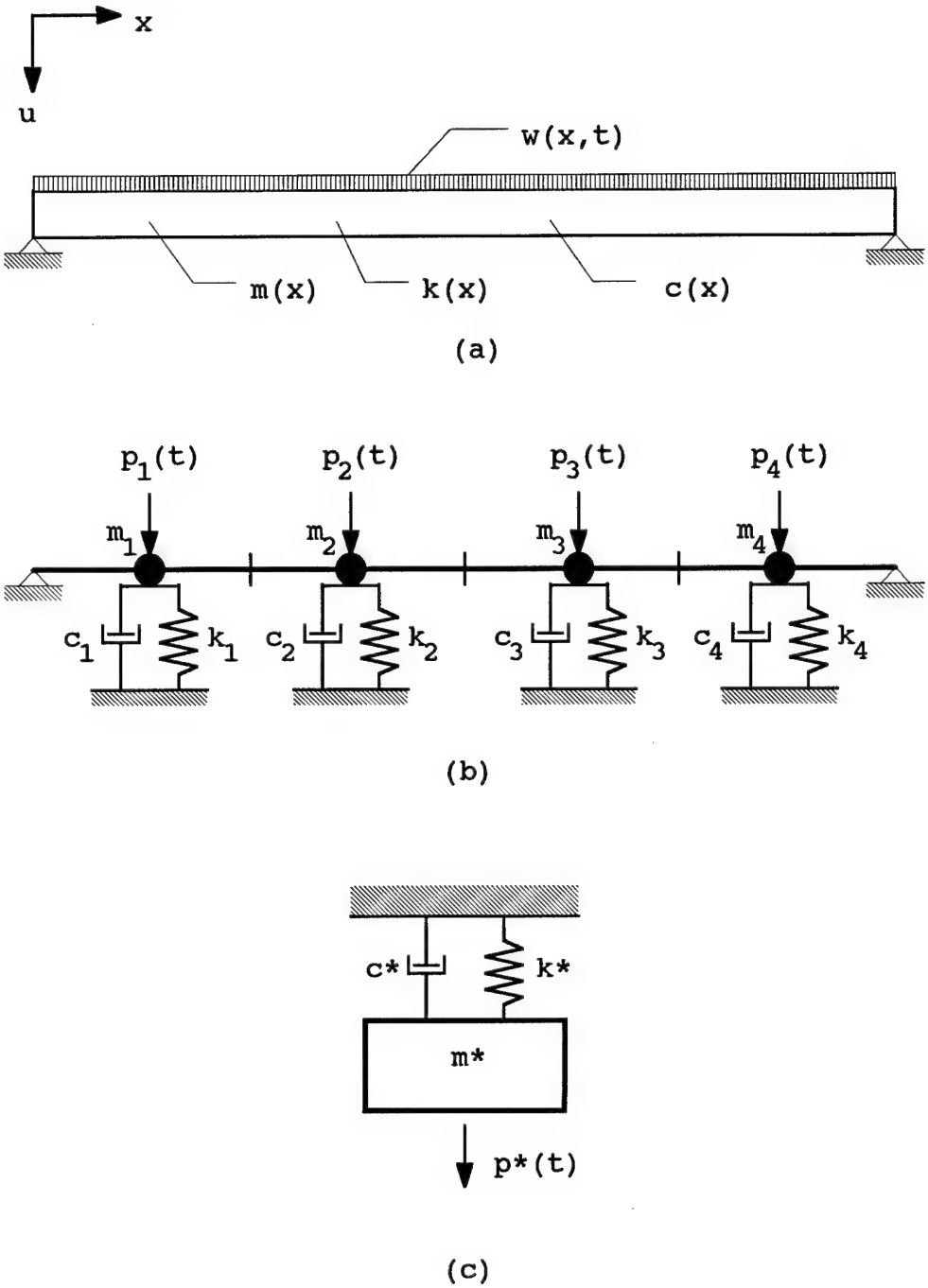

Figure 4.1 Idealized Beams

as discussed in Chapter 2. The dynamic equation of motion which must be satisfied at any time t can be written as

$$\mathbf{M}*\ddot{\mathbf{U}} + \mathbf{C}*\dot{\mathbf{U}} + \mathbf{K}*\mathbf{U} = \mathbf{P}(t) \tag{4.1}$$

where $\mathbf{M}$ = Lumped mass matrix (diagonal)

$\ddot{\mathbf{U}}$ = Acceleration vector

$\mathbf{C}$ = SSI damping matrix (diagonal)

$\dot{\mathbf{U}}$ = Velocity vector

$\mathbf{K}$ = Stiffness matrix

$\mathbf{U}$ = Displacement vector

$\mathbf{P}$ = Applied load vector

The $\mathbf{K}*\mathbf{U}$ term represents the resisting force vector, $\mathbf{F}(U)$, in the structure for some displaced shape $\mathbf{U}$. It is equal to the statically applied force required to cause the displaced shape $\mathbf{U}$ as shown in Figure 4.2. $\mathbf{F}(U)$ will be determined by a static nonlinear analysis using ABAQUS and UMAT91 with an assumed load distribution and will then be used as input into the dynamic analysis. This will account for the nonlinear stiffness of the concrete member during the dynamic analysis. Equation 4.1 can

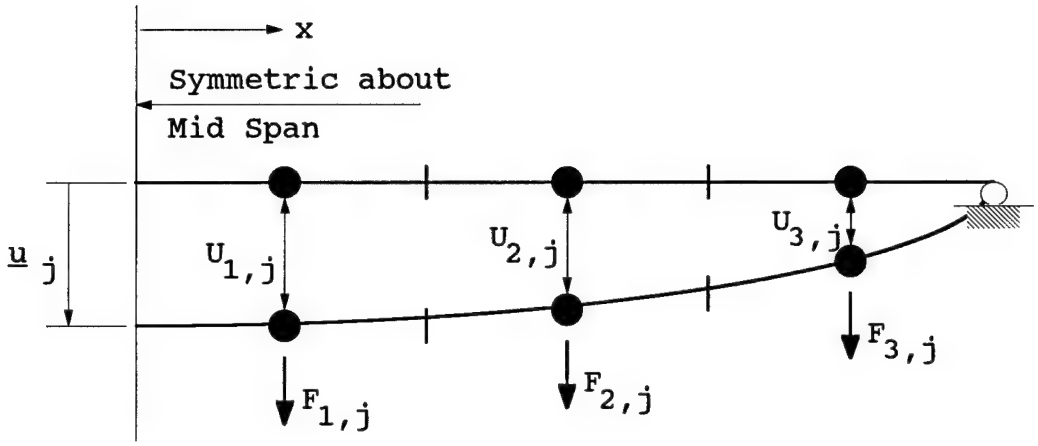

Figure 4.2 Static Shape and Load Vector

then be rewritten as

$$\mathbf{M}*\ddot{\mathbf{U}} + \mathbf{C}*\dot{\mathbf{U}} + \mathbf{F}(U) = \mathbf{P}(t) \qquad (4.2)$$

Figure 4.1.b, a finite multiple-degree-of-freedom (MDOF) system, can be further idealized as shown in Figure 4.1.c, a SDOF system, by selecting the deflection at mid span as the variable. The discretized mass, damping, stiffness, and applied load which are distributed across the span of the member can be reduced to a single effective mass, damping, stiffness, and applied load, respectively, which are applied at the mid span of the member where the dynamic response is desired.

A series of load vectors ($\mathbf{F}_j$) can be statically applied to the member during a nonlinear analysis using ABAQUS and UMAT91, and the corresponding displacement vectors or shape functions ($\mathbf{U}_j$) can be obtained

where $\mathbf{F}_j^T = \{F_{1,j}, F_{2,j}, \cdots, F_{nel,j}\}$

$\mathbf{U}_j^T = \{U_{1,j}, U_{2,j}, \cdots, U_{nel,j}\}$

j = Static load step

nel = Number of discrete elements

The shape function, $\mathbf{U}_n$, shown in Figure 4.3 and the corresponding structural resistance, $\mathbf{F}_n$, at any time step 'n' during the dynamic analysis can be approximated using linear interpolation as

$$\mathbf{U}_n = \mathbf{U}_j + \{[(u_n - \underline{u}_j)/\Delta\underline{u}_{j+1}] * \Delta\mathbf{U}_{j+1}\} \qquad (4.3)$$

$$\mathbf{F}_n = \mathbf{F}_j + \{[(u_n - \underline{u}_j)/\Delta\underline{u}_{j+1}] * \Delta\mathbf{F}_{j+1}\} \qquad (4.4)$$

where $\Delta\mathbf{U}_{j+1} = \mathbf{U}_{j+1} - \mathbf{U}_j$

$\Delta\underline{u}_{j+1} = \underline{u}_{j+1} - \underline{u}_j$

$\Delta\mathbf{F}_{j+1} = \mathbf{F}_{j+1} - \mathbf{F}_j$

as long as $\underline{u}_j \leq u_n \leq \underline{u}_{j+1}$

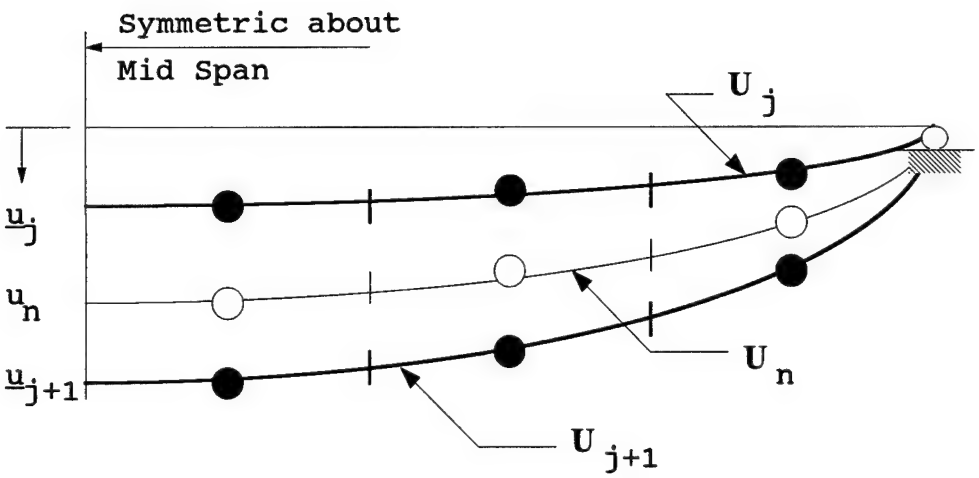

Figure 4.3 Approximate Shape Function

Taking the first and second derivative of Equation 4.3 with respect to time gives, respectively,

$$\dot{\mathbf{U}}_n = \dot{u}_n * (\Delta \mathbf{U}_{j+1}/\Delta \underline{u}_{j+1}) \tag{4.5}$$

$$\ddot{\mathbf{U}}_n = \ddot{u}_n * (\Delta \mathbf{U}_{j+1}/\Delta \underline{u}_{j+1}) \tag{4.6}$$

Substituting Equations 4.4, 4.5, and 4.6 into Equation 4.2 gives at any time step 'n'

$$\begin{aligned} &\mathbf{M}(\Delta \mathbf{U}_{j+1}/\Delta \underline{u}_{j+1})\ddot{u}_n + \mathbf{C}(\Delta \mathbf{U}_{j+1}/\Delta \underline{u}_{j+1})\dot{u}_n + \\ &\quad + (\Delta \mathbf{F}_{j+1}/\Delta \underline{u}_{j+1})u_n = \\ &\quad = \mathbf{P}_n(t) - \mathbf{F}_j + \Delta \mathbf{F}_{j+1}(\underline{u}_j/\Delta \underline{u}_{j+1}) \end{aligned} \tag{4.7}$$

Premultiplying Equation 4.7 by $\Delta \mathbf{U}^T_{j+1}$, reduces it to a scalar form corresponding to a SDOF system and yields

$$
\begin{aligned}
&[(\Delta \mathbf{U}^T_{j+1}\mathbf{M}\Delta \mathbf{U}_{j+1})/\Delta \underline{u}_{j+1}]\ddot{u}_n + \\
&\quad + [(\Delta \mathbf{U}^T_{j+1}\mathbf{C}\Delta \mathbf{U}_{j+1})/\Delta \underline{u}_{j+1}]\dot{u}_n + \\
&\quad + [(\Delta \mathbf{U}^T_{j+1}\Delta \mathbf{F}_{j+1})/\Delta \underline{u}_{j+1}]u_n = \\
&\quad = \Delta \mathbf{U}^T_{j+1}\mathbf{P}_n(t) - \Delta \mathbf{U}^T_{j+1}\mathbf{F}_j + \\
&\quad + [(\Delta \mathbf{U}^T_{j+1}\Delta \mathbf{F}_{j+1})(\underline{u}_j/\Delta \underline{u}_{j+1})]
\end{aligned}
\tag{4.8}
$$

Defining

$$m^*_n = (\Delta \mathbf{U}^T_{j+1}\mathbf{M}\Delta \mathbf{U}_{j+1})/\Delta \underline{u}_{j+1} \tag{4.9}$$

$$c^*_n = (\Delta \mathbf{U}^T_{j+1}\mathbf{C}\Delta \mathbf{U}_{j+1})/\Delta \underline{u}_{j+1} \tag{4.10}$$

$$f^*_n = (\Delta \mathbf{U}^T_{j+1}\Delta \mathbf{F}_{j+1})/\Delta \underline{u}_{j+1} \tag{4.11}$$

$$p^*_n = \Delta \mathbf{U}^T_{j+1}\mathbf{P}_n(t) \tag{4.12}$$

$$l^*_n = \Delta \mathbf{U}^T_{j+1}\mathbf{F}_j \tag{4.13}$$

and substituting into Equation 4.8 gives the SDOF dynamic equation of motion

$$m^*_n\ddot{u}_n + c^*_n\dot{u}_n + f^*_n u_n = p^*_n - l^*_n + f^*_n\underline{u}_j \tag{4.14}$$

A central difference formulation was chosen to solve the dynamic equation of motion, Equation 4.14. The quadratic central difference equations

$$\ddot{u}_n = (u_{n+1} - 2u_n + u_{n-1})/\Delta t^2 \tag{4.15}$$

$$\dot{u}_n = (u_{n+1} - u_{n-1})/2\Delta t \tag{4.16}$$

substituted into Equation 4.14 give

$$\begin{aligned} m^*_n[(u_{n+1} - 2u_n + u_{n-1})/\Delta t^2] &+ \\ + c^*_n[(u_{n+1} - u_{n-1})/2\Delta t] &+ \\ + f^*_n u_n = p^*_n - l^*_n + f^*_n \underline{u}_j & \end{aligned} \tag{4.17}$$

Rearranging Equation 4.17 and solving for u_{n+1} gives

$$\begin{aligned} u_{n+1} = [(m^*_n/\Delta t^2) + (c^*_n/2\Delta t)]^{-1} &* \\ * \{(p^*_n - l^*_n + f^*_n \underline{u}_j) &+ \\ + [(2m^*_n/\Delta t^2) - (f^*_n)]u_n &+ \\ + [(c^*_n/2\Delta t) - (m^*_n/\Delta t^2)]u_{n-1}\} & \end{aligned} \tag{4.18}$$

Knowing all the values on the right hand side of Equation 4.18, including u_n and u_{n-1}, one can project forward in time by Δt and find the mid span displacement u_{n+1} at time t_{n+1} (equal to t_n plus Δt). The process is then repeated determining the mid span displacement as it varies with time, u(t). The FORTRAN source code of the SDOF program, BLASTSDF.FOR, which implements this algorithm is provided in Appendix II.

4.2.2 Program Characteristics

BLASTSDF determines the mid span deflection, $u_n(t)$, of a member subjected to a blast load as it varies with time. The origin is set at the time when the blast load first reaches the member at mid span. The subroutine DYNLOAD in BLASTSDF adjusts the dynamic time to the explosive time when determining the magnitude of the ground shock at the structure and accounts for the time and spatial differences of the loading along the top surface of the structure. The mid span deflection, u_n, that BLASTSDF initially determines is the dynamic deflection and does not include the static deflection from the dead load of the soil and concrete. However, the static dead load does affect the values of the vectors $\mathbf{U}_j$ and $\mathbf{F}_j$ used in the dynamic analysis, and this effect is taken into account. The total mid span deflection is then determined by simply adding the static and dynamic deflections.

Throughout the development and source code of BLASTSDF, three indices or subscripts are used consistently; their meanings are

$j \rightarrow$ static values (j^{th} load increment)

$i \rightarrow$ node along the span of the member

$n \rightarrow$ dynamic time step increment

BLASTSDF was written taking into account symmetry and follows the layout shown in Figure 4.2. The mass, SSI damping, structural resistance, applied load, and shape functions are at the center of the elements as shown in Figure 4.1.b and Figure 4.2.

The mid span deflection is determined as a function of time using the algorithm developed above, Equation 4.18, for all time steps where 'n' is greater than or equal to 2. To evaluate the first time step, 'n' equal 1, we must apply the initial conditions at time equal zero. In general, we can write the dynamic equation of motion as

$$m\ddot{u} + c\dot{u} + ku = p(t) \tag{4.19}$$

Initial conditions at t_0, t=0, are

$$u_0 = u(0) = 0 \tag{4.20}$$

$$\dot{u}_0 = \dot{u}(0) = 0 \tag{4.21}$$

$$p_0 = p(0) = 0 \tag{4.22}$$

Applying Equation 4.21 to Equation 4.16 gives

$$\dot{u}_0 = (u_1 - u_{-1})/2\Delta t = 0$$

Therefore, $u_1 = u_{-1}$ (4.23)

Applying Equation 4.20 and 4.23 to Equation 4.15 gives

$$\ddot{u}_0 = (u_1 - 2u_0 + u_{-1})/\Delta t^2 = 2u_1/\Delta t^2 \qquad (4.24)$$

Substituting initial conditions u_0, $\dot{u}_0$, $\ddot{u}_0$, and p_0 into Equation 4.19 gives

$$m(2u_1/\Delta t^2) = p_0 \qquad \rightarrow \qquad u_1 = p_0 * \Delta t^2/2m$$

With an initial value of p_0 equal zero, the displacement u at time t equal Δt will also be zero. This introduces a small error in the first time step but has little impact on subsequent values of mid span displacements due to the small time steps used.

The procedure for using ABAQUS and BLASTSDF follows. First, an input file (*filename*.INP) for ABAQUS to generate the static nonlinear shape functions for an assumed load distribution is generated. Second, ABAQUS is used to complete a static nonlinear analysis and generate a data output file (*filename*.DAT). Third, *filename*.DAT is modified into the format shown in Appendix III to create a static input file (*filename*.SIN)

for BLASTSDF. Fourth, a dynamic input file (*filename*.DIN) for BLASTSDF must be created in the form shown in Appendix IV. Fifth, BLASTSDF.EXE is executed with the names of the two input files and the name of the dynamic output file (*filename*.OUT) provided interactively during execution.

The initial static load used in ABAQUS to generate the nonlinear shape and resistance functions, $\mathbf{U}_j$ and $\mathbf{F}_j$, respectively, was the commonly used cubic distribution

$$\sigma_N = \alpha * \sigma_o * (D/R)^3 \tag{4.25}$$

where

σ_N = Pressure normal to the member

α = Proportionality constant ($0.0 \leq \alpha \leq 1.0$)

σ_o = Peak pressure at mid span of member

D = Normal distance from charge to member

R = Radial distance from charge to load point

However, the dynamic output from BLASTSDF showed that the actual blast load distribution approached a uniform distribution after 11 milliseconds when the SSI effects were included. A second option was then incorporated into BLASTSDF to allow the nonlinear shape and resistance

functions, $\mathbf{U}_j$ and $\mathbf{F}_j$, respectively, to be developed from a uniform load distribution. Results from the two assumed static load distributions are compared in Section 4.2.3.

4.2.3 Validation

The dynamic response of a buried reinforced concrete one-way slab reported on by Weidlinger and Hinman[20] was used to validate BLASTSDF. The geometry and material properties are provided in Figure 4.4. The models for ABAQUS and BLASTSDF are shown in Figure 4.5. The ABAQUS model consists of a uniform 14 by 8 mesh of 8-noded plane strain elements with an element aspect ratio of 2.7 to 1.0. An additional 36 inches of a very stiff material, 'Stiffmat,' was used to model the end conditions. Initially, the ends were completely fixed which caused the development of tensile membrane action making the member too stiff. The member was then modeled as shown in Figure 4.5.a to fix the ends against rotation while allowing lateral translation of the ends, thereby eliminating the development of the tensile membrane action. A nonlinear static finite element analysis was also run using a finer mesh of 28 by 10. The finer mesh,

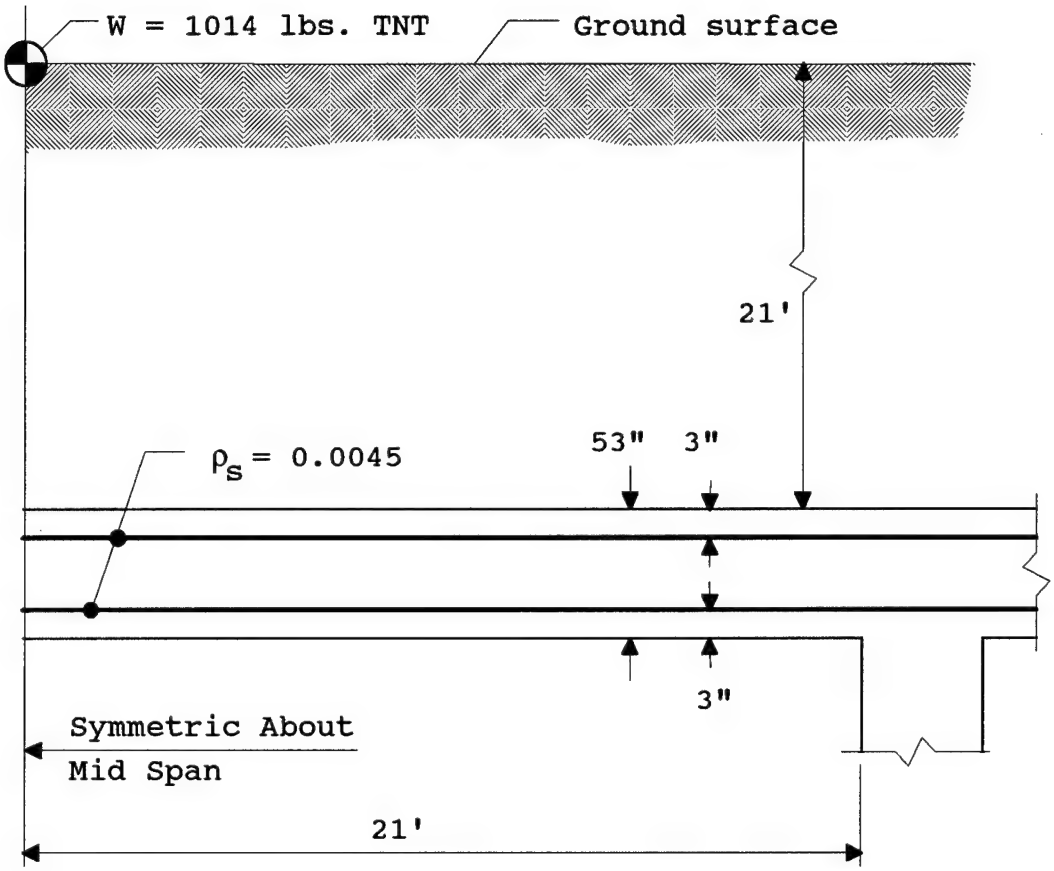

f'_c = 6,125 psi f_y = 72,000 psi

<u>Free Field Soil Parameters:</u>

f = 0.4 c = 1000 fps

ρ c = 22 psi/fps n = 2.75

Figure 4.4 Weidlinger One-way R/C Slab

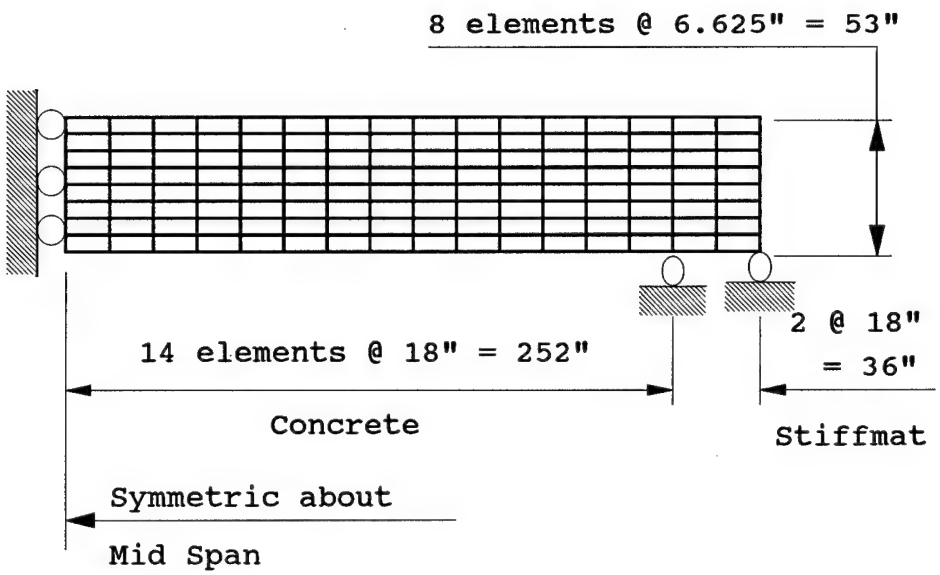

(a) ABAQUS

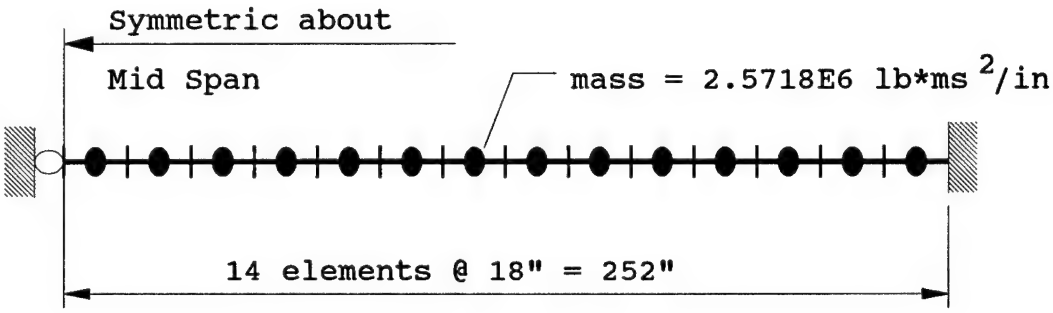

(b) BLASTSDF

Figure 4.5 ABAQUS and BLASTSDF Slab Models

requiring 2.5 times as much CPU time on the Cray computer, provided almost identical results to those of the coarser mesh. The concrete slab was also modeled using 14 uniform elements for the SDOF dynamic analysis using BLASTSDF as shown in Figure 4.5.b.

A linear dynamic analysis using BLASTSDF with static input from ABAQUS was conducted and the results compared to those of a linear dynamic analysis using ABAQUS alone. The deflection-time curves are almost identical as shown in Figure 4.6. This supports the validity of the theory developed and the FORTRAN code used in BLASTSDF.

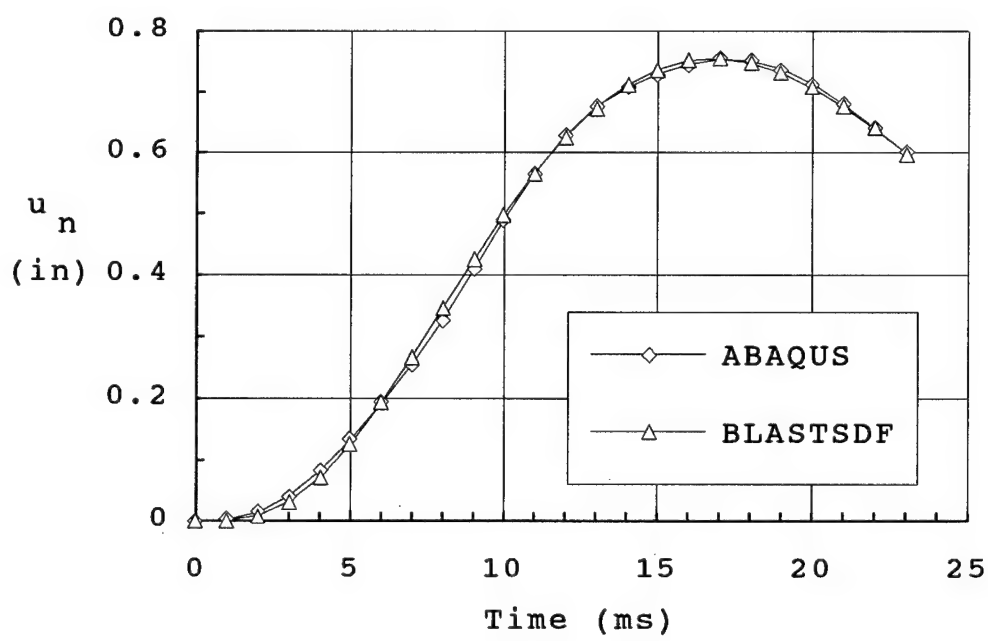

Figure 4.6 Linear Dynamic Analysis

A dynamic nonlinear analysis of the one-way concrete slab was then performed using BLASTSDF with the static nonlinear shape and stiffness functions generated by a cubic load distribution using ABAQUS. The results of this analysis, shown in Figure 4.7, are compared to the results of a finite element analysis reported by Weidlinger and Hinman.[20] Weidlinger and Hinman[20] reported that the finite element procedure they used had "been successfully used in the prediction of displacement and strain response of various tests and experimental investigations." Considering the uncertainties and variations in the details of the Weidlinger and Hinman model which include forcing function, soil overburden, material models, and end restraint, the agreement between the results of the two analyses seems satisfactory. This appears to further validate the present approach.

BLASTSDF was modified following the initial dynamic analysis above when it was observed that the blast load distribution approached a uniform distribution after 11 milliseconds when SSI effects were considered. The dynamic nonlinear response of the one-way slab was then obtained using BLASTSDF and the two static load distributions, cubic and uniform. The near identical

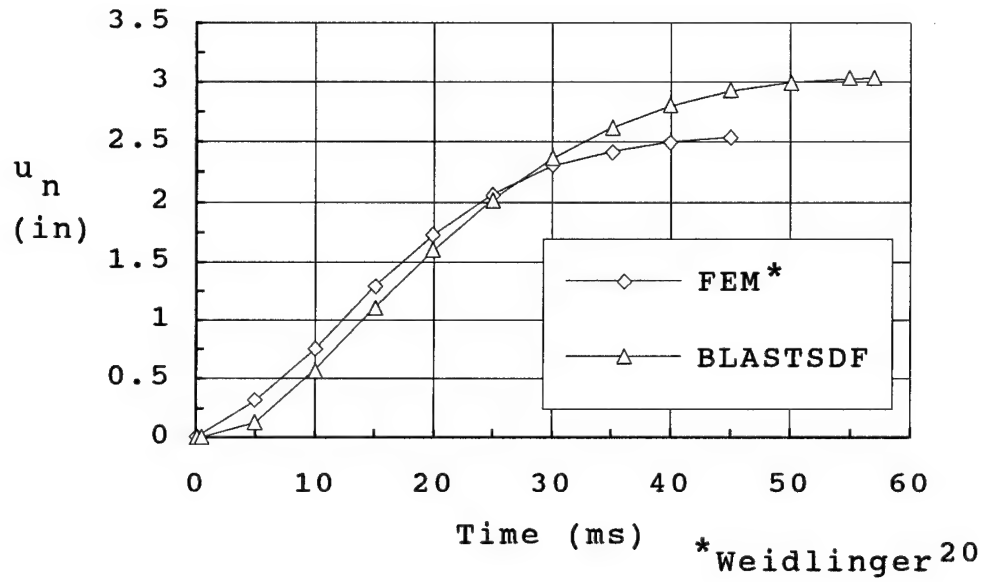

Figure 4.7 Dynamic Nonlinear Analysis

results shown in Figure 4.8 indicate no real difference between the two static load distributions when considering the dynamic response. However, one should note that these load distributions will affect the deflected shapes and the distribution of the internal forces along the member. The uniform distribution does prove favorable for load step control during the nonlinear static analysis and for modification of the ABAQUS output file to create the BLASTSDF static input file. Therefore, the uniform static load distribution was selected for use during the remainder of this study.

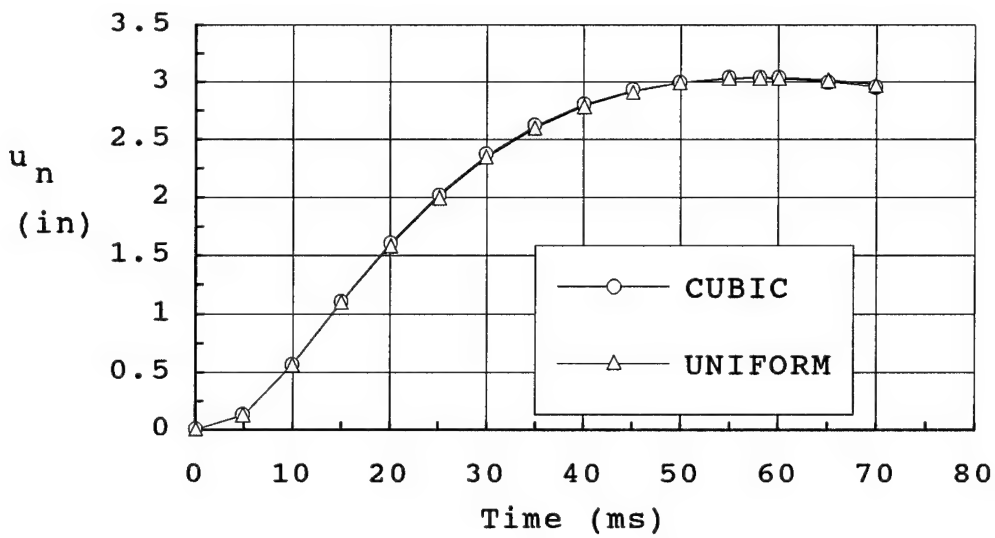

Figure 4.8 Load Distribution Effects

The explicit central difference method used in solving the dynamic equation of motion is conditionally stable. However, the small time steps required to simulate the blast load removes any problems with stability. Dynamic analyses were performed using time steps of 0.1 ms, 0.5 ms, 1.0 ms, 2.0 ms, and 4.0 ms. Nearly identical deflection-time curves were obtained after 12 ms for these time steps; even for the largest time step of 4.0 ms which introduces some error in the representation of the forcing function. The maximum deflection occurred well after 12 ms in each analysis. The near identical results of these analyses indicates no

real need for the smaller time steps. However, a time step of 1.0 ms will be used in BLASTSDF to better reproduce the forcing function by allowing two or three load steps to be applied during the rise time of the ground shock.

4.3 Dynamic Nonlinear Finite Element

A special version of ABAQUS was later obtained that allowed nonlinear dynamic finite element analyses to be completed using UMAT91. A dynamic nonlinear finite element analysis of the Weidlinger[20] slab (WS53-2.7) was completed using ABAQUS coupled with UMAT91. The one-way slab was modeled as described in Section 4.2.3, except fourteen vertical dashpots were added along the top of the slab to approximate SSI effects. The results of this analysis and an analysis using BLASTSDF are shown in Figure 4.9 with nearly identical results being obtained. The maximum response as predicted by the two methods differed by less than 0.5 percent while the time of maximum response differed by 5 ms.

Dynamic nonlinear analyses using BLASTSDF and using ABAQUS were also conducted on member PC53-6. Details of member PC53-6 are provide in Section 6.2. The analyses used soil and blast load parameters as shown in

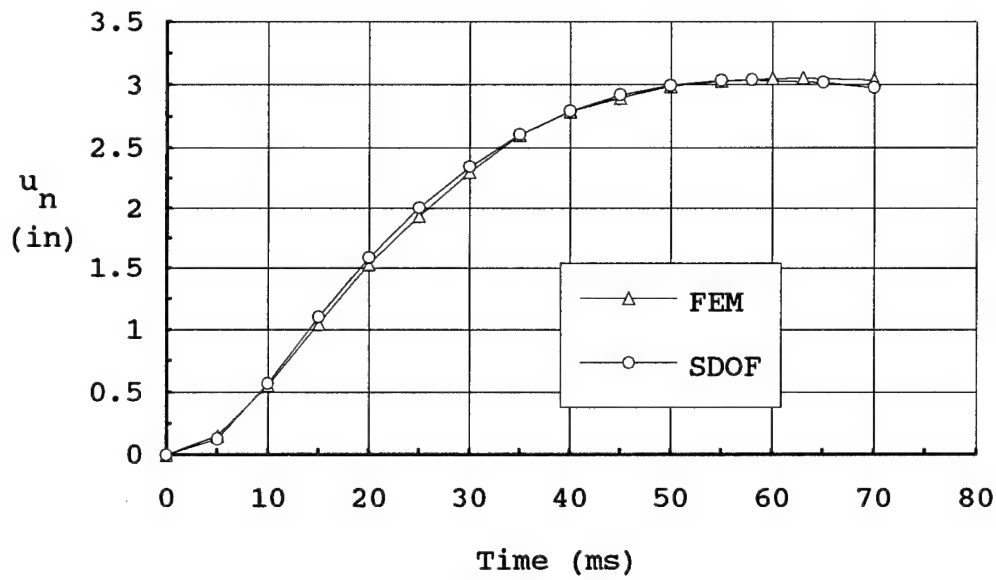

Figure 4.9 Dynamic Nonlinear Analysis: WS53-2.7

Figure 4.4 and used the soil restraint parameters of Case VI as detailed in Section 5.2. Again, vertical dashpots (21) were used along the top of the member to approximate SSI effects. The ABAQUS input file used during the dynamic nonlinear finite element analysis of member PC53-6 is provided in Appendix V.

The dynamic response of member PC53-6 from the two analyses is shown in Figure 4.10 with very close correlation between the two methods. Maximum response as predicted by the two methods differed by 3 percent while the time of maximum response differed by 5 ms. The deflected shape of the member determined by the two

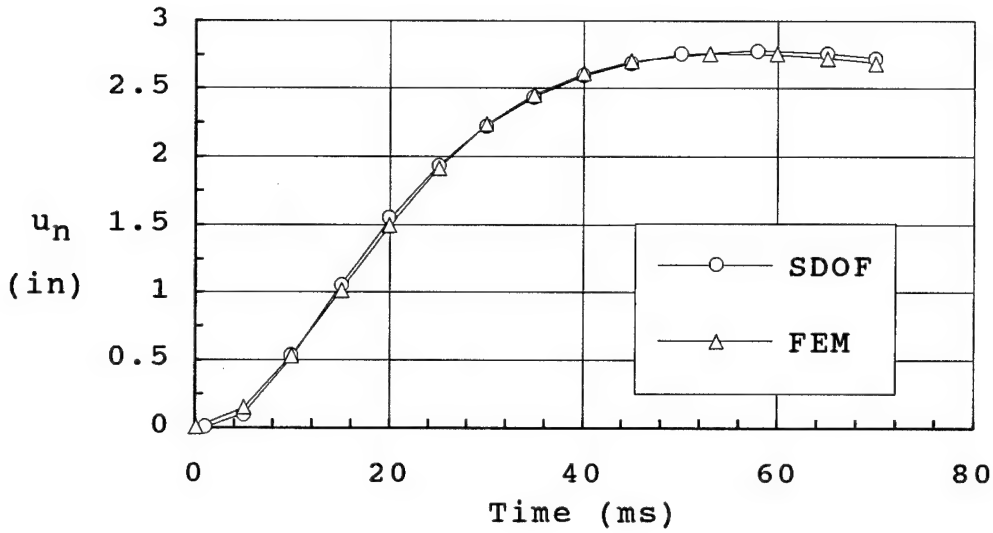

Figure 4.10 Dynamic Nonlinear Analysis: PC53-6

methods for a mid span deflection near the maximum value is shown in Figure 4.11. Close correlation is again seen, further confirming the validity of the SDOF model and assumed uniform static load distribution.

First cracking of the concrete in member PC53-6 occurred at mid span deflections of 0.1057 and 0.1453 inches during the dynamic and static analyses, respectively, using ABAQUS linked with UMAT91. For any given mid span deflection once cracking had occurred, the number of integration points cracked as predicted during the dynamic finite element analysis was approximately twice the number predicted during the static finite

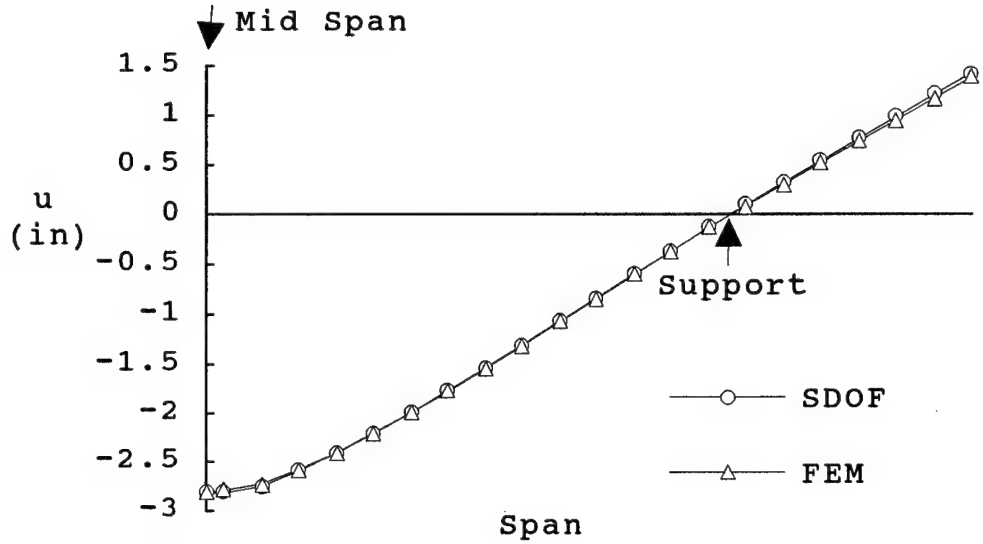

Figure 4.11 Deflected Shape: PC53-6

element analysis. However, this increase in cracking had no apparent influence on the dynamic response of the member as shown in Figure 4.10.

Good correlation between the two dynamic nonlinear analysis methods (SDOF and finite element) has been shown for the overall response of the two members discussed above. However, the computer time required to complete the dynamic nonlinear finite element analyses was at least twice the time required to complete the corresponding static nonlinear analyses which were used to develop input for BLASTSDF. Run time for BLASTSDF to complete the dynamic portion of the SDOF analyses was

insignificant. BLASTSDF would provide additional computer run time and cost savings for analyses using larger charge weights because smaller time steps would be required to control load increment size. For a particular member, BLASTSDF would also show a significant computer run time and cost savings advantage over the dynamic nonlinear finite element method when used to conduct parametric studies for various soil properties or weights of explosive where the member was kept constant.

Chapter 5

Soil Effects

5.1 Introduction

The effect of the soil on the magnitude and shape of a blast-created pressure pulse as it moves through the soil is well established as was discussed in Chapter 2. It can be predicted using the commonly accepted empirical equations developed by Drake and Little[17] and will not be discussed further here. The two aspects that were investigated in this phase of the study relate to the additional restraint of the soil on the cantilevered portion of the member. The effect of the additional strength and stiffness of the soil was investigated as was the effect of additional inertia forces caused by the mobilization of the soil above the cantilevered portion of the member during dynamic loading.

5.2 Soil Strength and Stiffness

Six cases using varying assumptions about the soil were investigated for possible use in this study to determine their effect on the static response. The six cases utilized three different geometric configurations

which are shown in Figure 5.1. Member PC53-8, which is detailed in Chapter 6, was used for this phase of the study.

A static nonlinear finite element analysis was completed for each case, and the corresponding load-deflection curve was plotted in Figure 5.2. A uniform load which is not shown in Figure 5.1 was superimposed on the top surface of each member in addition to the soil. The concrete weight was included in all six cases. The assumptions used in each case are discussed below and are summarized in Table 5.1.

Case I, shown in Figure 5.1.a, is a lower bound and considers only the dead weight of the soil with no additional resistance provided by the shear strength or stiffness of the soil. At a total applied pressure of 55.0 psi, the mid span and cantilevered tip deflections were predicted to be 5.3 inches downward and 3.5 inches upward, respectively. An upward movement of 3.5 inches by the cantilevered tip would cause the soil to develop significant forces and provide additional restraint to the end of the member.

Case II, shown in Figure 5.1.a, is an upper bound which was run to bracket the true response. Case II is identical to Case I except the cantilever tip, point 'A',

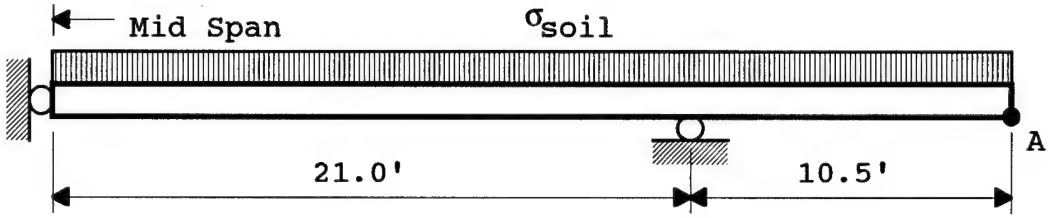

(a) Case I and Case II

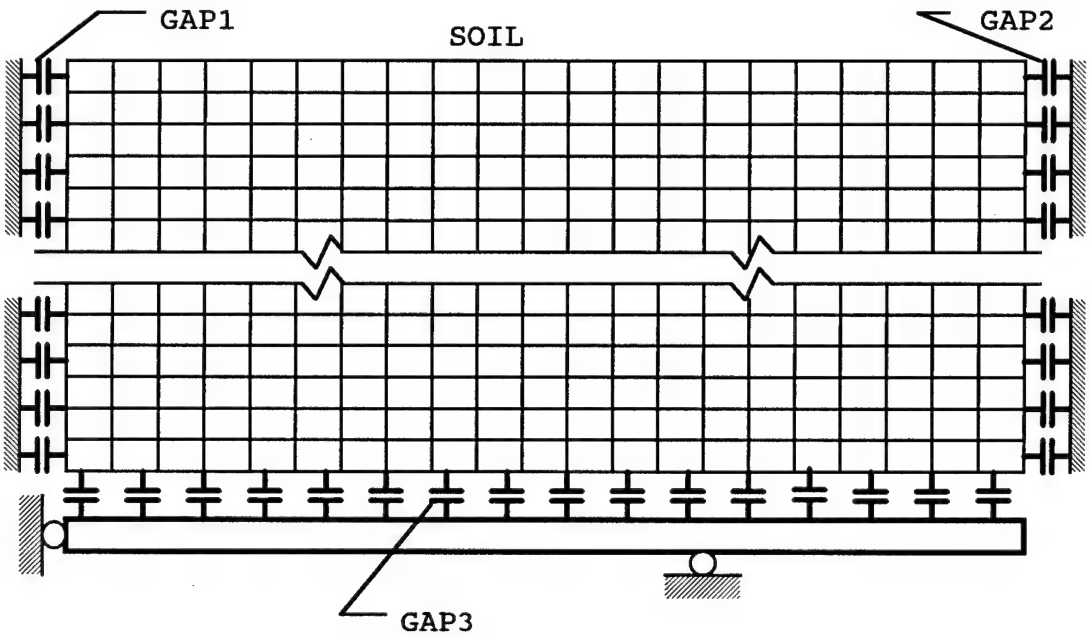

(b) Case III, Case IV, and Case V

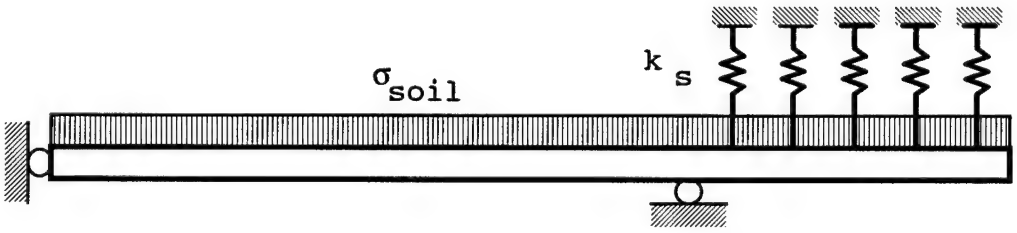

(c) Case VI

Figure 5.1 Soil Effects Case Geometries

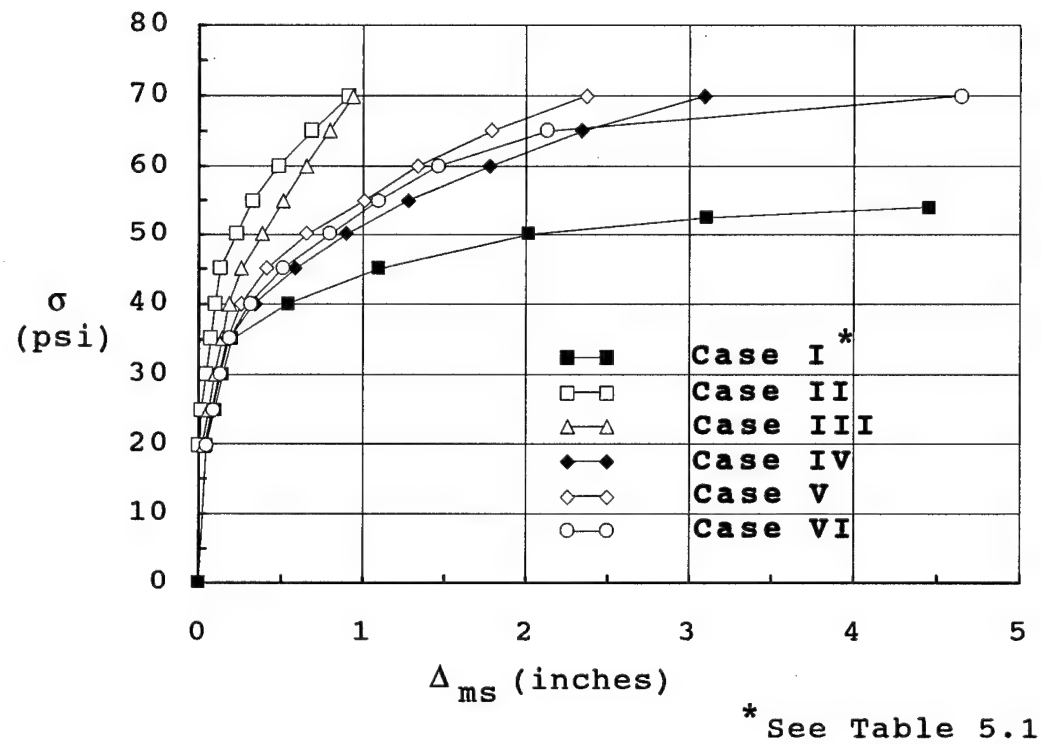

Figure 5.2 Load-Deflection for Soil Effects

is fixed against vertical movement. This greatly increased the stiffness and load carrying capacity of the member when compared to Case I as shown in Figure 5.2. This concept could be implemented in a final design to provide improved response of the roof member by anchoring the end of the cantilever to the floor of the structure or to a soil anchor.

Table 5.1 Soil Effects Case Assumptions

Case*	Assumptions
I	Soil Dead Weight
II	Soil Dead Weight: Point 'A' Fixed
III	Deep Linear Soil Beam E_{soil} = 16,000 psi No Friction in Gap Elements
IV	Deep Linear Soil Beam E_{soil} = 3,000 psi No Friction in Gap Elements
V	Deep Linear Soil Beam E_{soil} = 3,000 psi Friction Coefficient in Gap Elements: GAP1 - 0.0 GAP2 - 0.5 GAP3 - 0.2
VI	Soil Dead Weight and Soil Springs k_s = 12,960 lbs/in (60 lbs/in^3) Spring linear elastic limit: 0.75 inches

* See Figure 5.1

Case III, shown in Figure 5.1.b, modeled the soil as a deep linear beam on top of the concrete member. The soil model consisted of 21 one foot layers using 12 inch by 18 inch 8-noded plane strain elements. The soil was assigned an elastic modulus of 16,000 psi which

corresponds to an assumed compressive wave speed velocity of 1000 fps. The compressive wave speed velocity and elastic modulus of the soil are related by Bowles[80] by

$$E_s = c^2 \rho (1+\nu)(1-2\nu)/(1-\nu) \tag{5.1}$$

where E_s = Elastic modulus of soil

c = Compressive wave speed of soil

ρ = Mass density of soil

ν = Poisson's ratio (assumed = 0.3)

Gap elements were used at the soil boundaries to prevent the development of tension at the interfaces. No shear or friction was assumed to occur at the interfaces in Case III. The response of Case III, as shown in Figure 5.2, was very close to the response of Case II and was considered to be unreasonable. It was then decided to reduce the modulus of elasticity of the soil to better account for its nonlinear behavior.

Case IV, shown in Figure 5.1.b, is identical to Case III except that the modulus of elasticity was reduced to a value of 3,000 psi which is in the range of typical values given by Bowles[80] for the assumed soil type. As shown in Figure 5.2, the response of Case IV falls in the

midrange of the lower and upper bounds, Case I and Case II, respectively, and is believed to be a more realistic representation of the true response.

Case V, shown in Figure 5.1.b, is identical to Case IV except friction was added to the gap elements identified as GAP2 and GAP3 to account for the shear that occurs at the soil/concrete interface and in the soil. Coefficients of friction for gap elements (GAP2 and GAP3) were set at 0.5 and 0.2, respectively. As shown in Figure 5.2, the inclusion of shear at the interfaces does improve the response of the member, but the change is relatively small.

Case VI, shown in Figure 5.1.c, models the dead weight of the soil as an applied pressure and models the stiffness and shear strength of the soil using 7 elastic, perfectly plastic springs on the cantilevered portion of the member. Several typical values for the modulus of subgrade reaction of the soil as given by Bowles[80] were used as soil spring stiffnesses in preliminary analyses. A modulus of subgrade reaction of 60 lbs/in^3, which corresponds to a spring stiffness of 12,960 lbs/in, produced results similar to those of Case IV and Case V. A maximum elastic displacement of 0.75 inches, which is within the range of typical values suggested by Bowles,[80]

was used to define the elastic limit of the soil springs. As shown in Figure 5.2, the response of Case VI closely follows the response of Case IV and Case V until an applied pressure of 60 psi when the soil springs go into their plastic range. The modeling of Case VI and its response is believed to be more realistic and provides significant computer run time savings. Case VI and the soil spring values identified in Table 5.1 were therefore selected for use in this study.

5.3 Inertia Forces

The inertia forces caused by the mobilization of the soil above the cantilevered portion of the member were investigated to determine their effect on the dynamic response of the member. BLASTSDF was modified to allow different values of mass to be assigned to elements along the member. The dynamic response of member PC53-8 was determined using BLASTSDF with an additional soil mass corresponding to 2, 5, and 10 feet of soil added to the mass of the elements in the cantilevered portion of the member.

The results of the three dynamic analyses were compared to the response of member PC53-8 with no additional soil mass. The results are shown in

Figure 5.3. The maximum dynamic response of the member changed less than 0.5 percent when the 10.0 feet of soil mass was included in the analysis. Overall, there was no significant inertia effect from the soil mass on the dynamic response of the member as investigated in this phase of the study. Therefore, the mass of the soil above the cantilevered portion of the members was neglected in this study.

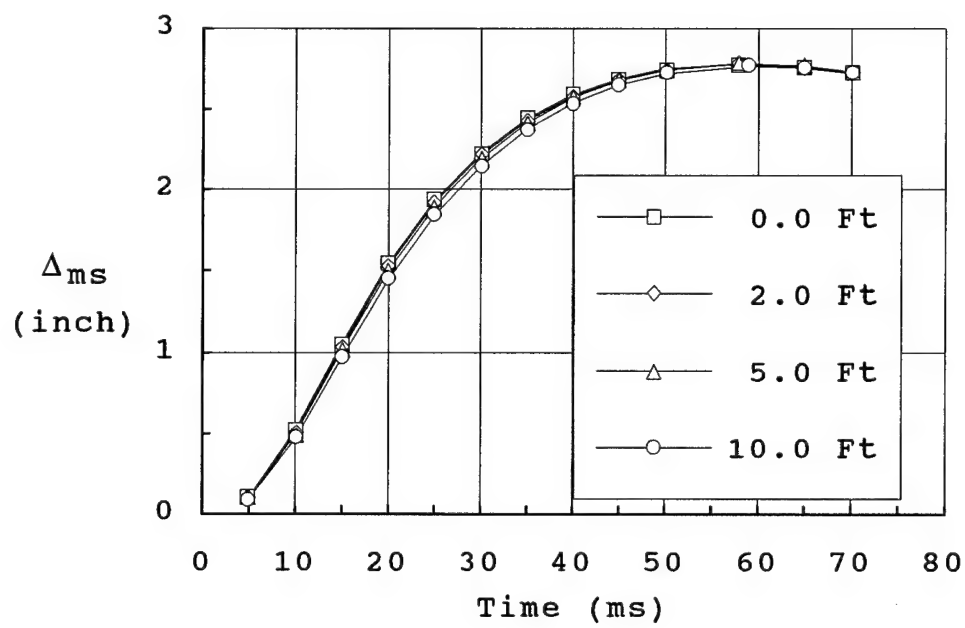

Figure 5.3 Soil Mass Effect on Response

Chapter 6

Static and Dynamic Response

6.1 Introduction

Four concrete members, three prestressed and one conventionally reinforced, were used in this phase of the study in addition to the buried reinforced concrete one-way slab reported by Weidlinger and Hinman.[20] Details of the additional concrete members and the Weidlinger slab are provided in Sections 6.2 and 4.2.3, respectively. A conventionally reinforced concrete member having structure geometry and end restraint conditions similar to the prestressed members was included in this study for comparative purposes.

Static nonlinear finite element analyses were initially completed using ABAQUS linked with UMAT91. Loads were applied uniformly along the entire length of the member with additional soil restraint being provided by nonlinear springs as discussed in Section 5.2. Service load condition was assumed as the dead weight of the concrete and soil overburden and was estimated at 20 psi. These analyses indicated significant advantages and one main disadvantage of prestressed concrete when

compared to conventionally reinforced concrete. Static responses of the members are discussed in detail in Section 6.3 where response is defined in terms of the mid span deflection.

Dynamic nonlinear analyses were then conducted on selected members using the computer code BLASTSDF, which was developed in Chapter 4, with input from the static nonlinear analyses discussed above. Initially, the members were loaded by a blast from a weight of explosive identical to that used in the Weidlinger example. However, the dynamic and total responses of the members were well below their failure ranges, and further dynamic nonlinear analyses using increased weights of explosive were conducted to push two of the members to their limits. The dynamic response is defined as the mid span deflection beyond the static service load deflection while the total response is defined as the total mid span deflection, static and dynamic. The results of these analyses showed improved total responses for the prestressed members when compared to the conventionally reinforced member and similar dynamic responses for the

prestressed and conventionally reinforced concrete members. An in-depth discussion is provided in Section 6.4.

6.2 Member Details

Details and dimensions for the members are provided in Figure 6.1 and Table 6.1. Member designators used in Table 6.1 were developed to allow identification of member properties. The first two letters, PC or RC, identify the member as a prestressed or conventionally reinforced concrete member, respectively. The second two numbers, 53 or 41, identify the overall depth of the member in inches. The number following the dash indicates either the number of 1/2 inch diameter strands used or the area of the conventional longitudinal reinforcing used at each face. The Weidlinger slab referenced above was assigned a member designator of WS53-2.7.

Two preliminary member configurations were considered in addition to those detailed in Table 6.1 but were rejected for further investigation. First, a simply supported single span with no cantilever end portion was considered. This configuration was rejected

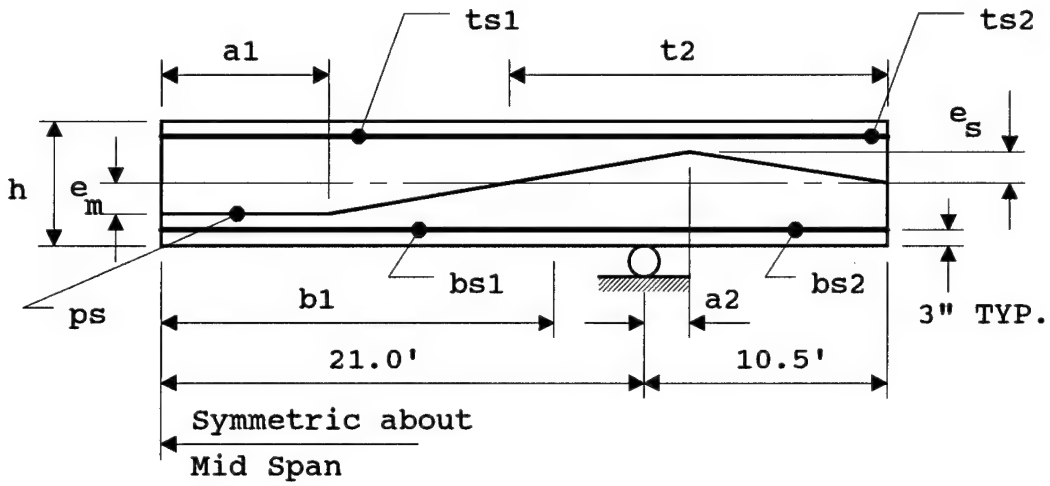

(a) Concrete and Flexural Steel

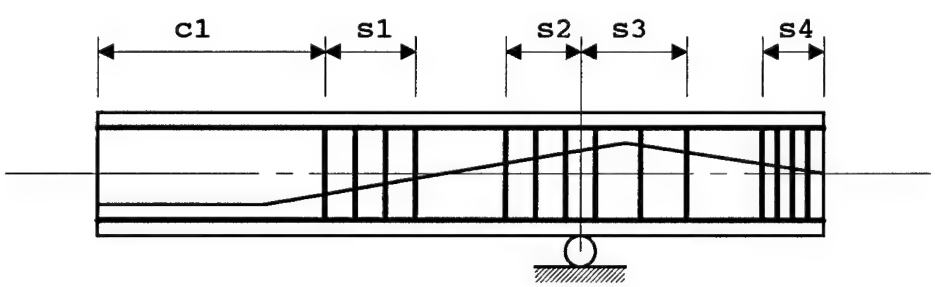

(b) Stirrups

Note: See Table 6.1 for dimensions.

Figure 6.1 Member Details

Table 6.1 Member Details

Member	Concrete	F E Model		
	h	Mesh	Element Dimensions	Aspect Ratio
PC53-8	53"	8 x 21	6.625" x 18.0"	2.7 x 1
PC53-6	53"	8 x 21	6.625" x 18.0"	2.7 x 1
PC41-8	41"	6 x 21	6.833" x 18.0"	2.6 x 1
RC53-3.1	53"	8 x 21	6.625" x 18.0"	2.7 x 1

	Strand					
	e_m	e_s	a1	a2	ps	f_{se}
PC53-8	21.5"	16"	54"	18"	8 - 1/2"	182 ksi
PC53-6	21.5"	17"	90"	0.0	6 - 1/2"	182 ksi
PC41-8	15.5"	12.5"	90"	0.0	8 - 1/2"	170 ksi
RC53-3.1	N/A	N/A	N/A	N/A	N/A	N/A

	Flexural Rebar					
	b1	bs1	bs2	t2	ts1	ts2
PC53-8	16.5'	2#3	2#9	13.5'	4#9	2#9
PC53-6	15'	2#3	2#8	15'	4#8	2#8
PC41-8	15'	2#5	2#9	15'	4#9	2#9
RC53-3.1	N/A	4#8	4#8	N/A	4#8	4#8

Table 6.1 continued on page 109

Table 6.1 Member Details (continued)

Member	Stirrups						
	c1	s1			s2		
		No	Bar	Space	No	Bar	Space
PC53-8	90"	7	1#3	18" c/c	0	0	0
PC53-6	0	0	0	0	4	1#3	9" c/c
PC41-8	57"	7	1#3	18" c/c	4	2#3	9" c/c
RC53-3.1	0	0	0	0	15	1#4	9" c/c

	Stirrups (continued)					
	s3			s4		
	No	Bar	Space	No	Bar	Space
PC53-8	0	0	0	4	1#3	2.5" c/c
PC53-6	2	1#3	9" c/c	4	1#3	2.5" c/c
PC41-8	4	2#3	12" c/c	3	2#3	2.5" c/c
RC53-3.1	4	1#4	18" c/c	0	0	0

because of the large increase in the ultimate moment capacity of the section that would be required to make the member of comparable capacity to that of WS53-2.7 as the assumed end conditions went from fixed/fixed to simple/simple. The simply supported configuration would also require additional attention to seating restraint

during large end rotations to prevent slip-off. Second, a preliminary configuration was considered similar to PC53-8 but with only a single harp point in the center section at mid span. This configuration was rejected because a double harp point near mid span would better offset the applied load moments and provide a higher level of precompression over a larger zone.

The initial design, PC53-8, was developed to provide a static load capacity similar to that of WS53-2.7 using the soil restraint and loading condition of Case I identified in Chapter 5. The static load-deflection behavior of members PC53-8 and WS53-2.7 is shown in Figure 6.2. The additional soil restraint on the cantilevered portion of the member provided by Case VI, the case selected for use in the remainder of this study, increased the static load capacity of PC53-8 above that of WS53-2.7 making it of no further use in this study. PC53-6 was then designed considering the additional soil restraint to provide a static load capacity similar to that of WS53-2.7. The force-displacement relation for member PC53-6 is also shown in Figure 6.2.

PC41-8 was then designed with an overall depth of 41 inches, which is 77 percent of the depth of WS53-2.7, in

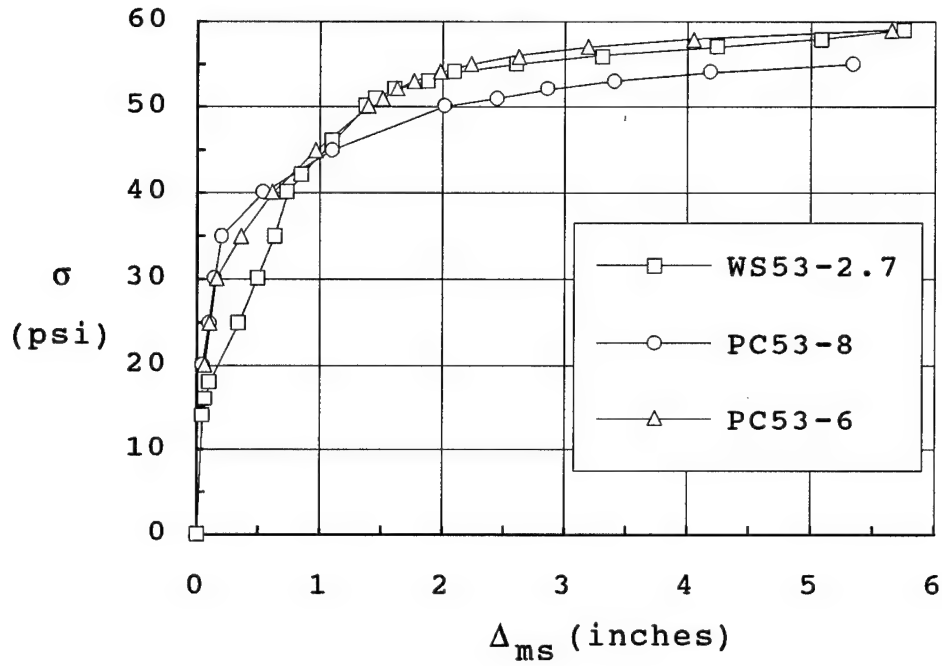

Figure 6.2 Static Load Capacities

an effort to provide a more economical section. Lin and Burns[1] noted that, in general, prestressed concrete sections are more economical at a depth of 70 to 80 percent of reinforced concrete sections. The cross section of PC41-8 was designed to have an ultimate moment capacity approximately equal to that of PC53-6.

RC53-3.1 was then designed for comparison since the geometry and end restraint assumptions for WS53-2.7 were different than those of the prestressed members. The

cross section of RC53-3.1 was also designed to have an ultimate moment capacity approximately equal to that of PC53-6 and included strain hardening of the longitudinal reinforcement.

All the members in Table 6.1 were designed with the ultimate moment capacity of the section at the support larger than the resisting moment that could be developed by the soil and load applied to the cantilevered portion of the member. This was done to maximize any restraint provided by the cantilevered portion of the member, thereby minimizing the mid span deflection. All members were designed with enough steel at mid span and at the support in the applied load compression face to provide comparable ultimate moment capacities during rebound.

All members in Table 6.1 were designed with stirrups so that the steel would carry any shear forces that exceeded the shear strength of the concrete in accordance with ACI 318-89[47] except that the strength reduction factor was neglected. Stirrups were included even though the failure mode was expected to be flexure because of the span to depth ratio of 10 or larger. PC53-8 was designed for shear at an ultimate uniform static load consistent with Case I in Chapter 5 while the remainder

of the members in Table 6.1 were designed for an ultimate static load consistent with Case VI in Chapter 5 with all the soil springs assumed to be in the plastic range. Stirrups were also provided in the anchorage zone of the member to control horizontal cracking. Anchorage zone stirrups were designed in accordance with AASHTO Bridge Specifications (1977 edition), Article 1.6.15.

All members were designed and analyzed as 12 inch wide sections. They were analyzed using 8-noded isoparametric plane strain elements which are standard in ABAQUS.[5] Finite element dimensions, aspect ratios, and meshes for the members are given in Table 6.1. Material properties used in the finite element analyses for the reinforcing steel, prestressing strand, and concrete are provided in Table 6.2. Free-field soil parameters used to determine the blast loading within BLASTSDF are the same as those used by Weidlinger and Hinman[20] and are shown in Figure 4.4. All conventional reinforcing steel was assumed as Grade 60. However, the nominal yield stress of the flexural reinforcement was increased to 72.0 ksi to account for the effects observed at the high strain rates encountered during blast loading. Dede and Dobbs[13] indicated that only a little high strain rate

Table 6.2 Material Properties

Rebar		Strand		Concrete
E_s = 29,000 ksi		E_{ps} = 28,000 ksi		E_c = 4,500 ksi
ν = 0.3		ν = 0.3		ν = 0.15
Flexural		f_{ps} (ksi)	ε_{ps}	f'_c = 6.125 ksi
f_s (ksi)	ε_s	224.0	0.008	ε_{cr} = 0.0001
72.0	0.0025	246.6	0.010	
72.0	0.0091	259.2	0.015	
105.0	0.0729	262.4	0.020	
93.0	0.1542	263.9	0.025	
Stirrup		264.8	0.030	
f_y (ksi)	ε_y	270.0	0.050	
60.0	0.0021			

effects are observed in the strength of the steel in the ultimate and failure ranges. Therefore, the values used to model the strain hardening of the steel, as shown in Table 6.2, are typical values reported by Wang,[81] et al, for Grade 60 steel with a yield stress of 60.0 ksi. Stirrup steel was modeled as elastic, perfectly plastic with no increase for strain rate effects. The prestressing steel was assumed as 7-wire, low-relaxation, 1/2 inch diameter, Grade 270 strand. The material

stress-strain properties were modeled as piecewise linear using the typical stress-strain properties in the *PCI Design Handbook*.[46] Dede and Dobbs[13] indicated very little increase in strength due to high strain rates for high strength steels; therefore, none was included in the model for the prestressing steel.

The concrete strength was modeled by Weidlinger and Hinman[20] and in this study as 6,125 psi to account for strength increase at high strain rates as reported by Dede and Dobbs.[13] Other concrete properties shown in Table 6.2 are default values used by UMAT91.[78]

6.3 Static Nonlinear Analysis (FE)

Static nonlinear finite element analyses were completed on members PC53-6, PC41-8, and RC53-3.1 using ABAQUS and UMAT91. A typical ABAQUS input file is provided in Appendix VI for member PC53-6. The load versus mid span deflection curves are shown in Figure 6.3. The curve for member PC53-6 stops at a mid span deflection of approximately 6.6 inches because of failure of the prestressing strand. The curves for members PC41-8 and RC53-3.1 stop at mid span deflections of 9.0 inches which corresponds to member rotation at the supports of

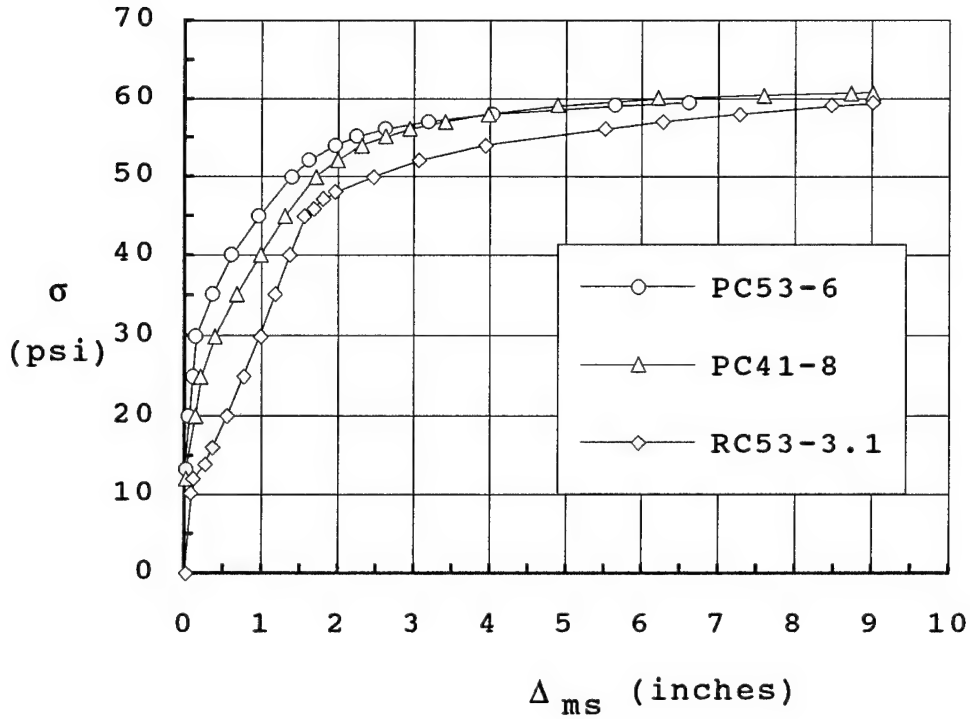

Figure 6.3 Static Load-Deflection Curves

approximately 2 degrees. Two degrees of member rotation at the support was recommended by Dede and Dobbs[15] as a limit for precast members. However, their recommendation was made for conventional precast concrete applications where member rotation greater than 2 degrees at the supports could create significant seating problems and could cause horizontal forces to be applied to the vertical supports. A member rotation greater than 2

degrees at the supports could probably be allowed for the geometry used in this study because the cantilevered portion of the member would minimize seating problems and the soil around the structure would supply horizontal restraint to the vertical supports. Further research is required to determine specific limits.

Finite element analyses to simulate transfer conditions were completed on members PC53-6 and PC41-8 with concrete properties adjusted to transfer values of f'_{ci} equal to 3,500 psi and E_{ci} equal to 3,500,000 psi. Prestressing was applied to the members as an initial condition in the strand and was applied as an effective prestress value which was held constant by the '*PRESTRESS HOLD' option available in ABAQUS[5] until the concrete reached equilibrium. The effective prestress values for the strand at transfer accounted for losses due to elastic shortening of the concrete and were input as 199.8 ksi and 181.4 ksi for PC53-6 and PC41-8, respectively. At transfer, values of extreme fiber concrete stresses from the finite element analyses compared well with those predicted by standard prestress theory. At service load, values of extreme fiber

concrete stresses also compared well with standard prestress theory.

Load was applied to the members PC53-6, PC41-8, and RC53-3.1 in three steps during the static nonlinear analyses. The magnitudes of the load steps and the increments within each step are provided in Table 6.3. The first load step from zero to 20 psi (service load) was applied to all three members. The prestress was applied to the members PC53-6 and PC41-8 as described above but with the effective prestress values used at transfer adjusted for additional losses in the concrete due to creep and shrinkage and for losses in the strand due to relaxation. Effective prestress values used are shown in Table 6.3. Smaller load increments, as shown in Table 6.3, were used during the third load step to better reproduce the nonlinear behavior of the concrete in the upper load ranges.

The static responses of the members PC53-6, PC41-8, and RC53-3.1 are shown in Figure 6.3 with significant events being summarized in Table 6.4. The overall static responses of the three members were as anticipated with PC53-6 being the stiffest, RC53-3.1 the least stiff, and PC41-8 falling in an intermediate range. All three

members exhibited an approximately trilinear response as can be seen in Figure 6.3. The three members responded as linearly elastic until first cracking at mid span which was followed by a significant decrease in member stiffness. The members then continued to respond in an approximately linear fashion, with a decreased stiffness, until a mid span deflection of about 1.5 inches was reached when yielding of the steel at mid span occurred or the soil springs began plastic behavior. This was

Table 6.3 Static Load Steps

Load Step	Member		
	PC53-6	PC41-8	RC53-3.1
Step 1			
f_{se} (ksi)	182	170	N/A
Range (psi)	0 - 20	0 - 20	0 - 20
Increment (psi)	20.0	20.0	1.0
Step 2			
Range	20 - 50	20 - 50	20 - 45
Increment	1.0	1.0	1.0
Step 3			
Range	50 - 60	50 - 61	45 - 60
Increment	0.25	0.25	0.25

Table 6.4 Significant Events

Member PC53-6			
Load (psi)	Significant Event	Δ_{ms} (in)	I.P.* Cracks
20.0	Service Load: f_c = 35 psi, bottom fiber at mid span	0.06	0
29.0	Concrete Cracks: Mid span	0.15	2
50.0	Strand Yields: Mid span	1.39	103
52.0	Plastic Behavior: Soil spring	1.63	109
54.0	Concrete Cracks: Support	1.98	121
59.5	Strand fails: Mid span, ε_{ps} = 0.051	6.61	177
Member PC41-8			
Load (psi)	Significant Event	Δ_{ms} (in)	I.P.* Cracks
20.0	Service Load: f_c = 123 psi, bottom fiber at mid span	0.13	0
26.0	Concrete Cracks: Mid span	0.25	1
45.0	Concrete Cracks: Support	1.31	81
50.0	Plastic Behavior: Soil spring	1.71	96
54.0	Strand Yields: Mid span	2.31	124
60.8	Limiting Deflection: ε_{ps} = 0.034	9.00	180

Table 6.4 Continued on page 121

* Number of integration points cracked in half span.

Table 6.4 Significant Events (continued)

Member RC53-3.1			
Load (psi)	Significant Event	Δ_{ms} (in)	I.P.* Cracks
12	Concrete Cracks: Mid span	0.12	15
20.0	Service Load	0.55	102
25.0	Concrete Cracks: Support	0.76	143
46.0	Lower Bar Yields: Mid span	1.67	289
49.0	Plastic Behavior: Soil spring	2.21	296
59.3	Limiting Deflection: ε_{ps} = 0.033	9.00	347

* Number of integration points cracked in half span.

followed by another significant decrease in member stiffness. All three members then continued to respond in an approximately linear fashion, with further reduced stiffness, until failure.

The precompression in the concrete bottom fiber at mid span of the member PC53-6 was gone at service load condition with a tensile stress of 35 psi being present in the concrete. The response of PC53-6 was linearly elastic until an applied load of 30 psi which immediately followed first concrete cracking at mid span. No additional significant change in stiffness was observed

until a load of 50 to 52 psi when the prestressing strand reached its theoretical yield strain of 0.01 and when the first soil spring began to behave plastically. An approximately linear response of the member PC53-6 continued then until the strand at mid span failed at an assumed ultimate strain of 0.05 with a corresponding load just less than 59.5 psi. Tension first appeared in the precompression zone at the support at a load of 40 psi. Cracking at this location occurred later at a load of 54 psi with no observable immediate change in member stiffness. Following the cracking of the concrete at the support, the prestressing strand and the conventional reinforcing at the support remained linearly elastic until failure of the strand at mid span.

The precompression in the concrete bottom fiber at mid span of the member PC41-8 was gone at service load condition with a tensile stress of 123 psi being present in the concrete. The response of PC41-8 was linearly elastic until an applied load of 26 psi which corresponds to first concrete cracking at mid span. No additional significant change in stiffness was observed until a load of 50 psi when the 2-#5 bars in the lower portion of the member at mid span yielded and when the first soil spring

began to behave plastically. An approximately linear response of PC41-8 continued until the mid span deflection reached its limiting value of 9.0 inches which corresponds a member rotation of 2 degrees at the support. The analysis was then stopped. The strain in the prestressing strand at mid span reached its theoretical yield strain of 0.01 at a load of 54 psi with no observable change in member stiffness. At a load of 60.8 psi which corresponds to the 9.0 inch mid span deflection, the strain in the prestressing strand was 0.034 which is 68 percent of the assumed ultimate failure strain. Tension first appeared in the precompression zone at the support at a load of 34 psi. Cracking at this location occurred later at a load of 45 psi, again with no observable immediate change in member stiffness. Following cracking of the concrete at the support, the prestressing strand and conventional reinforcing at the support remained linearly elastic until the analysis was stopped at a mid span deflection of 9.0 inches.

Member RC53-3.1 had no precompression and already had 102 integration points cracked at service load. RC53-3.1 initially responded as linearly elastic until first concrete cracking at mid span at a load of 12 psi.

Following a significant reduction in member stiffness, the member RC53-3.1 continued with a linear incremental response until a load of 45 psi when the bottom conventional reinforcing steel at mid span yielded causing another significant reduction in member stiffness. The approximately linear response of the member continued until the limiting mid span deflection of 9.0 inches was reached at a corresponding load of 59.3 psi. At this load, the bottom reinforcing at mid span was at a strain of 0.033 which is less than 22 percent of the assumed ultimate failure strain. Cracking in the concrete at the support first occurred at a load of 25 psi, again with no observable change in member stiffness. Following cracking of the concrete at the support, the upper reinforcing steel in that region remained linearly elastic until the analysis was stopped at the limiting mid span deflection.

There are two readily apparent advantages that the members PC53-6 and PC41-8 have over the member RC53-3.1. First and foremost, both prestressed members are linearly elastic and uncracked at and beyond service load condition. Remaining uncracked at service load condition will provide better protection for the steel through the

years that the member is buried. This will better insure that its original strength is available when the member is subjected to a blast load in addition to the service load. Second, the prestressed members have a larger load capacity at any given level of deflection. An additional significant advantage would be realized for the prestressed members if the depth of burial were reduced, thereby reducing the service load. If the depth of burial were reduced by one-half, the service load would be approximately 12 psi. At this load level, the member RC53-3.1 would still be cracked, but the members PC53-6 and PC41-8 would have an additional load capacity of 17 psi and 15 psi, respectively, before cracking would occur. This would allow the prestressed members to respond to surface explosions not located directly above them and possibly remain uncracked while any additional loading applied to RC53-3.1 would result in further cracking.

The main disadvantage of the members PC53-6 and PC41-8 when compared to the member RC53-3.1 is their reduced ductility as shown in Figure 6.4. At a mid span deflection of 6 inches, the prestressing strand in PC53-6 is approaching the assumed ultimate failure strain while

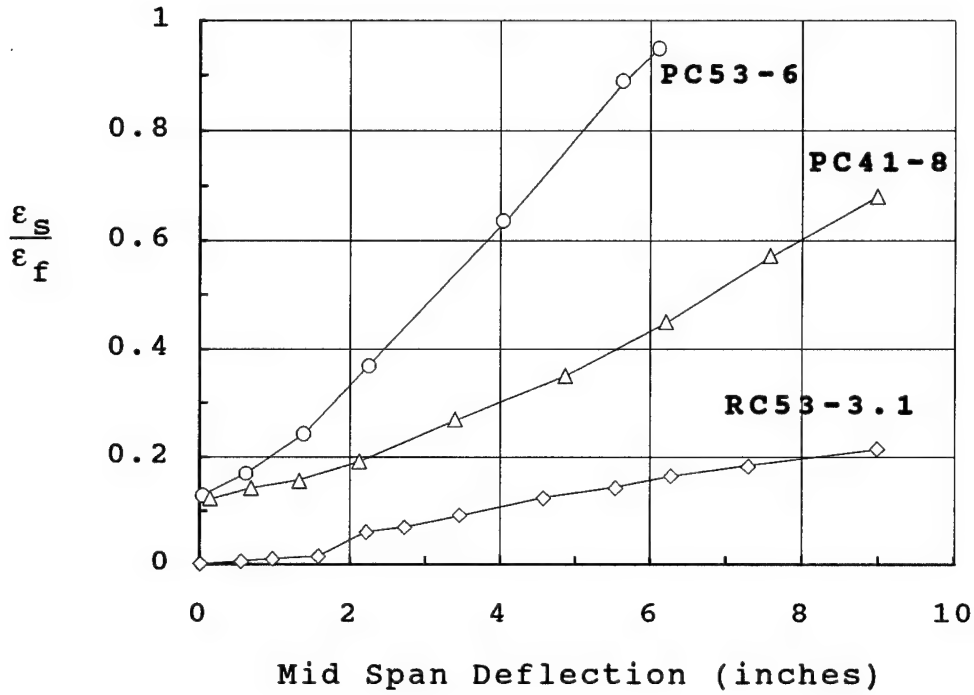

Figure 6.4 Member Ductility

the conventional reinforcing steel in RC53-3.1 is at a level of strain that is less than 16 percent of its assumed ultimate failure strain. However, PC41-8 does show a significant improvement over PC53-6. At the same mid span deflection of 6 inches, the prestressing strand in PC41-8 is at a level of strain that is approximately 43 percent of its assumed ultimate failure strain which is less than half the level of strain in the strand of PC53-6. At a mid span deflection of 9.0 inches, the

strain in the prestressing strand of PC41-8 and in the conventional reinforcing of RC53-3.1 is at a value of 68 and 21 percent of their assumed failure strains, respectively. The disadvantage of reduced ductility as discussed above should not prohibit the use of prestressed concrete members, but it should be considered when developing member details during design. Because of the differences in the stress-strain behavior of prestressing strand and conventional reinforcing bar, further research is required to determine the limiting value for the ductility (defined by Equation 2.17) of prestressed concrete members. Further research is also required to define the maximum elastic deflection as used in Equation 2.17 for prestressed concrete members.

Two preliminary designs for prestressed members were investigated for possible use in this study in an effort to correct the disadvantage of reduced ductility. PC41-8 was modified by reducing the number of prestressing strands to 4 and 6. The area of the conventional reinforcing was also increased in each design to maintain a similar ultimate moment capacity. Even with the strands prestressed to the maximum allowed by ACI 318-89,[47] the 4-strand member was cracked at service load

while the 6-strand member was very near cracking. As discussed earlier in this section, keeping the member uncracked at and beyond service load condition is a significant advantage. Therefore, no further investigation was conducted on the two preliminary designs described above. However, a combination of prestressing and conventional reinforcing may prove to be a viable option for improved overall response when the ultimate moment capacity of the section is not limited or when the service loads are reduced.

6.4 Dynamic Nonlinear Analysis (SDOF)

Dynamic nonlinear analyses were conducted on the members PC53-6, PC41-8, and RC53-3.1 using the methodology and computer code (BLASTSDF) which were described, developed, and validated in Chapter 4. Static nonlinear shape functions and member stiffness functions were obtained for all three members from the analyses described in Section 6.3. Nonlinear shape and stiffness functions were developed which corresponded to mid span deflection increments of approximately 0.2 inches except for the extreme upper load range where the mid span deflection increment was allowed to increase due to the

larger changes in deflection between load increments. Dynamic analyses on all three members were performed using a time step increment of 1.0 ms which was determined as acceptable in Chapter 4.

Dynamic analyses were carried out on all three members using the identical soil and blast load parameters used by Weidlinger and Hinman.[20] The total responses of the members are shown in Figure 6.5 and are as anticipated with the mid span deflections at any given time increasing from PC53-6 to RC53-3.1 with PC41-8 in between. Maximum mid span responses, given in Table 6.5, show that prestressing of a member improves its total response for this range of loading when compared to a conventionally reinforced member with a comparable ultimate section moment capacity. The increased time of maximum total response is justifiable for RC53-3.1 due to its overall reduced stiffness as seen in Figure 6.3 from the static analyses. Little difference is noted in the total responses of the two prestressed members. At the maximum total response, the tension steel at mid span in all three members has yielded.

The dynamic responses of the members PC53-6, PC41-8, and RC53-3.1 are shown in Figure 6.6. As can be seen,

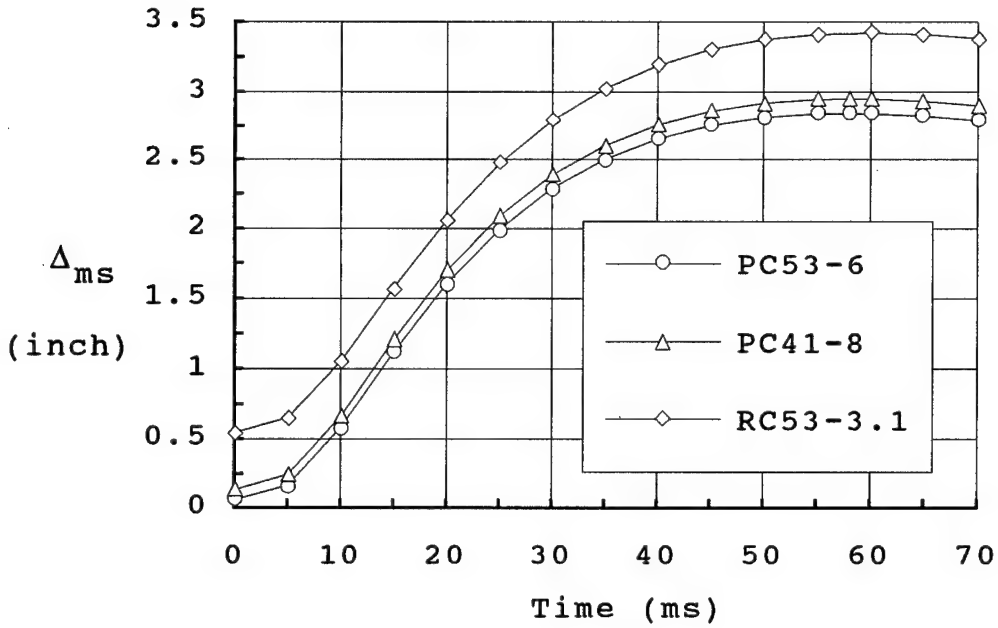

Figure 6.5 Total Response (W = 1014 lbs)

Table 6.5 Maximum Responses (W = 1014 lbs)

Member	Total Δ_{ms} (inch)	Dynamic Δ_{ms} (inch)	Time (ms)
PC53-6	2.8431	2.7812	58.0
PC41-6	2.9527	2.8193	58.0
RC53-3.1	3.4207	2.8722	60.0

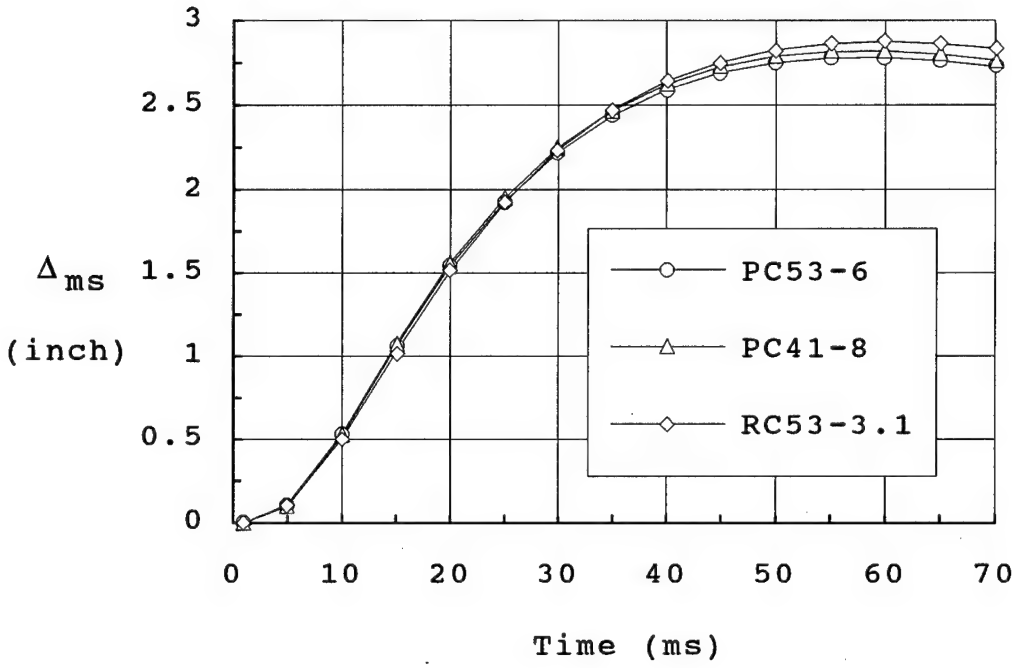

Figure 6.6 Dynamic Response (W = 1014 lbs)

the dynamic response from the static service load condition is almost identical for all three members. This is believed to be caused in part by the fact that at a time of 20 ms (one-third of the maximum response time) all three members are in their upper load ranges where member stiffness and load capacity are similar. This would indicate that the increased stiffness and load capacity throughout the entire load range of the prestressed members has little impact on the dynamic

response when the static service load condition is the point of reference. However, it should be reiterated that prestressing does have a significant impact on the total response of a member subjected to a blast load.

Members PC41-8 and RC53-3.1 were selected for further dynamic investigation at increased levels of loading. All parameters were held constant except for the weight of explosive creating the blast load. Three factors contributed to the rejection of PC53-6 for further investigation. First, PC41-8 is a more economical section than PC53-6. Second, there is little difference in the total or dynamic responses of the two prestressed members. The higher stiffness and load capacity of PC53-6 has very little impact on its response when compared with PC41-8. Third and foremost, the ductility of PC53-6 is much less than that of PC41-8. At several levels of mid span deflections, the strain in the prestressing strand at mid span of PC41-8 is about 50 percent of that found in PC53-6.

Dynamic analyses were conducted on the members PC41-8 and RC53-3.1 using BLASTSDF at increased charge weights of 2000 and 3000 lbs of explosive. The results of these analyses and the analyses at a charge weight of 1014 lbs

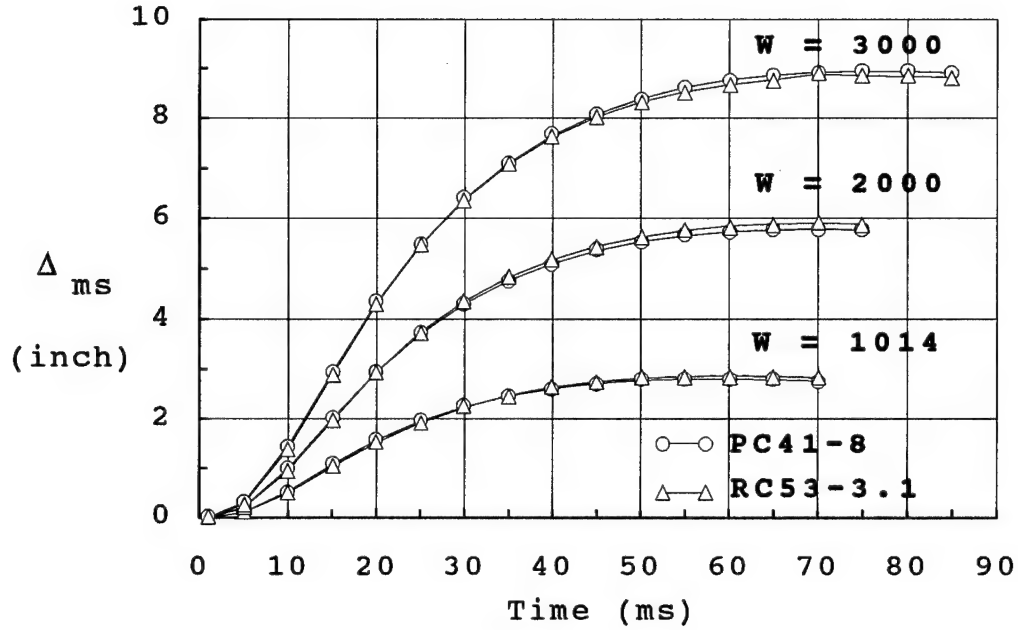

Figure 6.7 Dynamic Response for Various Weights

are shown in Figure 6.7 as the dynamic responses from their static service load positions. Maximum response and time of maximum response of both members for all three charge weights are given in Table 6.6. As expected, increases in the applied blast load increased the maximum response of each member and increased the time of maximum response. It is interesting to notice that the maximum deflection increases almost linearly with the charge weight. As with the initial charge weight of 1014 lbs, little difference in the dynamic

Table 6.6 Maximum Responses for Various Weights

Member	W (lbs)	Total Δ_{ms} (inch)	Dynamic Δ_{ms} (inch)	Time (ms)
PC41-8	1014	2.9527	2.8193	58.0
RC53-3.1		3.4207	2.8722	60.0
PC41-8	2000	5.9206	5.7872	69.0
RC53-3.1		6.4542	5.9057	70.0
PC41-8	3000	9.0711	8.9377	76.0
RC53-3.1		9.3901	8.8416	77.0

responses of the two members is observed with increased charge weight. However, the advantage previously observed in their total responses still exists due to the differences in their static service load deflections. The total response of each member is slightly over the limiting deflection of 9.0 inches at a weight of explosive equal to 3000 lbs. However, this level of total response was determined as acceptable for this phase of the study.

Chapter 7

Summary, Conclusions, and Recommendations

7.1 Summary

Dynamic nonlinear analyses were conducted on prestressed and conventionally reinforced concrete members used as roof elements of a buried shelter which was subjected to the detonation of a high explosive at the ground surface. The dynamic nonlinear analyses were conducted using BLASTSDF; a computer program developed and validated in this study. BLASTSDF implements a single-degree-of-freedom model to perform the dynamic analysis while using static nonlinear shape and stiffness functions generated by ABAQUS[6] linked with UMAT91,[77] a commercially available finite element program and concrete constitutive model, respectively. BLASTSDF was initially validated by comparing its results against those reported by Weidlinger and Hinman[20] which were obtained using a proven, more sophisticated dynamic nonlinear finite element procedure. Comparison of the results from the two procedures provided reasonable correlation considering several uncertainties about the Weidlinger[20] model. BLASTSDF was also validated against

dynamic linear and nonlinear finite element analyses conducted using ABAQUS linked with UMAT91 with excellent correlation.

Initial plans for this study were to conduct all dynamic nonlinear analyses using ABAQUS and its resident nonlinear concrete constitutive model. Preliminary nonlinear static analyses showed premature failure of the doubly reinforced members of interest in this study. The concrete constitutive model, UMAT91,[77] was selected as an alternate and was shown to provide good static nonlinear results when compared to ultimate design theory, experimental results, and commonly accepted concrete behavior. However, UMAT91 required a special option, which was not standard in the currently available version of ABAQUS (version 4.9), to conduct dynamic nonlinear analysis. BLASTSDF was then developed and validated. A special version of ABAQUS was later obtained which allowed the dynamic nonlinear analysis of concrete members using ABAQUS linked with UMAT91. Results of dynamic nonlinear analyses from BLASTSDF and ABAQUS linked with UMAT91 were then compared with excellent correlation.

The member configuration in this study was a single span with ends cantilevered past the supports to provide

additional restraint from the soil. Additional restraint provided by the soil was shown to significantly improve the response of the members. The members of interest in this study were modeled in plane strain using two-dimensional, 8-noded, isoparametric elements with reduced integration. The members were decoupled from the soil with soil-structure interaction effects approximated in the analyses. The prestressed concrete members showed significant advantages over the conventionally reinforced concrete member when considering their static and total dynamic responses but did show a reduced ductility.

7.2 Conclusions

7.2.1 Response of Concrete Members

The primary conclusion that comes from the design and analysis of the members investigated during this study is that prestressed concrete members are a viable option as roof elements for buried shelters subjected to a surface detonation of high explosives. Their overall responses showed several significant advantages and only minor disadvantages. The following conclusions and observations about the response of the prestressed and reinforced concrete members come from the design and analysis of the members investigated in this study.

1. In-depth static and dynamic nonlinear analyses were conducted on three concrete members (PC53-6, PC41-8, and RC53-3.1). The member PC53-6 was prestressed with six 1/2 inch diameter 7-wire strands and had a depth of 53 inches. The member PC41-8 was prestressed with eight 1/2 inch diameter 7-wire strands and had a depth of 41 inches. The member RC53-3.1 was not prestressed but contained 3.1 square inches of conventional reinforcing at each face and had a depth of 53 inches. All three members exhibited approximately trilinear static responses. The first significant reduction in stiffness followed first concrete cracking in the mid span region while the second significant reduction in stiffness followed yielding of mid span tensile steel or initiation of plastic soil spring behavior.

2. The precompression in the concrete at mid span of members PC53-6 and PC41-8 was gone at the service load condition. However, the members remained uncracked until a uniform static load of 29 and 26 psi, respectively. The reinforced concrete member (RC53-3.1) cracked at a uniform static load of 12 psi, well below the service load of 20 psi, and had 102 integration points cracked at service load.

3. The conventionally reinforced concrete member (RC53-3.1) had almost 50 percent more integration points cracked than the prestressed concrete member PC41-8 when they reached the limiting mid span deflection of 9 inches. However, at this limiting deflection, the strain in the tensile steel at mid span of RC53-3.1 and PC41-8 was at levels of 21 and 68 percent, respectively, of their respective tensile failure strains. The prestressing strand in member PC53-6 reached its failure strain at a mid span deflection of 6.6 inches.

4. The level of strain in the strand at mid span of the thinner prestressed member (PC41-8) was approximately 50 percent less than the level of strain in the strand at mid span of the thicker prestressed member (PC53-6) for all mid span deflections greater than 2.0 inches.

5. The strand and conventional reinforcing at the support remained linearly elastic throughout the entire static load range for all three members (PC53-6, PC41-8, and RC53-3.1) even after cracking of the concrete at the support. No significant change in stiffness was observed immediately following concrete cracking at the support for any of the three members.

6. At a charge weight of 1014 lbs of TNT, the prestressed members (PC53-6 and PC41-8) showed improved

total response (static and dynamic) when compared to the conventionally reinforced member (RC53-3.1). The prestressed members' total responses were very similar. For members PC53-6, PC41-8, and RC53-3.1, the maximum mid span deflection and time at which it occurred were 2.84 inches at 58 ms, 2.95 inches at 58 ms, and 3.42 inches at 60 ms, respectively.

7. As referenced from their static service load positions and at a charge weight of 1014 lbs of TNT, the dynamic responses of the members PC53-6, PC41-8, and RC53-3.1 were very similar with their maximum dynamic mid span deflections being 2.78 inches, 2.82 inches, and 2.87 inches, respectively. This is due in part to the fact that at a time of approximately one third of their maximum response time the members were all in their upper load ranges where their static capacities and stiffnesses are similar.

8. At the higher charge weights of 2000 lbs and 3000 lbs of TNT, the dynamic responses of the members PC41-8 and RC53-3.1 remained similar with their maximum mid span responses increasing approximately linearly with the charge weight (W). The time of maximum response also increased with increased charge weight. Member PC53-6 was not considered for these increased charge weights

because of its reduced ductility and its similar behavior when compared to PC41-8 at the initial charge weight of 1014 lbs of TNT.

7.2.2 Structure Configuration and Design

The following conclusions and observations about structure configuration and design come from the design and analysis of the members investigated in this study.

1. Higher levels of partial prestressing were considered in preliminary designs, but they did not prove favorable when evaluated using the constraints in this study. However, higher levels of partial prestressing may still prove favorable if higher ultimate moment capacities of the sections are allowed or if service loads are reduced and blast loads are increased as would occur if a shallower depth of burial was used.

2. Using double harp points for the prestressing strand near mid span of a member provides a higher level of precompression over a larger zone. This helps to delay the development of concrete cracks in that region which should improve the response of the member.

3. The cantilevered member configuration used in this study is better than a simply supported member

because any additional restraint provided to the cantilevered portion of the member significantly improves the load capacity of the member. The cantilevered member configuration should also reduce seating problems during large member rotation at the supports.

4. The effects of any additional inertia forces from the mobilized soil over the cantilevered portion of the members in this study were small.

7.2.3 Finite Element Models and Method

The following conclusions and observations about the finite element program ABAQUS,[6] the concrete constitutive model UMAT91,[77] and the finite element method come from the design and analysis of the members investigated in this study.

1. The algorithm in the concrete constitutive model resident in the finite element program ABAQUS developed numerical problems during the static nonlinear analysis of doubly reinforced concrete members. Numerical problems occurred at loads 50 to 73 percent of the members' predicted ultimate capacities.

2. The concrete constitutive model UMAT91 while linked to ABAQUS during static nonlinear analyses accurately predicted ultimate capacities of singly and

doubly reinforced concrete members, conventional and prestressed. Static nonlinear finite element analyses using ABAQUS linked with UMAT91 determined ultimate capacities within 4 percent of the ultimate capacities determined by ultimate design theory and by full scale test. These finite element analyses also produced results that were in good agreement with elastic beam theory and with commonly accepted concrete behavior.

3. The value of the concrete tensile cracking strain input into UMAT91 had a small influence on the overall static response of the prestressed concrete member tested by Hamilton,[43] but UMAT91's default value of 0.0001 provided good results when compared to the experimental results reported by Hamilton.

4. A special option for ABAQUS (version 4.9) was required to conducted dynamic nonlinear finite analysis while linked to UMAT91. It is the author's understanding that this special option is to be standard in ABAQUS, version 5.0.

7.2.4 Single-Degree-of-Freedom Model

The following conclusions and observations about the single-degree-of-freedom-model and the associated FORTRAN

computer code BLASTSDF come from the design and analysis of the members investigated in this study.

1. Significant computer run time and cost savings can be realized by using BLASTSDF to conduct dynamic nonlinear analyses in lieu of dynamic nonlinear finite element analyses using ABAQUS and UMAT91. This savings is especially significant when the member is kept unchanged while conducting parametric studies to investigate the effects of various soil properties or charge weights.

2. It was observed during the dynamic nonlinear analysis of the Weidlinger slab using BLASTSDF that after 11 ms the blast load approached a uniform distribution when the soil-structure interaction effects were considered. The assumed uniform static load distribution used to generate nonlinear stiffness and shape functions for input into BLASTSDF was validated by the close correlation shown for the dynamic responses of the members analyzed as predicted by BLASTSDF and by ABAQUS linked with UMAT91. The uniform static load distribution was further validated by the close correlation of the displaced shapes predicted by both methods.

7.3 Recommendations

The following recommendations for additional research can be made from the studies conducted.

1. Full scale testing of prestressed and conventionally reinforced concrete members should be conducted to verify the findings of this study and to further verify the analysis techniques and assumptions used in this study.

2. Non-solid sections (hollow or flanged) can provide more economical members, but the impact on the overall response of the members caused by local effects within the top flange should be investigated. The webs of the non-solid sections are also thinner and normally require more attention to shear details.

3. The overall geometry and configuration of the members investigated in this study may reduce the problems commonly associated with larger member end rotations of typical precast members. Specific limits of member rotation at the supports for the configuration used in this study should be determined.

4. The reduced ductility seen in the prestressed concrete members when compared to the conventionally reinforced concrete member and the lower failure strain of the prestressing strand as compared to the

conventional reinforcing steel indicate the need to determine acceptable levels of ductility for prestressed members subjected to blast loads.

5. For shelters with a shallower depth of burial which would cause an increased blast load and a decreased service load, the effects of higher levels of partial prestressing may prove favorable and should be investigated.

6. Additional restraint on the cantilevered portion of the members investigated in this study was shown to significantly improve member response. Ways to provided additional restraint such as soil anchors or ties to the bottom of the shelter should be identified and evaluated for their practicality and effectiveness.

7. Analyses in this study were limited in scope to a specific depth of burial, span length, overhang length, type of soil, and charge standoff distance. Further studies should be conducted to determine the response of prestressed concrete roof elements with variations in the above parameters.

8. Prestressed members in this study were limited to pretensioned members where cracking of the concrete at transfer controlled the prestressing force applied to the member. The post-tensioning method applies the

prestressing force to the concrete when the strength of the concrete is much greater than its strength at transfer during the pretensioned method. This allows a much larger prestressing force to be applied to the member yet allows control of concrete cracking. Larger prestressing forces should further improve the total response of a member and should be investigated.

Appendix I

ABAQUS Input File for Hamilton P/C Beam

```
*HEADING,PAGESIZE=990
 PC BEAM MODEL (HAMILTON 1967)  SIMPLE / SYMETRIC
 CPS8R, MESH 9 X 4,  NON-LINEAR, STATIC, ULTIMATE
*PREPRINT,LOCAL INFO=NO,HISTORY=NO,MODEL=NO,ECHO=YES
*NODE
1,0.0,0.0
801,0.0,10.0
19,54.0,0.0
819,54.0,10.0
*NGEN,NSET=MID
1,801,100
*NGEN,NSET=END
19,819,100
*NFILL
MID,END,18,1
*NSET,NSET=NAMID
401
*NSET,NSET=SUPPORT
17
*NSET,NSET=NLOAD
806,807
*ELEMENT,TYPE=CPS8R
1,1,3,203,201,2,103,202,101
*ELGEN,ELSET=ALLPS
1,9,2,1,4,200,100
*ELSET,ELSET=TOP,GENERATE
301,309,1
*ELSET,ELSET=BOT,GENERATE
```

```
1,9,1
*ELSET,ELSET=EMCOR
1,301
*ELSET,ELSET=ELMID,GENERATE
1,301,100
*ELSET,ELSET=ELSUP,GENERATE
8,308,100
*ELSET,ELSET=E301
301
*REBAR,ELEMENT=CONTINUUM,MATERIAL=REBAR,NAME=UBAR
TOP,0.22,8.0,0.0,0.8,3
*REBAR,ELEMENT=CONTINUUM,MATERIAL=STRAND,NAME=LBAR
BOT,0.178,8.0,0.0,0.8,1
*REBAR,ELEMENT=CONTINUUM,MATERIAL=REBAR,NAME=STIR1
ALLPS,0.22,8.0,0.0,0.5,4
*MATERIAL,NAME=CONC
*USER MATERIAL, CONSTANTS=4
3,5.88E+3,1.0E-4,4.37E+6
*DEPVAR
4
*MATERIAL,NAME=REBAR
*ELASTIC
29.0E+6,0.3
*PLASTIC
40000.0,0.0
*MATERIAL,NAME=STRAND
*ELASTIC
28.0E+6,0.3
*PLASTIC,HARDENING=ISOTROPIC
230000.0,0.0
246600.0,0.00119
254400.0,0.00292
259200.0,0.00574
```

```
262400.0,0.0106
264800.0,0.0205
270000.0,0.0508
*SOLID SECTION,ELSET=ALLPS,MATERIAL=CONC
8.0
*BOUNDARY
17,2
MID,1
*INITIAL CONDITIONS,TYPE=STRESS,REBAR
BOT,LBAR,118500.0
*STEP,INC=25,CYCLE=6
*STATIC,PTOL=100.0
0.04,1.0
*PRESTRESS HOLD
BOT,LBAR
*DLOAD
ALLPS,BY,-0.0868
*PRINT,FREQUENCY=25
*EL PRINT,SUMMARY=NO,ELSET=ELMID,FREQUENCY=25
S11,E11
*EL PRINT,SUMMARY=NO,ELSET=ELSUP,FREQUENCY=25
S11,E11
*EL PRINT,SUMMARY=NO,ELSET=EMCOR,REBAR,FREQUENCY=25
S,E
*NODE PRINT,NSET=NAMID,SUMMARY=NO,FREQUENCY=25
U2
*END STEP
*STEP,INC=25,CYCLE=3
*STATIC,PTOL=100.0,DIRECT=NOSTOP
0.5,10.0
*CLOAD
806,2,-7000.0
807,2,-3000.0
```

```
*PRINT,FREQUENCY=25
*EL PRINT,SUMMARY=NO,ELSET=E301,FREQUENCY=1
S,E
*EL PRINT,SUMMARY=NO,ELSET=E301,REBAR,FREQUENCY=1
S11,E11
*NODE PRINT,NSET=NAMID,SUMMARY=NO,FREQUENCY=1
U2
*NODE PRINT,NSET=NLOAD,SUMMARY=NO,TOTALS=YES,FREQUENCY=1
CF2
*END STEP
*STEP,INC=25,CYCLE=3
*STATIC,PTOL=100.0,DIRECT=NOSTOP
0.1,2.0
*CLOAD
806,2,-8000.0
807,2,-4000.0
*PRINT,FREQUENCY=25
*EL PRINT,SUMMARY=NO,ELSET=E301,FREQUENCY=1
S,E
*EL PRINT,SUMMARY=NO,ELSET=EMCOR,REBAR,FREQUENCY=1
S,E
*NODE PRINT,NSET=NAMID,SUMMARY=NO,FREQUENCY=1
U2
*NODE PRINT,NSET=NLOAD,SUMMARY=NO,TOTALS=YES,FREQUENCY=1
CF2
*END STEP
```

Appendix II

FORTRAN Source Code for BLASTSDF

```
      PROGRAM BLASTSDF
C
C     THIS PROGRAM DETERMINES THE DYNAMIC RESPONSE OF A
C     MEMBER TO A BLAST LOAD USING A SDOF APPROXIMATION.
C     SHAPE FUNCTIONS AND STIFFNESSES ARE DETERMINED FROM
C     STATIC FE ANALYSIS USING CUBIC OR UNIFORM LOAD
C     DISTRIBUTION.  DEGREE OF FREEDOM IS MID SPAN
C     DEFLECTION.
C
      IMPLICIT REAL (A-H,O-Z)
      IMPLICIT INTEGER (I-N)
      CHARACTER*1 YES,NO,STATECHO,LOADtype,UNIFORM,CUBIC
      CHARACTER*1 DMASSflg,DLOADflg,DAMPflg,TEMP1,TEMP2
      CHARACTER*12 DYNIN, DYNOUT, STATIN
      LOGICAL YESNO
      DIMENSION Ujo(40), SIGMA(40,41)
      COMMON /STATIC/ Uj(40,41),ubar(41),Fj(40,41)
      COMMON /DYNAMIC/ Pn(40),elMASS(2),dTIME,TAUmax,
     *nMASSgr,noelMgr1
      COMMON /GEOMETRY/ Rx(40),Xi(40),NOEL,ELLENGTH,
     *ELWIDTH
      COMMON /SOIL/ COUPLEf, RHOc, W, ATTENCO, Cfps
      YES='Y'
      NO='N'
      UNIFORM='U'
      CUBIC='C'
```

```
C
C     GIVE 'INPUT & OUTPUT' FILE NAMES FOR BLASTSDF
C
      WRITE (*,*)
  1   WRITE (*,'(A \)') 'ENTER DYNAMIC INPUT FILE NAME: '
      READ (*,'(A)') DYNIN
      WRITE (*,*)
      INQUIRE (FILE=DYNIN,EXIST=YESNO)
      IF (.NOT.YESNO) THEN
      WRITE (*,*)
      WRITE (*,*) 'DYNAMIC INPUT FILE DOES NOT EXIST! '
      WRITE (*,*)
      GO TO 1
      END IF
      WRITE (*,*)
  3   WRITE (*,'(A \)') ' ENTER OUTPUT FILE NAME:  '
      READ (*,'(A)') DYNOUT
      WRITE (*,*)
      INQUIRE (FILE=DYNOUT,EXIST=YESNO)
      IF (YESNO) THEN
      WRITE (*,*)
      WRITE (*,*) 'OUTPUT FILE ALREADY EXISTS! '
      WRITE (*,*)
      WRITE (*,*) 'WARNING:  UNLESS YOU SPECIFY A
     *DIFFERENT NAME, THE'
      WRITE (*,*) '        CURRENT OUTPUT FILE WILL BE
     *OVERWRITTEN!!'
      WRITE (*,*)
      WRITE (*,'(A \)') ' ENTER OUTPUT FILE NAME:  '
      READ (*,'(A)') DYNOUT
      WRITE (*,*)
      END IF
      WRITE (*,*)
```

```
  4   WRITE (*,'(A \)') 'ENTER STATIC INPUT FILE NAME:  '
      READ (*,'(A)') STATIN
      WRITE (*,*)
      INQUIRE (FILE=STATIN,EXIST=YESNO)
      IF (.NOT.YESNO) THEN
      WRITE (*,*) 'STATIC INPUT FILE DOES NOT EXIST!'
      WRITE (*,*)
      GO TO 4
      END IF
C
C     OPEN AND READ DYNAMIC INPUT FILE
C
      OPEN (10,FILE=DYNIN,FORM='FORMATTED',ACCESS
     *='SEQUENTIAL')
      READ (10,*) jSTEPS
      READ (10,*) NOEL,ELLENGTH,ELWIDTH
      READ (10,*) DOB
      READ (10,'(A)') LOADtype
      READ (10,'(A)') STATECHO
      READ (10,'(5A)') DLOADflg,TEMP1,DMASSflg,TEMP2,
     *DAMPflg
      READ (10,*) dTIME, TAUmax
      READ (10,*) nMASSgr,noelMgr1,(elMASS(I),
     *I=1,nMASSgr)
      READ (10,*) COUPLEf, RHOc, W, ATTENCO, Cfps
      CLOSE (10)
C
C     OPEN AND READ STATIC INPUT FILE
C
      OPEN (11,FILE=STATIN,FORM='FORMATTED',ACCESS
     *='SEQUENTIAL')
      IF (LOADtype.EQ.UNIFORM) THEN
      DO 20 J=1, jSTEPS+1
```

```
      READ (11,*) SIGMA(1,J)
      READ (11,*) NODEtemp, ubar(J)
      ubar(J)=-1.0*ubar(J)
      DO 20 I=1, NOEL
      READ (11,*) NODEtemp, Uj(I,J)
      Uj(I,J)=-1.0*Uj(I,J)
   20 CONTINUE
      ELSE IF (LOADtype.EQ.CUBIC) THEN
      DO 25 J=1, jSTEPS+1
      DO 21 I=1, NOEL
      READ (11,*) SIGMA(I,J)
   21 CONTINUE
      READ (11,*) NODEtemp, ubar(J)
      ubar(J)=-1.0*ubar(J)
      DO 25 I=1, NOEL
      READ (11,*) NODEtemp, Uj(I,J)
      Uj(I,J)=-1.0*Uj(I,J)
   25 CONTINUE
      ELSE
      WRITE (*,*)
      WRITE (*,*) 'ERROR IN STATIC LOAD TYPE! '
      STOP
      END IF
      CLOSE (11)
C
C     CONVERT INPUT PRESSURES TO FORCE
C
      IF (LOADtype.EQ.UNIFORM) THEN
      DO 30 J=1, jSTEPS+1
      Fj(1,J)=SIGMA(1,J)*ELLENGTH*ELWIDTH
   30 CONTINUE
      ELSE
      DO 35 J=1, jSTEPS+1
```

```
      DO 35 I=1, NOEL
      Fj(I,J)=SIGMA(I,J)*ELLENGTH*ELWIDTH
   35 CONTINUE
      END IF
C
C     OPEN OUTPUT FILE
C
      OPEN (12,FILE=DYNOUT,FORM='FORMATTED',ACCESS
     *='SEQUENTIAL')
C
C     PRINT INPUT FILE *.DIN VALUES
C
      WRITE (12,*) 'INPUT FROM FILE *.DIN'
      WRITE (12,*)
      WRITE (12,36) NOEL,ELLENGTH,ELWIDTH
   36 FORMAT (4X,'NUMBER OF ELEMENTS: ',7X,I3,/,4X,
     *'ELEMENT LENGTH: ',11X,F6.2,' inches',/,4X,
     *'MEMBER WIDTH: ',13X,F6.2,' inches',/)
      WRITE (12,37) DOB,W
   37 FORMAT (4X,'CHARGE STANDOFF: ',8X,F8.2,' inches',/,
     *4X,'CHARGE WEIGHT:   ',8X,F8.2,' lbs.',/)
      WRITE (12,38) COUPLEf,RHOc,ATTENCO,Cfps
   38 FORMAT (4X,'COUPLING FACTOR: ',8X,F8.2,/,4X,
     *'ACOUSTIC IMPEDANCE: ',5X,F8.2,' psi/fps',/,4X,
     *'ATTENUATION COEFFICIENT: ',2X,F6.2,/,4X,
     *'SEISMIC VELOCITY: ',7X,F8.2,' fps',/)
      IF (LOADtype.EQ.UNIFORM) THEN
      WRITE (12,*) ' STATIC LOAD APPROXIMATION:  UNIFORM'
      END IF
      IF (LOADtype.EQ.CUBIC) THEN
      WRITE (12,*) '   STATIC LOAD APPROXIMATION:  CUBIC'
      END IF
      WRITE (12,*)
```

```
C
C     SHIFT VALUES FOR Uj & ubar TO DYNAMIC INITIAL
C     CONDITIONS
C
      ubaro=ubar(1)
      DO 40 I=1, NOEL
      Ujo(I)=Uj(I,1)
   40 CONTINUE
      DO 50 J=1, jSTEPS+1
      ubar(J)=ubar(J)-ubaro
      DO 50 I=1, NOEL
      Uj(I,J)=Uj(I,J)-Ujo(I)
   50 CONTINUE
C
C     SHIFT VALUES OF Fj TO INITIAL DYNAMIC CONDITIONS
C     FOR UNIFORM LOAD & THEN DISPERSE THROUGH OUT
C     Fj(I,J). CUBIC LOADS ALREADY IN INITIAL DYNAMIC
C     CONDITIONS!
C
      IF (LOADtype.EQ.UNIFORM) THEN
      Fo=Fj(1,1)
      DO 60 J=1, jSTEPS+1
      Fj(1,J)=Fj(1,J)-Fo
      DO 60 I=1, NOEL
      Fj(I,J)=Fj(1,J)
   60 CONTINUE
      END IF
C
C     GENERATE Rx(I) & Xi(I) FOR EACH ELEMENT IN MEMBER.
C
      Xi(1)=ELLENGTH/2.0
      DO 70 I=2, NOEL
      Xi(I)=Xi(I-1)+ELLENGTH
```

```
 70   CONTINUE
      DO 80 I=1, NOEL
      Rx(I)=((DOB**2.0)+(Xi(I)**2.0))**0.5
 80   CONTINUE
C
C     PRINT STATIC INPUT IF STATECHO = "YES"
C
      IF (STATECHO.EQ.YES) THEN
      CALL STATPRT (jSTEPS,NOEL)
      END IF
C
C     BEGIN DYNAMIC ANALYSIS!  COMPLETED IN SUBROUTINE
C     DYNANAL
C
      CALL DYNANAL(DOB,jSTEPS,DLOADflg,DMASSflg, DAMPflg,
     *ubaro)
      CLOSE (12)
      STOP
      END


      SUBROUTINE STATPRT (jSTEPS,NOEL)
      IMPLICIT REAL (A-H,O-Z)
      IMPLICIT INTEGER (I-N)
      COMMON /STATIC/ Uj(40,41),ubar(41),Fj(40,41)
      WRITE (12,*) 'STATIC INPUT ECHO!'
      WRITE (12,*)
      jTOTAL=jSTEPS+1
      WRITE (12,*) 'TOTAL STATIC SHAPE/LOAD VECTORS: ',
     *jTOTAL
      WRITE (12,*) 'NUMBER OF ELEMENTS: ',NOEL
      WRITE (12,*)
      DO 30 J=1,jSTEPS+1
```

```
      WRITE (12,*)
      WRITE (12,*) 'STATIC SHAPE NUMBER:  ',J
      WRITE (12,5) ubar(J)
 5    FORMAT (1X,'CENTERLINE DEFLECTION: ',F8.4,
     *'  INCHES')
      WRITE (12,*)
      WRITE (12,6)
 6    FORMAT (1X,'ELEMENT',3X,'DISPLACED SHAPE',5X,
     *'LOAD',/,14X,'(INCHES)',9X,'(LBS)')
      DO 30 I=1, NOEL
      WRITE (12,7) I, Uj(I,J), Fj(I,J)
 7    FORMAT (2X,I3,9X,F8.4,7X,F9.1)
30    CONTINUE
      RETURN
      END


      SUBROUTINE DYNANAL(DOB,jSTEPS,DLOADflg,DMASSflg,
     *DAMPflg, ubaro)
      IMPLICIT REAL (A-H,O-Z)
      IMPLICIT INTEGER (I-N)
      CHARACTER*1 DLOADflg, DMASSflg, DAMPflg, YES, NO
      DIMENSION dUjp1(40), dFjp1(40), diaMASS(40),
     *diaC(40)
      COMMON /DYNAMIC/ Pn(40),elMASS(2),dTIME,TAUmax,
     *nMASSgr,noelMgr1
      COMMON /STATIC/ Uj(40,41), ubar(41), Fj(40,41)
      COMMON /GEOMETRY/ Rx(40), Xi(40), NOEL, ELLENGTH,
     *ELWIDTH
      COMMON /SOIL/ COUPLEf, RHOc, W, ATTENCO, Cfps
      YES='Y'
      NO='N'
```

```
C
C     COMPLETE DYNAMIC ANALYSIS WITHIN 'DO WHILE
C     (TAUn.LE.TAUmax)' LOOP
C
      WRITE (12,1)
    1 FORMAT (/,'DYNAMIC ANALYSIS OUTPUT!',/)
C
C     GENERATE LUMPED MASS MATRIX (diaMASS)
C
      WRITE (12,4)
    4 FORMAT (/,2X,'DYNAMIC MASS:  ')
      IF (DMASSflg.NE.YES) THEN
      DO 7 I=1, nMASSgr
      WRITE (12,6) I, elMASS(I)
    6 FORMAT (5X,'ELEMENT MASS OF GROUP',I3,' = ',F10.2,
     *' lb*ms**2/in')
    7 CONTINUE
      END IF
      DO 10 I=1, NOEL
      IF (I.LE.noelMgr1) THEN
      diaMASS(I)=elMASS(1)
      ELSE
      diaMASS(I)=elMASS(2)
      END IF
      IF (DMASSflg.EQ.YES) THEN
      WRITE (12,9) I, diaMASS(I)
    9 FORMAT (5X,'ELEMENT: ',I3,5X,'MASS: ',F10.2,
     *'lb*ms**2/in')
      END IF
   10 CONTINUE
C
C     DETERMINE DAMPING COEFFIEIENT 'Ci'
C
```

```
      Ci=RHOc*ELLENGTH*ELWIDTH*1000.0/12.0
      IF (DAMPflg.NE.YES) THEN
      WRITE (12,11) Ci
   11 FORMAT (/,2X,'DAMPING COEFFICIENT: ',F10.2,
     *' lb*ms/in')
      END IF
      unp1=0.0
      TAU=dTIME
      unTOTAL=ubaro
      WRITE (12,16) TAU, unp1, unTOTAL
   16 FORMAT (/,2X,'TIME = ',F6.2,' msec ',/,5X,
     *'CL DISPLACEMENT:', 4X,'DYNAMIC =',F8.4,' INCHES',
     *4X,'TOTAL =',F8.4,' INCHES')
      unm1=0.0
      un=0.0
      TAUn=dTIME
      DO 100 WHILE (TAUn.LT.TAUmax)
C
C     DETERIMINE WHICH STATIC SHAPE FUNCTION THE DYNAMIC
C     DISPLACEMENT IS BETWEEN DURING THIS DYNAMIC TIME
C     STEP
C
      J=1
      DO 20 WHILE (ubar(J).LE.un)
      J=J+1
      IF (J.GT.jSTEPS+1) THEN
      WRITE (*,*) 'WARNING:  DYNAMIC DISPLACEMENT HAS
     *EXCEEDED'
      WRITE (*,*) '          STATIC VALUES!!!'
      WRITE (12,19)
   19 FORMAT (//,2X,'WARNING:  DYNAMIC DISPLACEMENT HAS
     *EXCEEDED',/,2X,'          STATIC VALUES!!!',//,
     *'EXECUTION TERMINATED!')
```

```
      STOP
      END IF
   20 END DO
      jSTATIC=J-1
      WRITE (12,22) jSTATIC
   22 FORMAT (5X,'jSTATIC = ',I4)
C
C     DETERMINE DYNAMIC LOAD VECTOR Pn(NOEL) FOR CURRENT
C     DYNAMIC TIME STEP!
C
      CALL DYNLOAD(TAUn, DOB, DLOADflg)
C
C     DETERMINE DAMPING MATRIX diaC(I)
C
      IF (DAMPflg.EQ.YES) THEN
      WRITE (12,25)
   25 FORMAT (/,2X,'DAMPING MATRIX:')
      END IF
      DO 30 I=1, NOEL
      IF (Pn(I).GT.0.0) THEN
      diaC(I)=Ci
      ELSE
      diaC(I)=0.0
      END IF
      IF (DAMPflg.EQ.YES) THEN
      WRITE (12,26) I, diaC(I)
   26 FORMAT (2X,'ELEMENT: ',I3,5X,'DAMPING: ',F10.2)
      END IF
   30 CONTINUE
C
C     DETERMINE STATIC VECTOR CONSTANTS FOR DYNAMIC TIME
C     STEP 'n'
C
```

```
      DO 40 I=1, NOEL
      dUjp1(I)=Uj(I,jSTATIC+1)-Uj(I,jSTATIC)
      dFjp1(I)=Fj(I,jSTATIC+1)-Fj(I,jSTATIC)
   40 CONTINUE
      dubarjp1=ubar(jSTATIC+1)-ubar(jSTATIC)
C
C     DETERMINE SCALAR CONSTANTS FOR DYNAMIC TIME
C     STEP 'n'
C
      mSTAR=0.0
      cSTAR=0.0
      fSTAR=0.0
      pnSTAR=0.0
      dUFSTAR=0.0
      DO 50 I=1, NOEL
      mSTAR=(dUjp1(I)**2.0)*diaMASS(I)+mSTAR
      cSTAR=(dUjp1(I)**2.0)*diaC(I)+cSTAR
      fSTAR=dUjp1(I)*dFjp1(I)+fSTAR
      pnSTAR=dUjp1(I)*Pn(I)+pnSTAR
      dUFSTAR=dUjp1(I)*Fj(I,jSTATIC)+dUFSTAR
   50 CONTINUE
      mSTAR=mSTAR/dubarjp1
      cSTAR=cSTAR/dubarjp1
      fSTAR=fSTAR/dubarjp1
      fSTARu=fSTAR*ubar(jSTATIC)
C
C     DO ACTUAL DYNAMIC TIME INCREMENT FROM nSTEP
C     TO GET 'unp1'
C
      mdT2=mSTAR/(dTIME**2.0)
      c2dT=cSTAR/(2.0*dTIME)
      unp1=pnSTAR-dUFSTAR+fSTARu-(((-2.0)*mdT2+fSTAR)*un)
      unp1=unp1-((mdT2-c2dT)*unm1)
```

```
      unp1=unp1/(mdT2+c2dT)
      TAUnp1=TAUn+dTIME
      unTOTAL=unp1+ubaro
      WRITE (12,16) TAUnp1, unp1, unTOTAL
      unm1=un
      un=unp1
      TAUn=TAUnp1
      WRITE (*,99) TAUn
   99 FORMAT (2X,'DYNAMIC ANALYSIS:  TIME = ', F8.3)
  100 END DO
      RETURN
      END


      SUBROUTINE DYNLOAD (TAU,Dinch,DLOADflg)
C
C     THIS SUBROUTINE GENERATES THE DYNAMIC LOAD VECTOR
C     Pn(NOEL) AS A FUNCTION OF DYNAMIC TIME AND LOCATION
C     ALONG SPAN
C
      IMPLICIT REAL (A-H,O-Z)
      IMPLICIT INTEGER (I-N)
      CHARACTER*1 DLOADflg, YES, NO
      COMMON /DYNAMIC/ Pn(40),elMASS(2),dTIME,TAUmax,
     *nMASSgr,noelMgr1
      COMMON /GEOMETRY/ Rx(40), Xi(40), NOEL, ELLENGTH,
     *ELWIDTH
      COMMON /SOIL/ COUPLEf, RHOc, W, ATTENCO, Cfps
      YES='Y'
      NO='N'
      EXPON=1.0/3.0
      IF (DLOADflg.EQ.YES) THEN
      WRITE (12,5) TAU
```

```
5  FORMAT (/,2X,'LOAD VECTOR Pn FOR TIME: ',F8.4,/2X,
     *'ELEMENT',5X,'LOAD')
      END IF
      DO 10 I=1, NOEL
      THETA=ATAN(Xi(I)/Dinch)
      THETA2=2.0*THETA
      Rft=Rx(I)/12.0
      Po=COUPLEf*RHOc*160.0*((Rft/(W**EXPON))**ATTENCO)
      Ta=(Rft/Cfps)*1000.0
      Tr=0.1*Ta
      TaMS=(Dinch/(12.0*Cfps))*1000.0
      TIME=TAU+TaMS
      TIMEo=Ta+Tr
      IF (TIME.LT.Ta) THEN
      Pr=0.0
      ELSE IF (TIME.GE.Ta.AND.TIME.LE.TIMEo) THEN
      Pr=Po*(TIME-Ta)/Tr
      ELSE
      Pr=Po*EXP((Ta-TIME)/Ta)
      END IF
C
C     Pn(NOEL) IS NORMAL PRESSURE AT A POINT Xi &
C     INCLUDES A REFLECTION FACTOR OF 2!
C
      Pn(I)=Pr*(1.5+0.5*COS(THETA2))
C
C     CONVERT PRESSURE 'Pn' TO FORCE 'Pn'
C
      Pn(I)=Pn(I)*ELLENGTH*ELWIDTH
      IF (DLOADflg.EQ.YES) THEN
      WRITE (12,9) I, Pn(I)
```

```
 9  FORMAT (5X,I3,2X,F10.2)
    END IF
10  CONTINUE
    RETURN
    END
```

Appendix III

BLASTSDF Static Input File Format

<u>Cubic Distribution</u>:

$\sigma_{d1}(I)=0.0$ for I = 1 to NOEL

Node, $\underline{u}_{d1}$

Node, $\mathbf{U}_{d1}(I)$ for I = 1 to NOEL

for j = 2 to jSTEPS+1

$\sigma_j(I)$ for I = 1 to NOEL

Node, $\underline{u}_j$

Node, $\mathbf{U}_j(I)$ for I = 1 to NOEL

<u>Uniform Distribution</u>:

σ_{d1}

Node, $\underline{u}_{d1}$

Node, $\mathbf{U}_j(I)$ for I = 1 to NOEL

for j = 2 to jSTEPS+1

σ_j

Node, $\underline{u}_j$

Node, $\mathbf{U}_j(I)$ for I = 1 to NOEL

Nomenclature:

σ - Pressure load on structure

NOEL - Number of elements

Node - Node number

$\underline{u}$ - Static centerline deflection

U - Static shape function vector

jSTEPS - Number of static shape functions

Subscripts:

dl - Dead load (soil & concrete)

j - Static load step

Sample Cubic Load Distribution Input File (Partial File)

```
0.0
0.0
0.0
0.0
0.0
0.0
0.0
0.0
0.0
0.0
0.0
0.0
0.0
0.0
     801        -0.2189
     802        -0.2182
     804        -0.2117
     806        -0.2000
     808        -0.1847
```

```
    810        -0.1682
    812        -0.1508
    814        -0.1326
    816        -0.1138
    818        -9.4650E-02
    820        -7.5443E-02
    822        -5.6454E-02
    824        -3.8016E-02
    826        -2.0350E-02
    828        -5.3998E-03
4.990448903239
4.915122173223
4.770032257099
4.565376471272
4.314395329755
4.031542380427
3.730823875733
3.424580260171
3.122802478722
2.83293016211
2.56
2.30699689089
2.075284338945
1.865029503007
    801        -0.3084
    802        -0.3076
    804        -0.2994
    806        -0.2841
    808        -0.2624
    810        -0.2391
    812        -0.2146
    814        -0.1891
    816        -0.1629
    818        -0.1361
    820        -0.1092
    822        -8.2448E-02
    824        -5.6448E-02
    826        -3.0544E-02
    828        -5.8785E-03
8.982808025829
8.847219911801
8.586058062779
8.21767764829
7.765911593559
7.256776284768
6.71548297632
6.164244468308
5.6210444617
5.099274291798
```

```
4.608
4.152594403602
3.735511810101
3.357053105412
    801        -0.4063
    802        -0.4055
    804        -0.3966
    806        -0.3787
    808        -0.3525
    810        -0.3211
    812        -0.2878
    814        -0.2532
    816        -0.2179
    818        -0.1820
    820        -0.1461
    822        -0.1105
    824        -7.5050E-02
    826        -4.1864E-02
    828        -9.4311E-03
```

Sample Uniform Load Distribution Input File (Partial)

```
20.00
    801        -6.1925E-02
    802        -6.1824E-02
    804        -6.1023E-02
    806        -5.9457E-02
    808        -5.7191E-02
    810        -5.4364E-02
    812        -5.1363E-02
    814        -4.8171E-02
    816        -4.4411E-02
    818        -3.9983E-02
    820        -3.4850E-02
    822        -2.9010E-02
    824        -2.2478E-02
    826        -1.5286E-02
    828        -7.5742E-03
    830         4.0460E-04
    832         8.6258E-03
    834         1.7263E-02
    836         2.6384E-02
    838         3.5966E-02
    840         4.5938E-02
    842         5.6156E-02
```

30.00

801	-0.1548
802	-0.1545
804	-0.1525
806	-0.1486
808	-0.1429
810	-0.1355
812	-0.1269
814	-0.1172
816	-0.1061
818	-9.3555E-02
820	-7.9755E-02
822	-6.4814E-02
824	-4.8926E-02
826	-3.2300E-02
828	-1.5344E-02
830	1.3136E-03
832	1.7594E-02
834	3.3948E-02
836	5.0621E-02
838	6.7667E-02
840	8.5077E-02
842	0.1028

34.00

801	-0.3230
802	-0.3221
804	-0.3142
806	-0.2991
808	-0.2818
810	-0.2624
812	-0.2415
814	-0.2192
816	-0.1953
818	-0.1698
820	-0.1429
822	-0.1147
824	-8.5638E-02
826	-5.5861E-02
828	-2.5971E-02
830	3.4451E-03
832	3.2301E-02
834	6.0988E-02
836	8.9891E-02
838	0.1191
840	0.1487
842	0.1785

Appendix IV

BLASTSDF Dynamic Input File Format

Format:

```
jSTEPS
NOEL,ELLENGTH,ELWIDTH
DOB
LOADtype
STATECHO
DLOADflg,DMASSflg,DAMPflg
dTIME,TAUmax
nMASSgr,noelMgr1,elMASS(I)          For I = 1 to nMASSgr
COUPLEf,RHOc,W,ATTENCO,Cfps
```

Nomenclature:

```
jSTEPS    - Number of static load/shape vectors
NOEL      - Number of elements along span
ELLENGTH  - Element length (inches)
ELWIDTH   - Element width (inches)
DOB       - Depth of burial of structure (inches)
LOADtype  - Static load approximation,
            Cubic (C) or Uniform (U)
STAECHO   - Output flag to print static input values (Y/N)
DLOADflg  - Output flag to print dynamic load (Y/N)
DMASSflg  - Output flag to print mass vector (Y/N)
DAMPflg   - Output flag to print SSI damping vector (Y/N)
```

dTIME - Time step increment for use in dynamic analysis (milliseconds, ms)

TAUmax - Dynamic time at which to stop analysis (ms)

nMASSgr - Number of mass groups (1 or 2)

noelMgr1 - Number of elements in mass group 1

elMASS - Value of lumped element mass ($lb \cdot ms^2/in$)

COUPLEf - Coupling factor

RHOc - ρc, soil parameter (psi/fps)

W - Charge weight (lbs of TNT)

ATTENCO - Soil attenuation coefficient

Cfps - Seimic velocity of soil (ft/sec)

<u>Sample File</u>:

```
38
21,18.0,12.0
252.0
U
N
N,N,N
1.0,100.0
1,21,2.5718E6
0.4,22.0,1014.0,-2.75,1000.0
```

Appendix V

ABAQUS Dynamic Input File for Member PC53-6

```
*HEADING, PAGESIZE=2000
 PC BEAM  SIMPLE / CANTILEVER ENDS
 h=53"    6 - 1/2" 7W STRAND (LR)    (HARP @ 7.5')
 BLAST LOAD (W=1014 lbs TNT), DYNAMIC, NONLINEAR, UMAT91
 CPE8R,  MESH 21 (14 + 7) X 8  (ASPECT 2.7 TO 1.0)
 ELASTIC-PLASTIC SOIL SPRINGS  &  SSI-DASHPOTS
*PREPRINT, LOCAL INFO=NO, HISTORY=NO, MODEL=NO, ECHO=YES
*NODE
1,0.0,0.0
43,378.0,0.0
1601,0.0,53.0
1643,378.0,53.0
*NGEN,NSET=MID
1,1601,100
*NGEN,NSET=END
43,1643,100
*NFILL
MID,END,42,1
*NSET,NSET=NAXIS,GENERATE
801,843,1
*NSET,NSET=BOTEDGE,GENERATE
1,43,1
*NSET,NSET=N29
29
*NSET,NSET=N801
801
*ELEMENT,TYPE=CPE8R
1,1,3,203,201,2,103,202,101
```

```
*ELGEN,ELSET=ALLCON
1,21,2,1,8,200,100
*ELEMENT, TYPE=SPRING1
815,1630
*ELGEN, ELSET=SPRINGS
815,7,2,1,1
*ELEMENT,TYPE=DASHPOT1
901,1602
*ELGEN,ELSET=DASHPOTS
901,21,2,1,1
*ELSET,ELSET=PRESTR1
1,2,3,4,5,6,106,107,108,208,209,309,310,311,411,412
*ELSET,ELSET=PRESTR2
512,513,514,614,615,616,516,517,518,519,419,420,421
*ELSET,ELSET=PRESTR
PRESTR1,PRESTR2
*ELSET,ELSET=TOP,GENERATE
701,721,1
*ELSET,ELSET=T4BAR8,GENERATE
701,711,1
*ELSET,ELSET=T2BAR8,GENERATE
712,721,1
*ELSET,ELSET=BOT,GENERATE
1,21,1
*ELSET,ELSET=B2BAR3,GENERATE
1,10,1
*ELSET,ELSET=B4BAR8,GENERATE
11,21,1
*ELSET,ELSET=THARPDIS
714,715
*ELSET,ELSET=SUPDISC
14,15
*ELSET,ELSET=CONCSTR
```

```
1,701,THARPDIS,SUPDISC
*ELSET,ELSET=STLSTR
1,614,615,THARPDIS
*ELSET,ELSET=STIR13,GENERATE
13,713,100
*ELSET,ELSET=STIR14,GENERATE
14,714,100
*ELSET,ELSET=STIR15,GENERATE
15,715,100
*ELSET,ELSET=STIR21,GENERATE
21,721,100
*ELSET,ELSET=E701
701
*REBAR,ELEMENT=CONTINUUM,MATERIAL=MSTRAND,GEOMETRY=SKEW,
  NAME=STRAND
1,0.918,12.0,0.0
0.0,0.649,0.0,0.351
2,0.918,12.0,0.0
0.0,0.649,0.0,0.351
3,0.918,12.0,0.0
0.0,0.649,0.0,0.351
4,0.918,12.0,0.0
0.0,0.649,0.0,0.351
5,0.918,12.0,0.0
0.0,0.649,0.0,0.351
6,0.918,12.0,0.0
0.0,0.0,0.466,0.351
106,0.918,12.0,0.0
0.534,0.307,0.0,0.0
107,0.918,12.0,0.0
0.0,0.964,0.0,0.693
108,0.918,12.0,0.0
0.0,0.0,0.945,0.036
```

208,0.918,12.0,0.0
0.055,0.621,0.0,0.0
209,0.918,12.0,0.0
0.0,0.0,0.424,0.379
309,0.918,12.0,0.0
0.576,0.279,0.0,0.0
310,0.918,12.0,0.0
0.0,0.936,0.0,0.721
311,0.918,12.0,0.0
0.0,0.0,0.903,0.064
411,0.918,12.0,0.0
0.097,0.594,0.0,0.0
412,0.918,12.0,0.0
0.0,0.0,0.382,0.406
512,0.918,12.0,0.0
0.618,0.251,0.0,0.0
513,0.918,12.0,0.0
0.0,0.909,0.0,0.749
514,0.918,12.0,0.0
0.0,0.0,0.861,0.091
614,0.918,12.0,0.0
0.139,0.566,0.0,0.0
615,0.918,12.0,0.0
0.0,0.199,0.0,0.434
616,0.918,12.0,0.0
0.544,0.0,0.0,0.801
516,0.918,12.0,0.0
0.0,0.833,0.456,0.0
517,0.918,12.0,0.0
0.0,0.466,0.0,0.167
518,0.918,12.0,0.0
0.0,0.100,0.0,0.534
519,0.918,12.0,0.0

```
0.272,0.0,0.0,0.900
419,0.918,12.0,0.0
0.0,0.733,0.728,0.0
420,0.918,12.0,0.0
0.0,0.367,0.0,0.267
421,0.918,12.0,0.0
1.0,0.0,0.0,0.633
*REBAR,ELEMENT=CONTINUUM,MATERIAL=FLEXBAR,NAME=LBAR
B2BAR3,0.22,12.0,0.0,0.453,1
B4BAR8,3.16,12.0,0.0,0.453,1
*REBAR,ELEMENT=CONTINUUM,MATERIAL=FLEXBAR,NAME=UBAR
T4BAR8,3.16,12.0,0.0,0.453,3
T2BAR8,1.58,12.0,0.0,0.453,3
*REBAR,ELEMENT=CONTINUUM,MATERIAL=STIRUP,NAME=STIRS
STIR13,0.11,12.0,0.0,0.25,2
STIR13,0.11,12.0,0.0,0.25,4
STIR14,0.11,12.0,0.0,0.25,2
STIR14,0.11,12.0,0.0,0.25,4
STIR15,0.11,12.0,0.0,0.25,2
STIR15,0.11,12.0,0.0,0.25,4
STIR21,0.11,12.0,0.0,0.14,2
STIR21,0.11,12.0,0.0,0.28,2
STIR21,0.11,12.0,0.0,0.42,2
STIR21,0.11,12.0,0.0,0.56,2
*MATERIAL, NAME=CONC
*USER MATERIAL, CONSTANTS=4
3,6125.0,1.0E-4,4.5E6
*DEPVAR
4
*DENSITY
224.7
*MATERIAL, NAME=FLEXBAR
*ELASTIC
```

```
29.0E6,0.3
*PLASTIC,HARDENING=ISOTROPIC
72000.0,0.0
72000.0,0.0066
105000.0,0.0693
93000.0,0.1510
*DENSITY
734.0
*MATERIAL, NAME=STIRUP
*ELASTIC
29.0E6,0.3
*PLASTIC
60000.0,0.0
*DENSITY
734.0
*MATERIAL, NAME=MSTRAND
*ELASTIC
28.0E6,0.3
*PLASTIC, HARDENING=ISOTROPIC
224000.0,0.0
246600.0,0.0012
259200.0,0.0057
262400.0,0.0106
263900.0,0.0156
264800.0,0.0205
270000.0,0.0404
*DENSITY
734.0
*SPRING,ELSET=SPRINGS,NONLINEAR
2
0.0,-2.0
0.0,0.0
9720.0,0.75
```

```
**  COMMENT:  DASHPOTS USED TO APPROX. SSI EFFECTS
*DASHPOT,ELSET=DASHPOTS
2
396000.0
*SOLID SECTION, ELSET=ALLCON, MATERIAL=CONC
12.0
*BOUNDARY
MID,1
N29,2
*INITIAL CONDITIONS, TYPE=STRESS, REBAR
PRESTR,STRAND,182000.0
*USER SUBROUTINES
      SUBROUTINE DLOAD(PN,KSTEP,KINC,TAU,NOEL,NPT,
                       COORDS, JLTYP)
C
C     THIS SUBROUTINE DEFINES NORMAL PRESSURE FROM BLAST
C     AS A FUNCTION OF TIME AND DISTANCE FROM BLAST  &
C     DOES NOT INCLUDE SSI EFFECTS
C
      DIMENSION COORDS(3)
      CFACTOR=0.4
      RHOC=22.0
      W=1014.0
      D=252.0
      THETA=ATAN2(COORDS(1),D)
      THETA2=2.0*THETA
      ATTENCO=-2.75
      EXPON=1.0/3.0
      RFT=(COORDS(1)/SIN(THETA))/12.0
      CFPS=1000.0
      PO=CFACTOR*RHOC*160.0*((RFT/(W**EXPON))**ATTENCO)
      TA=(RFT/CFPS)*1000.0
      TR=0.1*TA
```

```
      TAMS=(D/(12.0*CFPS))*1000.0
C     MINUS 500.0 ms ADJUSTS DYNAMIC TIME FOR LOAD
C     "TRICK" IN INITIAL LOAD STEP DESCRIBED BELOW
      TIME=TAU+TAMS-500.0
      IF (NOEL.EQ.701.AND.NPT.EQ.2) THEN
      WRITE (*,*) 'DYNAMIC BLAST TIME = ',TIME
      END IF
      TIMEO=TR+TA
      IF (TIME.LT.TA) THEN
      PN=0.0
      RETURN
      ELSE IF (TIME.GE.TA.AND.TIME.LE.TIMEO) THEN
      PR=PO*(TIME-TA)/TR
      ELSE
      PR=PO*EXP((TA-TIME)/TA)
      END IF
C
C     FORMULA FOR 'PN' CONTAINS A REFLECTION FACTOR OF 2
C
      PN=PR*(1.5+0.5*COS(THETA2))
      RETURN
      END
*AMPLITUDE,NAME=DEADLOAD,TIME=D,VALUE=A
0.0,0.0,200.0,20.0,500.0,20.0
**  COMMENT:  PROBLEMS ENCOUNTERED DURING INITIAL STATIC
**            LOAD STEP DUE TO DASHPOTS USED TO APPROX.
**            SSI EFFECTS.  "TRICK" - IMPLEMENT INITIAL
**            LOAD STEP AS DYNAMIC STEP WITH SHARP RISE
**            TIME THEN HOLD CONSTANT UNTIL VIBRATION
**            DISSIPATES:  500 ms.  ADJUST DYNAMIC TIME
**            IN SUBROUTINE DLOAD BY 500 ms.
*STEP, INC=1000, CYCLE=3
*DYNAMIC, PTOL=100.0, INITIAL=NO, NOHAF, DIRECT=NOSTOP
```

```
10.0,500.0
*PRESTRESS HOLD
PRESTR, STRAND
*DLOAD,AMPLITUDE=DEADLOAD
TOP,P3,20.0
*PRINT, FREQUENCY=1000
*EL PRINT, SUMMARY=NO, ELSET=E701, FREQUENCY=100
S11,E11
*NODE PRINT, SUMMARY=NO, NSET=N801, FREQUENCY=5
U2
*END STEP
*STEP, INC=800, CYCLE=3
*DYNAMIC, PTOL=100.0, INITIAL=NO, NOHAF, DIRECT=NOSTOP
1.0,80.0
*DLOAD
TOP,P3NU
*PRINT, FREQUENCY=1000
*EL PRINT, SUMMARY=NO, ELSET=CONCSTR, FREQUENCY=25
S11,E11
*EL PRINT, SUMMARY=NO, ELSET=STLSTR, FREQUENCY=25
S11,E11
*NODE PRINT,SUMMARY=NO,NSET=N801,FREQUENCY=1
U2
*NODE PRINT,SUMMARY=NO,NSET=NAXIS,FREQUENCY=55
U2
*END STEP
```

Appendix VI

ABAQUS Static Input File for Member PC53-6

```
*HEADING, PAGESIZE=2000
 PC BEAM  SIMPLE / CANTILEVER ENDS
 h=53"    6 - 1/2" 7W STRAND (LR)    (HARP @ 7.5')
 ULTIMATE UNIFORM LOAD,   STATIC,  NONLINEAR,   UMAT91
 CPE8R   MESH 21 (14 + 7) X 8  (ASPECT 2.7 TO 1.0)
 ELASTIC-PLASTIC SOIL SPRINGS
*PREPRINT, LOCAL INFO=NO, HISTORY=NO, MODEL=NO, ECHO=YES
*NODE
1,0.0,0.0
43,378.0,0.0
1601,0.0,53.0
1643,378.0,53.0
*NGEN,NSET=MID
1,1601,100
*NGEN,NSET=END
43,1643,100
*NFILL
MID,END,42,1
*NSET,NSET=PNAXIS,GENERATE
802,842,2
*NSET,NSET=NAXIS
801,PNAXIS
*NSET,NSET=BOTEDGE,GENERATE
1,43,1
*NSET,NSET=N29
29
*NSET,NSET=N801
```

```
801
*ELEMENT,TYPE=CPE8R
1,1,3,203,201,2,103,202,101
*ELGEN,ELSET=ALLCON
1,21,2,1,8,200,100
*ELEMENT, TYPE=SPRING1
830,1630
*ELGEN, ELSET=SPRINGS
830,7,2,2,1
*ELSET,ELSET=PRESTR1
1,2,3,4,5,6,106,107,108,208,209,309,310,311,411,412
*ELSET,ELSET=PRESTR2
512,513,514,614,615,616,516,517,518,519,419,420,421
*ELSET,ELSET=PRESTR
PRESTR1,PRESTR2
*ELSET,ELSET=TOP,GENERATE
701,721,1
*ELSET,ELSET=T4BAR8,GENERATE
701,711,1
*ELSET,ELSET=T2BAR8,GENERATE
712,721,1
*ELSET,ELSET=BOT,GENERATE
1,21,1
*ELSET,ELSET=B2BAR3,GENERATE
1,10,1
*ELSET,ELSET=B4BAR8,GENERATE
11,21,1
*ELSET,ELSET=THARPDIS
714,715
*ELSET,ELSET=SUPDISC
14,15
```

```
*ELSET,ELSET=CONCSTR
1,701,THARPDIS,SUPDISC
*ELSET,ELSET=STLSTR
1,614,615,THARPDIS
*ELSET,ELSET=STIR13,GENERATE
13,713,100
*ELSET,ELSET=STIR14,GENERATE
14,714,100
*ELSET,ELSET=STIR15,GENERATE
15,715,100
*ELSET,ELSET=STIR21,GENERATE
21,721,100
*ELSET,ELSET=E701
701
*REBAR,ELEMENT=CONTINUUM,MATERIAL=MSTRAND,GEOMETRY=SKEW,
  NAME=STRAND
1,0.918,12.0,0.0
0.0,0.649,0.0,0.351
2,0.918,12.0,0.0
0.0,0.649,0.0,0.351
3,0.918,12.0,0.0
0.0,0.649,0.0,0.351
4,0.918,12.0,0.0
0.0,0.649,0.0,0.351
5,0.918,12.0,0.0
0.0,0.649,0.0,0.351
6,0.918,12.0,0.0
0.0,0.0,0.466,0.351
106,0.918,12.0,0.0
0.534,0.307,0.0,0.0
107,0.918,12.0,0.0
0.0,0.964,0.0,0.693
```

```
108,0.918,12.0,0.0
0.0,0.0,0.945,0.036
208,0.918,12.0,0.0
0.055,0.621,0.0,0.0
209,0.918,12.0,0.0
0.0,0.0,0.424,0.379
309,0.918,12.0,0.0
0.576,0.279,0.0,0.0
310,0.918,12.0,0.0
0.0,0.936,0.0,0.721
311,0.918,12.0,0.0
0.0,0.0,0.903,0.064
411,0.918,12.0,0.0
0.097,0.594,0.0,0.0
412,0.918,12.0,0.0
0.0,0.0,0.382,0.406
512,0.918,12.0,0.0
0.618,0.251,0.0,0.0
513,0.918,12.0,0.0
0.0,0.909,0.0,0.749
514,0.918,12.0,0.0
0.0,0.0,0.861,0.091
614,0.918,12.0,0.0
0.139,0.566,0.0,0.0
615,0.918,12.0,0.0
0.0,0.199,0.0,0.434
616,0.918,12.0,0.0
0.544,0.0,0.0,0.801
516,0.918,12.0,0.0
0.0,0.833,0.456,0.0
517,0.918,12.0,0.0
```

```
0.0,0.466,0.0,0.167
518,0.918,12.0,0.0
0.0,0.100,0.0,0.534
519,0.918,12.0,0.0
0.272,0.0,0.0,0.900
419,0.918,12.0,0.0
0.0,0.733,0.728,0.0
420,0.918,12.0,0.0
0.0,0.367,0.0,0.267
421,0.918,12.0,0.0
1.0,0.0,0.0,0.633
*REBAR,ELEMENT=CONTINUUM,MATERIAL=FLEXBAR,NAME=LBAR
B2BAR3,0.22,12.0,0.0,0.453,1
B4BAR8,3.16,12.0,0.0,0.453,1
*REBAR,ELEMENT=CONTINUUM,MATERIAL=FLEXBAR,NAME=UBAR
T4BAR8,3.16,12.0,0.0,0.453,3
T2BAR8,1.58,12.0,0.0,0.453,3
*REBAR,ELEMENT=CONTINUUM,MATERIAL=STIRUP,NAME=STIRS
STIR13,0.11,12.0,0.0,0.25,2
STIR13,0.11,12.0,0.0,0.25,4
STIR14,0.11,12.0,0.0,0.25,2
STIR14,0.11,12.0,0.0,0.25,4
STIR15,0.11,12.0,0.0,0.25,2
STIR15,0.11,12.0,0.0,0.25,4
STIR21,0.11,12.0,0.0,0.14,2
STIR21,0.11,12.0,0.0,0.28,2
STIR21,0.11,12.0,0.0,0.42,2
STIR21,0.11,12.0,0.0,0.56,2
*MATERIAL, NAME=CONC
*USER MATERIAL, CONSTANTS=5
3,6125.0,1.0E-4,4.5E6,0.15
```

```
*DEPVAR
4
*MATERIAL, NAME=FLEXBAR
*ELASTIC
29.0E6,0.3
*PLASTIC,HARDENING=ISOTROPIC
72000.0,0.0
72000.0,0.0066
105000.0,0.0693
93000.0,0.1510
*MATERIAL, NAME=STIRUP
*ELASTIC
29.0E6,0.3
*PLASTIC
60000.0,0.0
*MATERIAL, NAME=MSTRAND
*ELASTIC
28.0E6,0.3
*PLASTIC, HARDENING=ISOTROPIC
224000.0,0.0
246600.0,0.0012
259200.0,0.0057
262400.0,0.0106
263900.0,0.0156
264800.0,0.0205
270000.0,0.0404
*SPRING,ELSET=SPRINGS,NONLINEAR
2
0.0,-2.0
0.0,0.0
9720.0,0.75
```

```
*SOLID SECTION, ELSET=ALLCON, MATERIAL=CONC
12.0
*BOUNDARY
MID,1
N29,2
*INITIAL CONDITIONS, TYPE=STRESS, REBAR
PRESTR,STRAND,182000.0
*STEP, INC=20, CYCLE=3
*STATIC, PTOL=100.0, DIRECT=NOSTOP
1.0,1.0
*PRESTRESS HOLD
PRESTR, STRAND
*DLOAD
TOP,P3,20.0
*PRINT, FREQUENCY=50
*EL PRINT, SUMMARY=NO, ELSET=E701, FREQUENCY=20
LOADS
*NODE PRINT, SUMMARY=NO, NSET=NAXIS, FREQUENCY=20
U2
*EL PRINT, SUMMARY=NO, ELSET=SPRINGS, FREQUENCY=20
S11
*END STEP
*STEP, INC=40, CYCLE=3
*STATIC, PTOL=100.0, DIRECT=NOSTOP
1.0,10.0
*DLOAD
TOP,P3,30.0
*PRINT, FREQUENCY=50
*EL PRINT, SUMMARY=NO, ELSET=E701, FREQUENCY=10
LOADS
*NODE PRINT, SUMMARY=NO, NSET=NAXIS, FREQUENCY=10
```

```
U2
*EL PRINT, SUMMARY=NO, ELSET=SPRINGS, FREQUENCY=10
S11
*END STEP
*STEP, INC=40, CYCLE=3
*STATIC, PTOL=100.0, DIRECT=NOSTOP
1.0,20.0
*DLOAD
TOP,P3,50.0
*PRINT, FREQUENCY=50
*EL PRINT, SUMMARY=NO, ELSET=E701, FREQUENCY=2
LOADS
*NODE PRINT, SUMMARY=NO, NSET=NAXIS, FREQUENCY=2
U2
*EL PRINT, SUMMARY=NO, ELSET=SPRINGS, FREQUENCY=2
S11
*END STEP
*STEP, INC=40, CYCLE=3
*STATIC, PTOL=100.0, DIRECT=NOSTOP
0.25,10.0
*DLOAD
TOP,P3,60.0
*PRINT, FREQUENCY=50
*EL PRINT, SUMMARY=NO, ELSET=E701, FREQUENCY=1
LOADS
*NODE PRINT, SUMMARY=NO, NSET=NAXIS, FREQUENCY=1
U2
*EL PRINT, SUMMARY=NO, ELSET=SPRINGS, FREQUENCY=1
S11
*END STEP
```

References

1. Lin, T. Y., and Burns, N. H., *Design of Prestressed Concrete Structures*, 3rd Edition, John Wiley and Sons, New York, NY, 1981.

2. Wang, C., and Salmon, C. G., *Reinforced Concrete Design*, 3rd Edition, Harper and Row Publishers, Inc., New York, NY, 1979.

3. Dobbs, N., *Structures to Resist the Effects of Accidental Explosions - Volume I (Introduction)*, Special Publication ARLCD-SP-84001, U. S. Army Armament Research, Development and Engineering Center, Armament Engineering Directorate, Picatinny Arsenal, Dover, NJ, December, 1987.

4. *Fundamentals of Protective Design for Conventional Weapons*, TM5-855-1, Department of the Army, Waterways Experiment Station, Structures Laboratory, Corps of Engineers, Vicksburg, MS, July, 1984.

5. *ABAQUS Users' Manual* (Version 4.8), Hibbitt, Karlsson, and Sorensen, Inc., Providence, RI, 1989.

6. *ABAQUS Theory Manual* (Version 4.8), Hibbitt, Karlsson, and Sorensen, Inc., Providence, RI, 1989.

7. *Symposium Proceedings on the Interaction of Non-Nuclear Munitions with Structures*, U. S. Air Force Academy, Colorado Springs, CO, May 10-13, 1983.

8. *Proceedings of the Second Symposium on the Interaction of Non-Nuclear Munitions with Structures*, Panama City Beach, FL, April 15-18, 1985.

9. *International Symposium Proceedings on the Interaction of Non-Nuclear Munitions with Structures*, Mannheim, West Germany, March 9-13, 1987.

10. *Proceedings of the Fourth International Symposium on the Interaction of Non-Nuclear Munitions with Structures*, Panama City Beach, FL, April 17-21, 1989.

11. Ayvazyan, H., Dede, M., Dobbs, N., Whitney, M., Bowles, P., and Baker, W., *Structures to Resist the Effects of Accidental Explosions - Volume II (Blast, Fragments, and Shock Loads)*, Special Publication ARLCD-SP-84001, U. S. Army Armament Engineering Directorate, Picatinny Arsenal, Dover, NJ, December 1986.

12. Dede, M., Sock, F., Lipvin-Schramm, S., and Dobbs, N., *Structures to Resist the Effects of Accidental Explosions - Volume III (Principles of Dynamics)*, Special Publication ARLCD-SP-84001, U. S. Army Research and Development Center, Large Caliber Weapon Systems Laboratory, Dover, NJ, June, 1984.

13. Dede, M., and Dobbs, N., *Structures to Resist the Effects of Accidental Explosions - Volume IV (Reinforced Concrete Design)*, Special Publication ARLCD-SP-84001, U. S. Army Armament Research, Development, and Engineering Center, Armament Engineering Directorate, Picatinny Arsenal, NJ, April, 1987.

14. Kossover, D., and Dobbs, N., *Structures to Resist the Effects of Accidental Explosions - Volume V (Structural Steel Design)*, Special Publication ARLCD-SP-84001, U. S. Army Research and Development Center, Large Caliber Weapon Systems Laboratory, Dover, NJ, May, 1987.

15. Dede, M., Lipvin-Schramm, S., and Dobbs, N., *Structures to Resist the Effects of Accidental Explosions - Volume VI (Special Conditions in Explosive Facility Design)*, Special Publication ARLCD-SP-84001, U. S. Army Armament Research and Development Center, Larger Caliber Weapon Systems Laboratory, Dover, NJ, April, 1985.

16. Drake, J. L., Twisdale, L. A., Frank, R. A., Dass, W. C., Rochefort, M. A., Walker, R. E., Britt, J. R., Murphy, C. E., Slawson, T. R., and Sues, R. H., *Protective Construction Design Manual*, Report ESL-TR-87-57, Air Force Engineering and Services Laboratory, Tyndall AFB, FL, November, 1989.

17. Drake, J. L., and Little, Jr., C. D., "Ground Shock from Penetration Conventional Weapons," *Symposium Proceedings on the Interaction of Non-Nuclear Munitions with Structures*, U. S. Air Force Academy, Colorado Springs, CO, May 10-13, 1983, pp. 1-6.

18. Henrych, J., *The Dynamics of Explosion and Its Use*, Elsevier Scientific Publishing Co., New York, NY, 1979.

19. Higgens, C. J., "Some Considerations in the Analysis and Prediction of Ground Shock from Buried Conventional Explosions," *Symposium Proceeding on the Interaction of Non-Nuclear Munitions with Structures*, U. S. Air Force Academy, Colorado Springs, CO, May 10-13, 1983, pp. 5-24.

20. Weidlinger, P., and Hinman, E., "Analysis of Underground Protective Structures," *Journal of Structural Engineering*, ASCE, V. 114, No. 7, July, 1988, pp. 1658-1673.

21. Clough, R. W., and Penzien, J., *Dynamics of Structures*, McGraw-Hill Inc., New York, NY, 1975.

22. Ross, C. A., Jerome, E. L., and Malvern, L. E., "Spatial and Time Variations of Loading on Buried Structures by Underground Cylindrical Explosives," *Proceedings of the Second Symposium on the Interaction of Non-Nuclear Munitions with Structures*, Panama City Beach, FL, April 15-18, 1985, pp. 235-241.

23. Higdon, A., Ohlsen, E. H., Stiles, W. B., Weese, J. A., and Riley, W. F., *Mechanics of Materials*, 3rd Edition, John Wiley and Sons, Inc., New York, NY, 1976.

24. Kiger, S. A., and Painter, J. T., "A Computational Procedure for Response of Buried Structures to Conventional Weapons," *Proceedings of Second Symposium on the Interaction of Non-Nuclear Munitions with Structures*, Panama City Beach, FL, April 15-18, 1985, pp. 41-44.

25. Drake, J. L., Frank, R. A., and Rochefort, M. A., "A Simplified Method for the Prediction of the Ground Shock Loads on Buried Structures," *International Symposium Proceedings on the Interaction of Non-Nuclear Munitions with Structures*, Mannheim, West Germany, March 9-13, 1987, pp. 3-14.

26. Wong, F. S., *A Study on the Effect of Structure/Medium Interaction on the Loading on a Buried Structure*, Report No. 7864, Weidlinger Associates, New York, NY, November, 1978.

27. Wong, F. S., and Weidlinger, P., "Damping of Shallow-Buried Structures Due to Soil-Structure Interaction," *The Shock and Vibration Bulletin*, V. 52, Part 5, May, 1982, pp. 149-154.

28. Wong, F. S., and Weidlinger, P., "Design of Underground Shelters Including Soil-Structure Interaction Effects," *Symposium Proceedings on the Interaction of Non-Nuclear Munitions with Structures*, U. S. Air Force Academy, Colorado Springs, CO, May 10-13, 1983, pp.174-176.

29. Wong, F. S., Mak, R. Y., Kufferman, D., and Weidlinger, P., "A Case Study in Design of Underground Shelters," *Proceedings of Second Symposium on the Interaction of Non-Nuclear Munitions with Structures*, Panama City Beach, FL, April 15-18, 1985, pp. 74-77.

30. Isenberg, J., and Levine, H., "Analysis of Reinforced Concrete Under Shock Loading," *Seminar Proceedings: Finite Element Analysis of Reinforced Concrete Structures*, Tokyo, Japan, May 21-24, 1985, ASCE, New York, NY, pp.445-464.

31. Hinman, E. E., and Weidlinger, P., "Single-Degree-of-Freedom Solution of Structure-Medium Interaction," *Proceedings of the International Symposium on the Interaction of Non-Nuclear Munitions with Structures*, Mannheim, West Germany, March 9-13, 1987, pp. 44-59.

32. LaHoud, P. M., "Improved Design Procedure for Shallow-Buried Structures to Resist Airblast Loading," *Proceeding of Structural Congress '87 Related to Dynamics of Structures*, August 17-20, 1987, Structural Division, ASCE, New York, NY, pp. 721-734.

33. Drake, J. L., Walker, R. E., and Slawson, T., "Backfill Effects on Buried Structure Response," *Proceedings of the Fourth International Symposium on the Interaction of Non-Nuclear Munitions with Structures*, Panama City Beach, FL, April 17-21, 1989, pp. 38-43.

34. Krauthammer, T., Bazeos, N., and Holmquist, T. J., "Modified SDOF Analysis of RC Box-Type Structures," *Journal of Structural Engineering*, ASCE, V. 112, No. 4, April, 1986, pp. 726-744.

35. McVay, M. C., and Zalzman, S., *Finite Element Analysis of an Underground Structure*, Report AFESC/ESL-TR-87-05, Air Force Engineering and Services Center Laboratory, Tyndall AFB, FL, 1987.

36. Nelson, I., "Numerical Solutions of Problems Involving Explosive Loading," *Proceedings of Dynamic Methods in Soil and Rock Mechanics*, September 5-16, 1977, Rotterdam, Holland, pp. 239-297.

37. Crawford, R. E., Higgins, C. J., and Bultmann, H. E., *The Air Force Manual for Design and Analysis of Hardened Structures*, Report AFWL-TR-74-102, Air Force Weapons Laboratory, Kirtland AFB, NM, 1974.

38. Wright, J. P., and Smilowitz, R., "Uncoupling Approximation for the Dynamic Analysis of Structures Embedded in Hysteretic Media," *Journal of Computers and Structures*, V. 24, No. 5, 1986, pp. 791-798.

39. Galletly, G. D., Hosking, N. G., and Ofjord, A., *Behavior of Structural Elements Under Impulsive Loads III*, Massachusetts Institute of Technology, Department of Civil and Sanitary Engineering, Cambridge, MA, July, 1951.

40. Bates, S. C. C., *The Effect of Impact Loading on Prestressed and Ordinary Reinforced Concrete Beams*, Research Paper No. 35, Department of Scientific and Industrial Research, Building Research Station, Garston, England, 1961.

41. Wadlin, G. K., and Stewart, J. J., "Comparison of Prestressed Concrete Beams and Conventionally Reinforced Concrete Beams Under Impulsive Loading," *Proceeding of American Concrete Institute*, V. 58, October, 1961, pp. 407-421.

42. Hamilton, W. A., *Dynamic Response of Pretensioned Prestressed Concrete Beams*, Ph.D. Dissertation, Oklahoma State University, Stillwater, OK, 1967.

43. Veeraiah, C., *Dynamic Behavior and Resistance of Prestressed Concrete Split Beams*, Ph.D. Dissertation, The University of Texas at Austin, Austin, TX, 1972.

44. Tansley, R. S., Cuzner, G. J., and Wilton, C., *Research on Upgrading Structures for Host and Risk Area Shelters*, Final Report SSI-8144-7, Scientific Services, Inc., Redwood City, CA, September, 1982.

45. Loo, Y. C., and Santos, A. P., "Impact Deflection Analysis of Concrete Beams," *Journal of Structural Engineering*, ASCE, V. 112, No. 6, June, 1986, pp. 1297-1312.

46. *PCI Design Handbook: Precast and Prestressed Concrete*, 3rd Edition, Prestressed Concrete Institute, Chicago, IL, 1985.

47. *Building Code Requirements for Reinforced Concrete and Commentary*, ACI 318-89/318R-89, American Concrete Institute, Detroit, MI, 1989.

48. Wong, F. S., and Weidlinger, P., "Design of Underground Protective Structures," *Journal of Structural Engineering*, ASCE, V. 109, No. 8, August, 1983, pp. 1972-1979.

49. *Finite Element Analysis of Reinforced Concrete*, Task Committee of Finite Element Analysis of Reinforced Concrete Structures, Structural Division Committee on Concrete and Masonry Structures, ASCE, New York, NY, 1982.

50. Kotsovos, M. D., and Pavlovic, M. N., "Non-Linear Finite Element Modeling of Concrete Structures: Basic Analysis, Phenomenological Insight, and Design Implications," *Engineering Computations*, V. 3, No. 3, September, 1986, pp. 243-250.

51. Stevens, D. J., and Krauthammer, T., "Combined Finite Difference/Finite Element Analysis for Soil-Structure Interaction," *Proceedings of the Structural Congress 1987 Related to Dynamics of Structures*, August 17-20, 1987, Structural Division, ASCE, New York, NY, pp. 485-496.

52. Balakrishnan, S., Elwi, A. E., and Murray, D. W., "Effect of Modeling NLFE Analysis of Concrete Structures," *Journal of Structural Engineering*, ASCE, V. 114, No. 7, July, 1988, pp. 1467-1487.

53. Razaqpur, A. G., Nofal, M., and Mirza, M. S., "Nonlinear Analysis of Prestressed Concrete Box Girder Bridges Under Flexure," *Canadian Journal of Civil Engineering*, V. 16, Issue 6, 1989, pp. 845-853.

54. Crouch, R. S., and Chrisp, T. M., "The Response of Reinforced Concrete Slabs to Non-Nuclear Blast Loading," *Proceedings of the First International Conference on Structures Under Shock and Impact*, Cambridge, MA, July, 1989, pp. 69-76.

55. Xia, Y., *Behavior of a Two-Layered Beam Under Impact Loading*, Report OUEL-1716-87, Oxford University, England, 1987.

56. Clough, R. W., "Original Formulation of Finite Element Method," *Proceedings from Structures Congress '89 (Computer Utilization in Structural Engineering)*, San Francisco, CA, May 1-5, 1989, ASCE, New York, NY, 1989, pp. 1-10.

57. Scordelis, A. C., "Past, Present, and Future Developments," *Seminar Proceedings: Finite Element Analysis of Reinforced Concrete Structures*, Tokyo, Japan, May 21-24, 1985, ASCE, New York, NY, pp. 656-666.

58. Ottosen, N. S., *Non-Linear Finite Element Analysis of Concrete Structures*, Report RISO-R-411, Risoe National Laboratory, Roskilde, Denmark, May, 1980.

59. Owen, D. R. J., Figueiras, J. A., and Damjanic, F., "Finite Element Analysis of Reinforced and Prestressed Concrete Structures Including Thermal Loading," *Computer Methods in Applied Mechanics and Engineering*, V. 41, 1983, pp. 323-336.

60. Gedling, J. S., Mistry, N. S., and Welch, A. K., "Evaluation of Material Models for Reinforced Concrete Structures," *Computers and Structures*, V. 24, No. 2, 1986, pp. 225-232.

61. Bedard, C., and Kotsovos, M. D., "Fracture Processes of Concrete for NLFEA Methods," *Journal of Structural Engineering*, ASCE, V. 112, No. 3, 1986, pp. 573-587.

62. Chang, T. Y., Taniguchi, H., and Chen, W. F., "Nonlinear Finite Element Analysis of Reinforced Concrete Panels," *Journal of Structural Engineering*, ASCE, V. 113, No. 1, 1987, pp. 122-140.

63. Ahmad, M., and Bangash, Y., "Three-Dimensional Bond Analysis Using Finite Element," *Computers and Structures*, V. 25, No. 2, 1987, pp. 281-296.

64. Pulmano, V. A., and Shin, Y. S., "Simplified Finite-Element Analysis of Deflections of Reinforced Concrete Beams," *ACI Structural Journal*, July-August, 1987, pp. 342-348.

65. Abdel-Halim, M., McClure, R. M., and West, H. H., "Overload Behavior of an Experimental Precast Prestressed Concrete Segmental Bridge," *Journal of Prestressed Concrete Institute*, V. 32, No. 6, November-December, 1987, pp. 102-123.

66. Bhatt, P., Abdel-Hafiz, L. M., and Green, D. R., "Nonlinear Analysis of Reinforced Concrete Slabs," *Updating the State-of-the-Art in Civil Engineering Computing Tools*, Third International Conference on Computing in Civil Engineering, August 10-12, 1988, Vancouver, B.C., Canada, pp. 225-232.

67. Elwi, A. E., and Hrudey, T. M., "Finite Element Model for Curved Embedded Reinforcement," *Journal of Engineering Mechanics*, ASCE, V. 115, No. 4, April, 1989, pp. 740-754.

68. Ghaboussi, J., Millavec, W. A., and Isenberg, J., "R/C Structures Under Impulsive Loading," *Journal of Structural Engineering*, ASCE, V. 110, No. 3, 1984, pp. 505-522.

69. Citernesi, F., Zurru, M., and Crutzen, Y., "Dynamic Analysis of a Buried Concrete Structure Subjected to Gas Pressure Loading," *Proceedings of Second Symposium on the Interaction of Non-Nuclear Munitions with Structures*," Panama City Beach, FL, April 15-18, 1985, pp. 101-106.

70. Van Mier, J. G. M., *Examples of Nonlinear Analysis of Reinforced Concrete Structures with DIANA*, Heron, V. 32, No. 3, 1987.

71. Weerheijm, J., Van Zantvoort, P. J. H., and Opschoor, G., "The Applicability of the FE-Technique to Dynamic Failure Analysis of Concrete Structures," *23rd DOD Explosive Safety Seminar*, Atlanta, GA, August 9-11, 1988, pp. 1005-1020.

72. Miyamoto, A., King, M. E., and Fujii, M., "Non-Linear Dynamic Analysis and Design Concepts for RC Beams Under Impulsive Loads," *Bulletin of the New Zealand National Society for Earthquake Engineering*, V. 22, No. 2, June, 1989, pp. 98-111.

73. Stevens, D. J., and Krauthammer, T., "Nonlinear Finite Element Analysis of Impulse Loaded RC Beams," *Proceedings of the First International Conference on Structures Under Shock and Impact*, Cambridge, MA, July, 1989, pp. 41-53.

74. Van Wees, R. M. M., and Weerheijm, J., "Simulation of Concrete Beams Under Explosive Loading with the Finite Element Method," *Proceedings of the First International Conference on Structures Under Shock and Impact*, Cambridge, MA, July, 1989, pp. 97-106.

75. Riva, P. and Cohn, M. Z., "Engineering Approach to Nonlinear Analysis of Concrete Structures," *Journal of Structural Engineering*, ASCE, V. 116, No. 8, August, 1990, pp. 2162-2186.

76. Smith, J. L., *Investigation of Existing Computer Codes with Linear and Nonlinear Dynamic Capabilities*, Report J650-88-001/1411, JAYCOR, Vicksburg, MS, February, 1988.

77. *ANACAP-U Theory Report (Version 90-2.0)*, ANATECH Research Corp., La Jolla, CA, February, 1991.

78. *ANACAP-U User's Manual (Version 90-2.0)*, ANATECH Research Corp., La Jolla, CA, February, 1991.

79. *ABAQUS Example Problems Manual (Version 4.8)*, Hibbitt, Karlsson, and Sorensen, Inc., Providence, RI, 1989.

80. Bowles, J. E., *Foundation Analysis and Design*, 3rd Edition, McGraw-Hill Book Company, New York, NY, 1982.

81. Wang, P. T., Shaw, S. P., and Naaman, A. E., "High-Strength Concrete in Ultimate Strength Design," *Journal of Structural Division*, ASCE, V. 104, No. ST11, November, 1978, pp. 1761-1773.

Vita

William Randal Burkett was born in El Dorado, Arkansas, on July 31, 1952, the son of Eldreadge Lynn Burkett and Sarah Jane (Starkey) Burkett. After completing work at Robert E. Lee High School, Baytown, Texas, in 1970, he entered Lamar University in Beaumont, Texas. He received the degrees of Associate of Applied Science in Drafting Technology in December 1972, Bachelor of Science in Industrial Technology in August 1975, and Bachelor of Science in Civil Engineering in August 1981, from Lamar University. As a student, he became a member of Chi Epsilon National Honorary Civil Engineering Fraternity in 1980. While in Beaumont, Texas, he was employed as a structural and mechanical draftsman by Dresser Ideco (May 1974 - August 1977) and as an instructor by Lamar University, College of Technical Arts (August 1977 - August 1982). As a drafting instructor, he received an "Award of Excellence" from the Halliburton Education Foundation in 1980.

The author entered Texas A&M University, College Station, Texas, in September 1982, and received the degree of Master of Engineering in Civil Engineering with a specialization in structures in May 1984.

The author received an active duty commission as an Ensign, Civil Engineer Corps, United States Navy in May 1984. His first assignment was Assistant Resident Officer in Charge of Construction, Northern Division Contracts Office, Naval Facilities Engineering Command, Brunswick Naval Air Station, Maine. He served in Maine (September 1984 - August 1986) administering general construction contracts for the Navy and was promoted to the rank of Lieutenant (Junior Grade) in March 1986. As part of an exchange program, his second assignment was Research Engineer, Headquarters Air Force Engineering and Services Center, Tyndall Air Force Base, Florida. He served in Florida (August 1986 - August 1988) developing and managing research, development, test, and evaluation (RDT&E) programs for the Air Force with an emphasis on conventional weapons effects and protective structural systems. He was promoted to the rank of Lieutenant in October 1987, and was released from active duty in August 1988. He now continues his military career as a reserve naval officer.

The author entered the Ph.D. program at The University of Texas at Austin, Austin, Texas, during the spring semester of 1989. Again, his emphasis was on structures in the Civil Engineering Department. While in

graduate school at Austin, he was awarded a fellowship (June 1989 - August 1992) under the United States Air Force Office of Scientific Research - Laboratory Graduate Fellowship Program.

The author was designated as an Engineer-in-Training in Texas, November 1984. He is also a member of the American Concrete Institute and the American Society of Civil Engineers.

The author married the former Donna Lynn Hazzard of Texas City, Texas, in December 1982. They have two precious children; a son, William Matthew, and a daughter, Leeanna Maelyn.

Permanent address: 2921 8th Avenue North
Texas City, Texas 77590

This dissertation was typed by the author.